Modern Depositional Environment in Lake Bosumtwi, Mapped by the Spatial Relationships of Bulk Sediment and Magnetic Mineral Grain Size.

A Thesis Submitted to the Kwame Nkrumah University Science and Technology, for the degree of Master of Science in Geophysics

by

James Nii Kamuah Addo (Bsc.)

College of Science
Department of Physics
Kwame Nkrumah University of Science and Technology

May 2005

QUOTATION

A lake is the landscape's most beautiful and expressive feature. It is the earth's eye; looking into which the beholder measures the depths of his own nature

Henry David Thoreau

Walden

DECLARATION

It is hereby declared that:

This thesis is a presentation of a work carried out by the author.

This report has not been submitted in any form to any organization, institution or body for the award of any degree.

All inclusions as well as references from works of previous authors have been duly acknowledged.

Signature: _____

James Nii Kamuah Addo
(Author)

Date: _____

Signature: _____

Prof. Aboagye Menyeh
(Supervisor)

Date: _____

DEDICATION

This work is dedicated to my beloved and wonderful wife Mrs. Emma Nana Ama Sefa-Addo, my father Mr. Emmanuel A. Addo and to all my brothers; Samuel, Sampson, Daniel, Stephen, Joseph and my sisters; Gladys and Victoria and finally, to my most cherished friends, Theodora Belba-Smith and Jarlvis Anum Yemoh.

ACKNOWLEDGEMENTS

I wish to express my sincerest and most heartfelt thanks to my project supervisors Prof. A. Menyeh and Dr. Sylvester K. Danuor for their support, suggestions and constructive criticisms during this work. Indeed, they have been more than just supervisor to me throughout this work period. Much thanks also to my colleague and junior course mates for their encouragement in all the various forms offered me.

I am deeply indebted to Prof. John A. Peck, from the University of Akron, Ohio, USA, for his role in assisting me work in his laboratory in the University. I am also very grateful to him for introducing me to the subject of environmental magnetics during my fieldwork section as part of the Lake Bosumtwi Drilling Project, which took place between July 1 and August 31, 2004, and his kind encouragement, guidance and hours of discussions throughout my stay in the USA while working on this thesis. Also many thanks to Andrea Mullen of University of Akron, Ohio, USA, for assisting me work on all the spatial maps used in this work.

Sincere thanks go to all friends of mine who have assisted me in any form to make this write-up a fruitful one, especially Jarlvis A. Yemoh of Miracle Life Ministries, Tema, and Miss Theodora Belba-Smith of the Biological Science Department, Kwame Nkrumah University of Science and Technology. Much thanks also go to Mr. Van Dyke Asare and all the staff of the Department of Physics (KNUST), for their technical assistance. I will like to express my gratitude to my father, Mr. Emmanuel A. Addo and all my brothers and sisters for their immense assistance in all they did to make this thesis a success.

Finally, I thank the Lord God almighty for His abundant love and mercy he showered on me during this period of schooling. I focused my mind on him and He fulfilled His word concerning my life, for He kept me in perfect peace during this time.

ABSTRACT

A study of the modern depositional environment mapped by the spatial relationships of bulk sediment and magnetic mineral grain size has been conducted at Lake Bosumtwi. A total of 134 sediment samples were collected from specific locations over the entire lake with sampling depths ranging from 2 cm to 8 cm using the Ekman dredge. Sample measurements include magnetic susceptibility, anhysteretic remanent magnetization, isothermal remanent magnetization, saturation isothermal remanent magnetization, loss-on-ignition as well as the determination of magnetic hysteretic parameters such as coercive force (H_c) and the remanent coercivity (H_{cr}). In addition, grain size analysis was performed on selected samples using the Rotap sieving method. The analysis of the measured results shows an increase in the magnetic concentration of the samples with increasing lake water depth. Coercivity values measured reveals that samples contain high proportions of magnetic minerals with low coercivity. The magnetic mineral grain size analyzed shows a decrease in size as lake water depth increases and bulk sediment grain size decreases with increasing water depth. The ratio of saturation remanent magnetization to saturation magnetization (M_{rs}/M_s) for selected samples were calculated. This ratio was observed to lie in the range of values, 0.21 – 0.31 indicating the presence of pseudo – single domain magnetic mineral grain size. Similarly, the percentage of organic content of the samples was found to increase with increasing lake water depth. From the results above, it can be concluded that, the uppermost 8 cm of surface sediment possibly accumulated under wet climatic conditions, which allowed the settling of sediments of reduced dust flux. The magnetic minerals present in the lake could be more of an authigenic and diagenetic origin than from allogenic origin.

CONTENTS **PAGE**

LIST OF FIGURES

LIST OF TABLES

CHAPTER ONE

INTRODUCTION

1.1 GENERAL INTRODUCTION

In recent years, lake sediments studies have become increasingly important in many branches of environmental science. This reflects both a natural scientific curiosity in the sediment-based reconstruction of past environmental conditions, and also, especially over the last decade, a need to set studies of present day environmental processes and problems in a longer time perspective. This is best achieved in the lake-watershed ecosystem framework (Oldfield, 1977).

Lake sediments are especially useful in historical monitoring for several reasons. Despite unresolved problems of mud-water exchange chemistry and early diagenesis, there is often a conformity of process linking past and present deposition mechanisms. The rate of sediment accumulation is normally more rapid in lakes than in marine environments. In consequence, the period of accelerating human impact on the environmental processes over the last one or two centuries is usually well resolved in the upper sediments of lakes. Finally, the lake-watershed ecosystem is material-bonded in large measure and thus provides a convenient and spatially finite framework for study (Thompson & Oldfield, 1986).

1.2 STATEMENT OF THE PROBLEM

Modern depositional environment in Lake Bosumtwi is mapped by the spatial relationships of bulk sediment and magnetic mineral grain size.

1.3 RESEARCH OBJECTIVES AND PURPOSE

The main objective of this research is to determine if sediment magnetic properties are related to lithologic variability (e.g., sandy, clayey, or mud layers) of the Lake Bosumtwi surfacial sediment. The collection of samples came from precisely known locations and depths therefore, it will be possible to determine variations in the bulk sediment grain size as a function of water depth wave orbital energy, and proximity to sources.

Because changes in lithology are related to depositional environment (i.e., the prevailing physical, chemical and biological conditions at the time of deposition), it will be possible to construct a map showing the present day depositional environment in the lake. Furthermore, it may be possible to correlate changes in magnetic mineralogy with depositional environment. One important control on the physical energy of a depositional environment is water level change (low or high stands), which has responded to climate variations since the formation of the lake. Understanding lake level variability is one of the vital aspects of the Lake Bosumtwi project. The results of this research will contribute to the drilling project goals by providing an understanding of the relationship between sediments and water level changes and therefore to the climatic conditions. The results will also contribute to the use of this technique in paleoclimatic studies.

1.4 SIGNIFICANCE OF THE STUDY

The Bosumtwi crater has been an object of scientific interest since the late 70's (Talbot & Delibrias, 1977). However, in spite of this long period of study, the determination of the relationship between sediment magnetic properties and lithology of the lake surface sediments has not been carried out. In addition, no lake surfacial sediment grain-size maps exist.

Understanding the magnetic mineral–lithology relationship is important because changes in surface magnetic minerals of the lake sediments might correlate with climatic conditions at the time sediments were deposited. A knowledge of the changing global

climate is important and inference from the past climatic conditions is vital for the prediction of future climate.

1.5 GEOLOGY OF THE LAKE BOSUMTWI CRATER AREA

The Bosumtwi impact event occurred about 1.07 ± 0.05 million years ago (Koeberl et al., 1997), in a target made of Precambrian crystalline rocks, the 2.1-2.2 Ga metasedimentary rocks in greenschist facies of the Lower Birimian System of phyllites, graywackes, quarzites, sandstones, shale, micaschist, as well as local granites (Jones et al., 1981; Wright et al., 1985; Leube et al., 1990; Reimold et. al., 1998). The Upper Birimian metamorphosed basalts and pyroclastic rocks (metavolcanics) occur in the Obuom Range, south-east of the crater. The Precambrian Tarkwaian metasedimentary rocks also occur to the east and south-east of the crater (Moon and Mason, 1967; Woodfield, 1966; Jones et al., 1981).

Regionally the geology is characterized by northeast-southwest trends with steep dips of 30° – 40° either to the northwest or south-east. However, variations in this trend, due to folding, have been observed (Reimold et al., 1998). The lithology at and around Lake Bosumtwi is dominated by metagraywackes and metasandstones, but some shale and mica schist are found, more often to the north-eastern and southern rim sectors (Reimold et al., 1997; Reimold et al., 1998). A variety of granitoid intrusions (mainly biotite or amphibole granites) have been mapped by Junner (1937) and Moon and Mason (1967). Small granite intrusions, probably connected with the Kumasi granite, crop out around the north-east, west, and south sides of the lake, the largest at Pepiakese on the north-east side of the crater (Jones et al., 1981). In addition, numerous, but generally less than 1-m-wide, dikes of biotite granitoid at many basement exposures in the crater rim have been observed. The overall granitoid component in the region is estimated at about 2 percent (Reimold et al., 1998).

Recent rock formations include the Bosumtwi lake beds, as well as soils and breccias associated with crater formation (Junner, 1937; Kolbe et al., 1967; Woodfield, 1966; Moon and Mason, 1967; Jones et al., 1981; Koeberl et al., 1997b, and Reimold et al., 1998).

CHAPTER TWO

THEORETICAL BACKGROUND: THE ORIGIN OF MAGNETIC MINERALS IN LAKE SEDIMENTS

2.1 INTRODUCTION

The magnetic minerals present in lakes are of varied types and origins. Interpreting the record of mineral magnetic variation in the sediments is therefore strongly dependent on evaluating alternative sources for a given lake and catchment, with a view to identifying the dominant types, sources, and pathways represented.

2.2 TYPES AND SOURCES OF MAGNETIC MINERALS IN LAKE SEDIMENTS

The conventional distinction between the three main mineral sediment types is useful in this respect (i.e., authigenic, diagenetic and allogenic sediment). Authigenic magnetic minerals are those formed by chemical or biogenic processes in situ after deposition of the sediment. Diagenetic magnetic minerals result from the transformation of existing magnetic or non-magnetic minerals to new magnetic types and allogenic magnetic minerals types are those brought into the lake from outside. They may have originated within the drainage basin of the lake or have been transported (for example by man or wind) from more distant sources beyond the immediate catchment. Thus the magnetic minerals in lake sediments are overwhelmingly regarded as allogenic except where there is positive evidence to the contrary (e.g. Hilton and Lishman, 1985). Table 2.1 identifies the main types and sources of magnetic minerals found in lake sediments.

Table 2.1 Magnetic minerals in lake sediments: major types and sources (Thompson & Oldfield, 1986).

Source type	Location origin	Major pathways	Magnetic mineral types
Bedrock	Lake catchment	Streams overland flow mass movement wind	Magnetites; haematite;pyrrhotite Multidomain/Single domain
Soils	Outside lake catchment		Impure magnetite; magnetite Singledomain/Superparamagnetic Goethite/haematite
Volcanic ash	Lake catchment	Streams, etc.	magnetites
	Outside lake catchment	Wind	
Fossil fuel combustion and industrial processes	Lake catchment	Streams, etc	
Lake sediments	Outside lake catchment Authigenic/diagenetic/post-depositional/in situ	Wind	Impure magnetite Haematite Magnetite Greigite

2.2.1 ALLOGENIC MAGNETIC MINERALS FROM WITHIN THE LAKE CATCHMENT

Lithology exerts an important control on the magnetic mineralogy of lake sediments. Modification of the primary iron compounds in bedrock during the course of weathering and soil formation provides also the basis for distinguishing magnetically between topsoil, subsoil and bedrock sediment sources in rivers. In the case of lake sediments, any part of the drainage basin regolith exposed to erosive processes is a potential sediment source and allogenic sediments will be a mixture of soil-, subsoil- and bedrock-derived material in widely varying proportions. Allogenic lake sediments therefore will be expected to come as a mixture of primary magnetic minerals in the catchment with the secondary magnetic minerals formed in the soil.

Human activity within the catchment or on the lake itself may also generate magnetic minerals, which pass into the lake sediments. Moreover, in recent sediments of the Grand Lac d'Annecy a striking susceptibility peak in several cores were shown to be the result of clinker from the coal barges, which plied the lake in the first half of the 20th century.

2.2.2 ALLOGENIC MAGNETIC MINERALS FROM OUTSIDE THE LAKE CATCHMENT.

All the magnetic mineral types encountered in the atmosphere contribute to the sedimentary records. However, contribution becomes significant only in specific circumstances such as volcanic activity, fossil-fuel combustion and from forest fires, in comparison with the input from the land surfaces around the lake.

There is strong evidence from the sediments of Newton Mere in the English Midlands and the nearby Whixall Moss, for the recent deposition of magnetic minerals resulting from fossil fuel combustion and industrial processes in areas lying down wind, but outside the tiny catchment. The evidence for fine soil and for wind erosion and charcoal dispersal associated with major forest and savannah fires suggests that these agencies may contribute magnetic minerals to lake sediments down wind. Ferrimagnetic minerals in high concentrations have been detected also in peat cores from Bega Swamp in S. E. Australia, at two horizons with high charcoal counts, and presumably, were caused by atmospheric transport of fire-enhanced topsoil (Thompson & Oldfield, 1986).

2.2.3 AUTHIGENIC AND DIAGENETIC MAGNETIC MINERALS

Goethite (presumably Fe_2O_3)**,** has been identified by electron microprobe analysis as the major mineral constituent of the iron-rich ferromanganese nodules recovered from Romahawk Lake, Wisconsin, and that both todorokite and goethite have been identified by X-ray diffraction there and at other sites including the Green Bay arm of the Lake Michigan. Greigite (Fe_3S_4) has been identified in sediment cores from Lake Superior (Thompson & Oldfield, 1986).

2.3 FACTORS THAT AFFECT LAKE SEDIMENT MAGNETISM

2.3.1 FIRE

A study at Llyn Gaddindum, lying only 1 km from Llyn Bychan, used a grid of cores in the correlation including many with high susceptibility, Π, and saturation isothermal remanent magnetization (SIRM) values in the top 10-20 cm. The increase in their magnetism, dated by ^{137}Cs in 1954, was ascribed to the major fire of 1951, which destroyed much of the forest in the eastern half of the catchment. Similarly, in the Landes, SIRM values shown from ^{210}Pb and ^{137}Cs dating was contemporary with massive forest fires of the 1940's culminating in 1949 (Thompson & Oldfield, 1986).

2.3.2 CLIMATIC CHANGES

Results from many site studies suggest that major climatic shifts control weathering and sedimentation regimes in ways, which give rise to distinctive mineral magnetic variations. Climatic episodes therefore marked by poorly developed vegetation cover, soil instability and active soil-fluction gives rise to peaks in Π. Episodes of developing plant cover and soil maturation under milder climatic conditions give rise to minimum Π values (Thompson & Oldfield, 1986).

2.3.3 PARTICLE SIZE

Magnetic properties of lake sediment and sediment source generally vary with particle size (Thompson & Morton, 1979; Dearing et al, 1981; Bradshaw & Thompson, 1985; Snowball, 1993). Hence, differences in particle size distribution within a core can be a major control on bulk sample magnetic property.

Different potential sources of sediment within a catchment may show similar and distinctive magnetic particle size relationships but the sorting effects of erosion, transport

and sedimentation processes can be expected to produce as much as five – fold differences between the magnetic concentrations of different texture sediment layers.

2.3.4 TIME DEPENDENCE OF MAGNETIZATION

Changes in magnetization with time are known as viscous with the most important one arising from thermal activation. Therefore, the effects of time on magnetic phenomena are of great importance, especially when geological time-scales are involved. Thermal activation causes magnetic viscosity in multi-domain grains by exciting domain wall movements and allowing the walls to cross otherwise impenetrable barriers. Thermal agitation can also cause the magnetic moments of single-domain grain to rotate from a minimum energy position to another across potential energy barriers which otherwise would not have been possible. Magnetic viscosity can therefore lead to a growth or loss in magnetization (Thompson & Oldfield, 1986).

2.3.5 GRAIN SIZE INTERACTIONS

When magnetic grains lie close to each other, there is the tendency of magnetostatic interaction arising between them and then modifying the overall magnetic behavior. Such grain interaction tends to lower bulk coercivity. Through these phenomena, coercivity has been realized to decrease with increasing packing where packing is defined as the fraction of the total volume occupied by magnetic particles. Magnetism tends to be made more difficult by grain interactions whereas demagnetization tends to become easier. In addition, the critical grain size of multi-/single-domain boundary is increased by interactions because of the changes in magnetostatic energy.

Finally, the susceptibility of magnetic assemblage may be lowered by magnetic interactions, ultimately, with interactions, which involve superparamagnetic grains (Thompson & Oldfield, 1986).

2.4 MAGNETIC REMANENCE

Rocks, soils and sediments can acquire remanent magnetization via natural processes. This remanence is therefore not as intense as those, which can be artificially imparted on a material in the laboratories using strong magnetic fields, but it is found to be stable.

For example, in igneous rocks, the event is simply the cooling of the magnetic minerals through their Curie and blocking temperatures, and in deep-sea sediments, the event is consolidation, which locks the tiny detrital, micron-sized magnetic minerals firmly into the bulk of the sediments (Thompson & Oldfield, 1986).

2.5 TYPES OF REMANENT MAGNETIZATION

2.5.1 NATURAL MAGNETIC REMANENCE

2.5.1.1 THERMOREMANENT MAGNETIZATION (TRM)

A thermoremanet magnetization is acquired by a magnetic mineral cooling from above its Curie temperature in a magnetic field. If the sample is isotropic, the magnetization is parallel to the applied field and, for small fields, the intensity of the remanence is proportional to the field. The remanence can survive with a little change through geological time, the reason being that it is remarkably stable. However, the thermoremanence of a multi-domain grain is much lower than that of a single domain grain with the remanence of mixtures of multi-domain, single-domain and superparamagnetic grains being overwhelmingly influenced by the single-domain fraction (Thompson & Oldfield, 1986).

Consequently, the thermoremanence of stable single-domain grains plays an important role in many palaeomagnetic studies (Nagata, 1961).

2.5.1.2 CHEMICAL REMANENT MAGNETIZATION (CRM)

This occurs when a magnetic mineral is produced by chemical changes at temperatures below its Curie temperature. This remanence is acquired in the direction of the ambient field and locked up in the grain when it grows larger than a critical size called the blocking volume.

Chemical remanence is of lower magnitude than thermoremanence because, the saturation magnetization and anisotropy energy are lower at temperatures well below the Curie temperature whilst the stability of both is similar.

2.5.1.3 DETRITAL REMANENT MAGNETIZATION (DRM)

Detrital remanent magnetization results mainly when detrital magnetic particles align themselves with an applied magnetic field (the earth's magnetic field) whilst they fall through water. It can also result after the particles have come to rest on a substrate, by the rotation of the magnetic grains in water-filled interstices. This post-depositional remanent magnetization is locked up into sediments by consolidation due to either compaction or to the growth of authigenic minerals or organic gels (Thompson & Oldfield, 1986).

2.5.2 LABORATORY - IMPACTED REMANENCES

2.5.2.1 VISCOUS REMANENT MAGNETIZATION (VRM)

This is acquired when a sample is exposed to a new magnetic field, which is by definition, time dependent. Decay of the natural remanence with time during a zero field storage, indicates the presence of 'soft' components of viscous remanence.

This component can therefore be removed by waiting for a few days or weeks so that the remanence stabilizes. Such remanences are commonly found in recent sediments, which have been stored for sometime (Thompson & Oldfield, 1986).

2.5.2.2 ISOTHERMAL REMANENT MAGNETIZATION (IRM)

This is the remanence acquired by deliberately exposing the material to a steady field at a given temperature (most commonly, room temperature), with magnitude depending on the strength of the steady field applied. The maximum remanences, which can be produced is called the saturation isothermal remanent magnetization (expressed by the symbols M_{rs} or SIRM). This dependence of magnetization on field can be illustrated or demonstrated by placing a specimen in stronger and stronger fields and measuring the remanence after each exposure as shown in Figure 2.1 (Thompson & Oldfield, 1986).

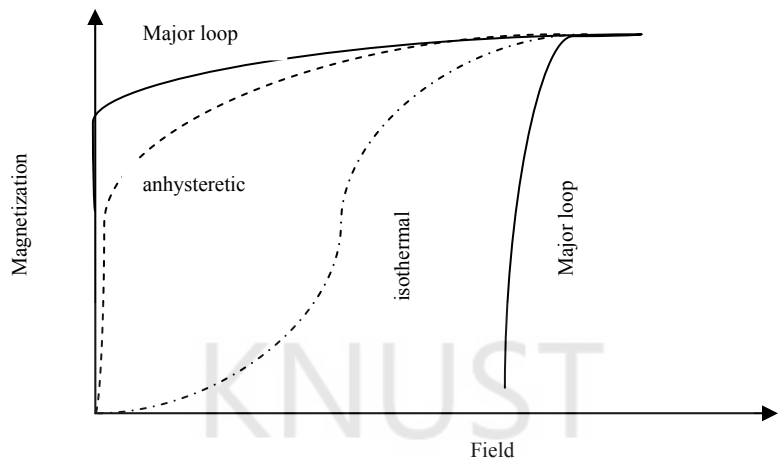

Figure 2.1 Diagram illustrating acquisition curves for anhysteretic (dashed) magnetizations. The isothermal magnetization curve increases slowly in low fields, then more rapidly before saturation.

IRM acquisition is a useful technique to distinguish between magnetite and hematite as shown below in the Fig. 2.2.

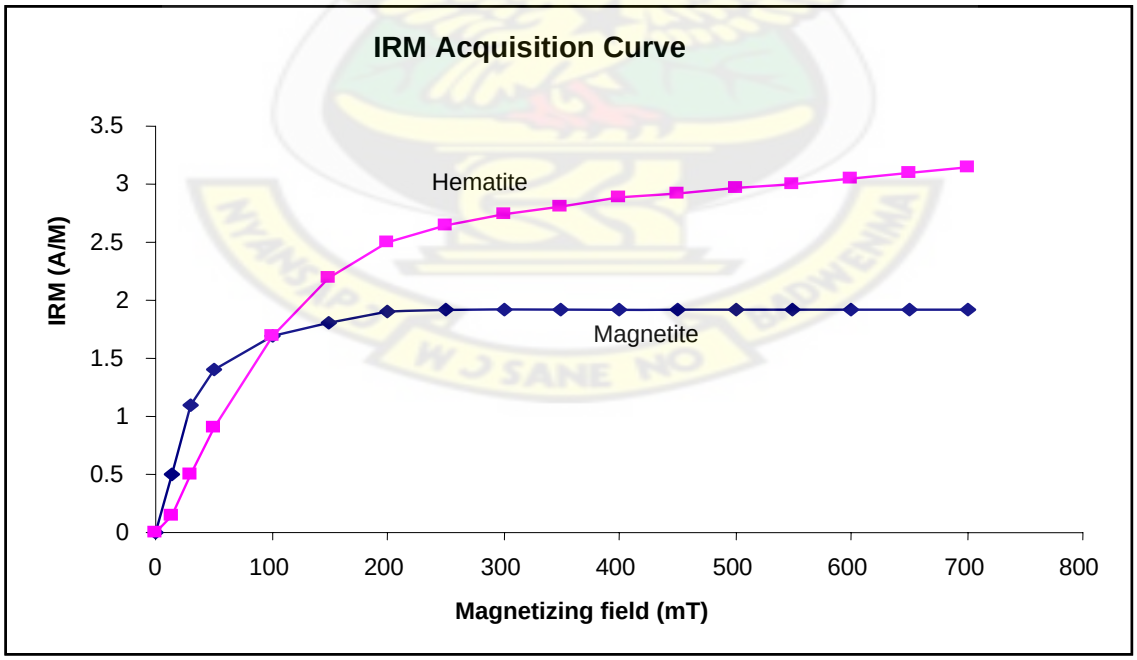

Figure 2.2 IRM acquisition curve and its usefulness to distinguish between magnetite and hematite (After Butler, 1982).

Coercivity in hematite is usually much larger than that observed in magnetite; hence, during IRM acquisition it is more difficult to saturate hematite than magnetite. Magnetite is typically saturated by 300 – 500 mT (Moskowitz, 1991).

2.5.2.3 ANHYSTERETIC REMANENT MAGNETIZATION (ARM)

This is generally impacted by the subjection of a sample to a strong alternating field, which is smoothly decreased to zero in the presence of a small steady field. Anhysteretic remanence increases in intensity with the application of either a stronger steady field or a stronger alternating field until saturation is reached.

The intensity of an ARM for weak – fields (< 10 mT) is always much larger than a comparable IRM given in the same DC field as shown in Fig. 2.3.

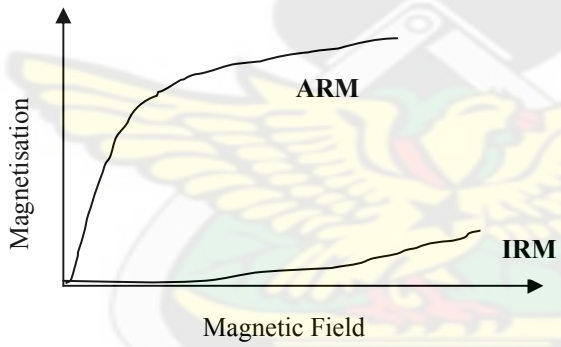

Figure 2.3 Illustration of the dissimilarity in ARM and IRM in magnetizing process (Moskowitz, 1991).

During ARM acquisition, the DC field is assisted by the AF field in the acquisition process. Likewise, the remanence coercivity fractions activated by the ARM and IRM processes will also be dissimilar (Thompson & Oldfield, 1986).

Dunlop and Yu [2003] however, have observed experimentally that ARM intensities diminish with increasing decay rate for single domain and pseudo-single domain assemblages, but increase for multi-domain grains (The IRM Quarterly, Fall 2003).

2.6 MAGNETIC PROPERTIES OF MATERIALS

2.6.1 INTRODUCTION

To the-man-in-the-street, matter is often thought to be either magnetic or non-magnetic due to the fact that ordinary magnet attracts magnetic materials, e.g. iron fillings, pins, lodestone, whereas non-magnetic materials e.g. wood, chalk, are not attracted by magnet. This means that all materials show some reaction to a magnetic field though the reaction will be very weak in the case of conventionally 'non-magnetic' materials, which therefore calls for a powerful electromagnet and sensitive measuring instrument to demonstrate these weak reactions.

At the atomic scale, magnetic fields arise from the motion of electrons. Two possible electron motions may be imagined within an atom; - the orbital rotation of an electron about the nucleus of an atom, and the spin motion of an electron about its own axis (Thompson & Oldfield, 1986).

2.6.2 DIAMAGNETISM

This is a property of all materials. It arises from the interaction of an applied magnetic field and the motion of electrons orbiting the nucleus. Because electrons carry charges, they experience a sideways Lorentz force when moving through a magnetic field. This force gives rise to a magnetic moment in the opposite direction to the applied field. This result to a negative magnetization (Fig. 2.4). The moment is typically a hundred times smaller than paramagnetism and a hundred-thousand times smaller than ferromagnetism, e.g. quartz (SiO_2), although, it is temperature independent compared to paramagnetism and ferromagnetism, which decrease markedly as temperature increases. There occur exceptional cases where some materials give an appreciable signal. An example is the weakly magnetized water-saturated sediment sometimes encountered in lake studies (Moskowitz, 1991).

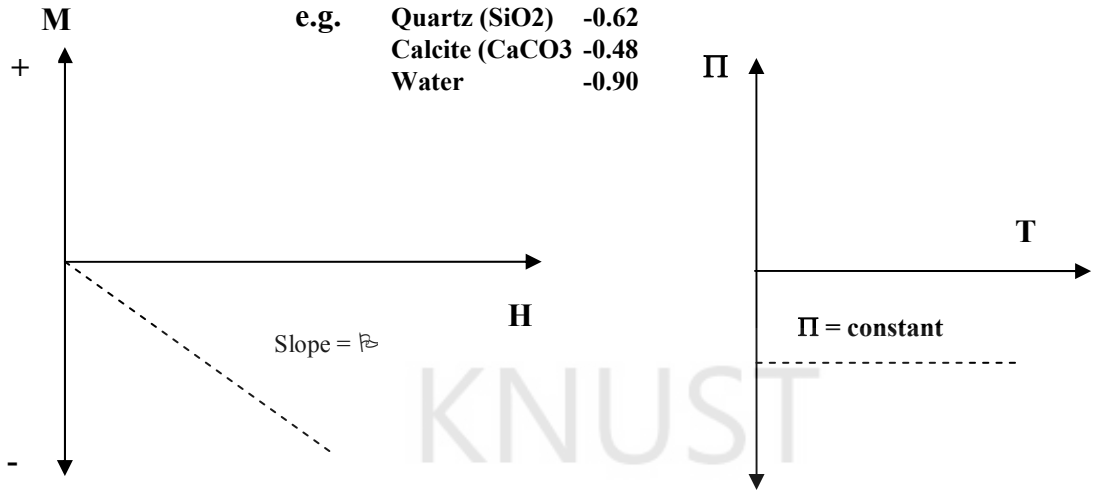

Figure 2.4 Shows the variation of magnetic susceptibility with magnetic field and temperature in diamagnetic materials.

2.6.3 PARAMAGNETISM

In the context of environmental magnetism, paramagnetism is much more important than diamagnetism. It arises by virtue of the fact that an electron behaves as though it were spinning about its own axis as well as orbiting the nucleus, which causes it to possess spin magnetic moment in addition to its orbital magnetic moment.

If the spin and orbital magnetic moments of an atom are oriented in such a way as to cancel one another out, the atom would have a zero magnetic moment. If on the other hand the cancellation is partial, the atom would have a permanent magnetic moment which leads to paramagnetism (Moskowitz, 1991). The graph of Π with variation in temperature and magnetic field is shown in Fig. 2.5 below.

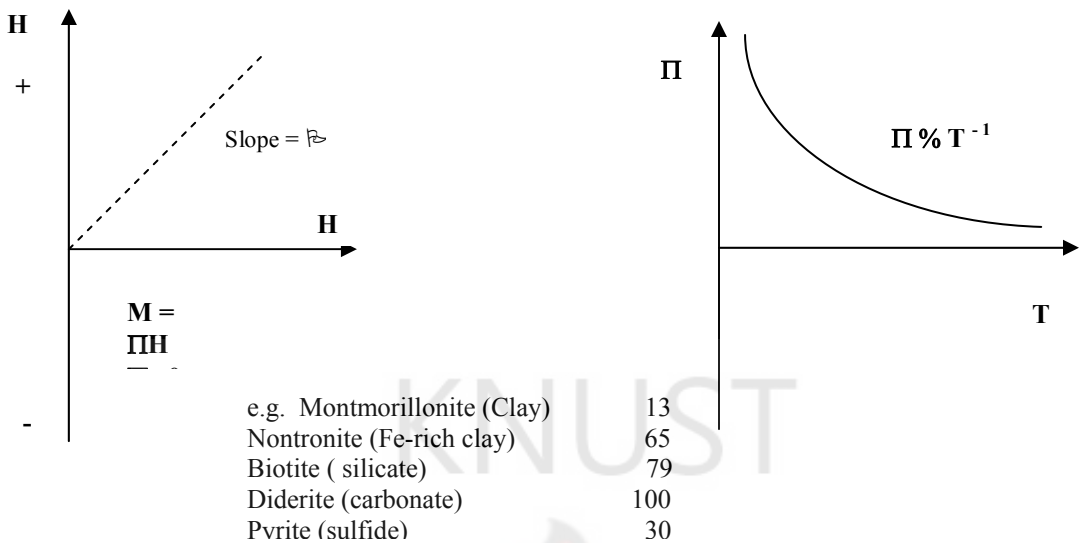

Figure 2.5 Variation of magnetic susceptibility with temperature and magnetic field strength in paramagnetic materials.

2.6.4 FERROMAGNETISM

This is much stronger than diamagnetism and paramagnetism. It is particularly associated with the elements iron (hence the name), nickel, and cobalt, but also occurs in many natural minerals such as certain very important iron oxides. Because of its unfilled 3*d* sub-shell, the iron atom possesses a fundamental magnetic moment of 4 Bohr magnetons ($4\mu_B$) (Niels Bohr, 1889 - 1962).

In the crystal lattice of a ferromagnetic material, adjacent atoms are sufficiently close together that some of the electron orbitals overlap and a strong interaction arises. This interaction (exchange coupling) means that rather than being directed in random, the magnetic moments of all the atoms in the lattice are aligned, giving rise to a strong magnetization. Exchange coupling can give rise also to a phenomenon called ferrimagnetism. Here, the crystal lattice contains two kinds of sites with cations in two types or different coordinates (Michael & Heller, 2003).

2.6.5 FERRIMAGNETISM

This is a form of magnetic ordering that occurs in ionic compounds such as oxides because of the crystal structure. Here the magnetic structure is composed of two magnetic sub-lattices (called A and B) separated by oxygens. The exchange interactions are mediated by the oxygen anions. When this happens, the interactions are said to be indirect or superexchange interactions. The strongest superexchange interactions result in an anti-parallel alignment of spins between the A and B sublattice (Fig. 2.6).

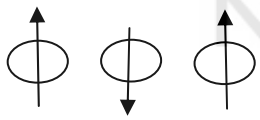

Unequal magnetic

Figure 2.6 Illustration of the alignment of an unequal magnetic moment in ferrimagnetism.

In ferrimagnets, the magnetic moments of the A and B sub-lattices are not equal as shown in the diagram above and result in a net magnetic moment. Ferrimagnetism is therefore similar to ferromagnetism with a famous example as **magnetite** (Fe_3O_4).

2.6.6 ANTIFERROMAGNETISM

This phenomenon occurs when the magnetic ordering in the sub-lattice structure A and B, is such that the sub-lattice moments are exactly equal but opposite, and therefore the moment is zero as shown in Fig. 2.7 below.

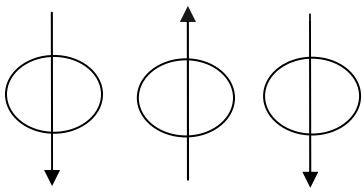

Equal but opposite magnetic moment

Figure 2.7 Illustration of the alignment of equal magnetic moment in antiferromagnetism.

Antiferromagnetic materials also have zero remanences, no hysteresis, but a small positive susceptibility that varies in a peculiar way with temperature.

Slight deviations from ideal antiferromagnetism can exist if the anti–parallelism is not exact. If neighboring spins are slightly tilted (< 1°) or canted, a very small net magnetization can be produced. Figure 2.8 below illustrates this phenomenon.

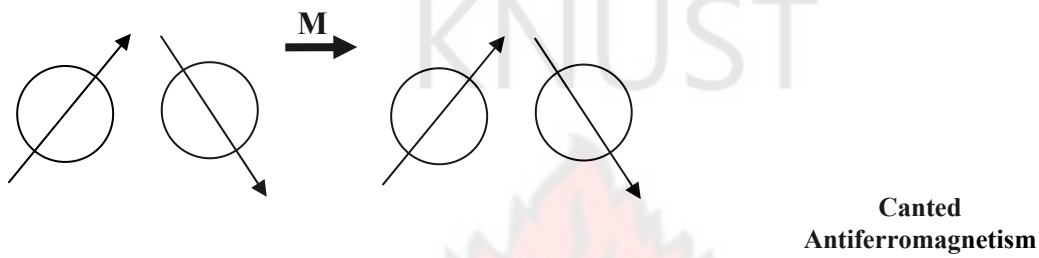

Figure 2.8 Illustration of the alignment of an equal but tilted magnetic moment in antiferromanetism.

This is called antiferromagnetism and **hematite** is a well known example. Canted antiferromagnets exhibit many of the typical magnetic characteristics of ferromagnets and ferrimagnets (e.g. hysteresis and remanences) (Moskowitz, 1991).

2.7 HYSTERESIS

A complete hysteresis loop is obtained by cycling the magnetic field from an extreme applied field in one direction to an extreme in the opposite direction and back.

The magnetic state of an iron bar will depend on two basic things;

That is
1. The magnetic field to which it was subjected to and
2. The history of the bar.

The field dependence of magnetization can be explained using the diagram below which plots magnetization on the vertical axis against magnetic field on the horizontal axis. Starting with an unmagnetized piece of iron, it is realized that its magnetization increases

slowly as a small field is applied and that if this field is removed, the magnetizations return to zero. When a strong field, beyond a certain critical field is applied, it is found that an important change (magnetic behavior takes place). Changes in magnetization associated with the removal of the field is different in that magnetization here is now no longer reversible in the straight forward way like the low field; instead, on removal of the field, a phenomenon referred to as hysteresis develops. This change is such that the magnetization lags behind the field as shown in Fig. 2.9 below.

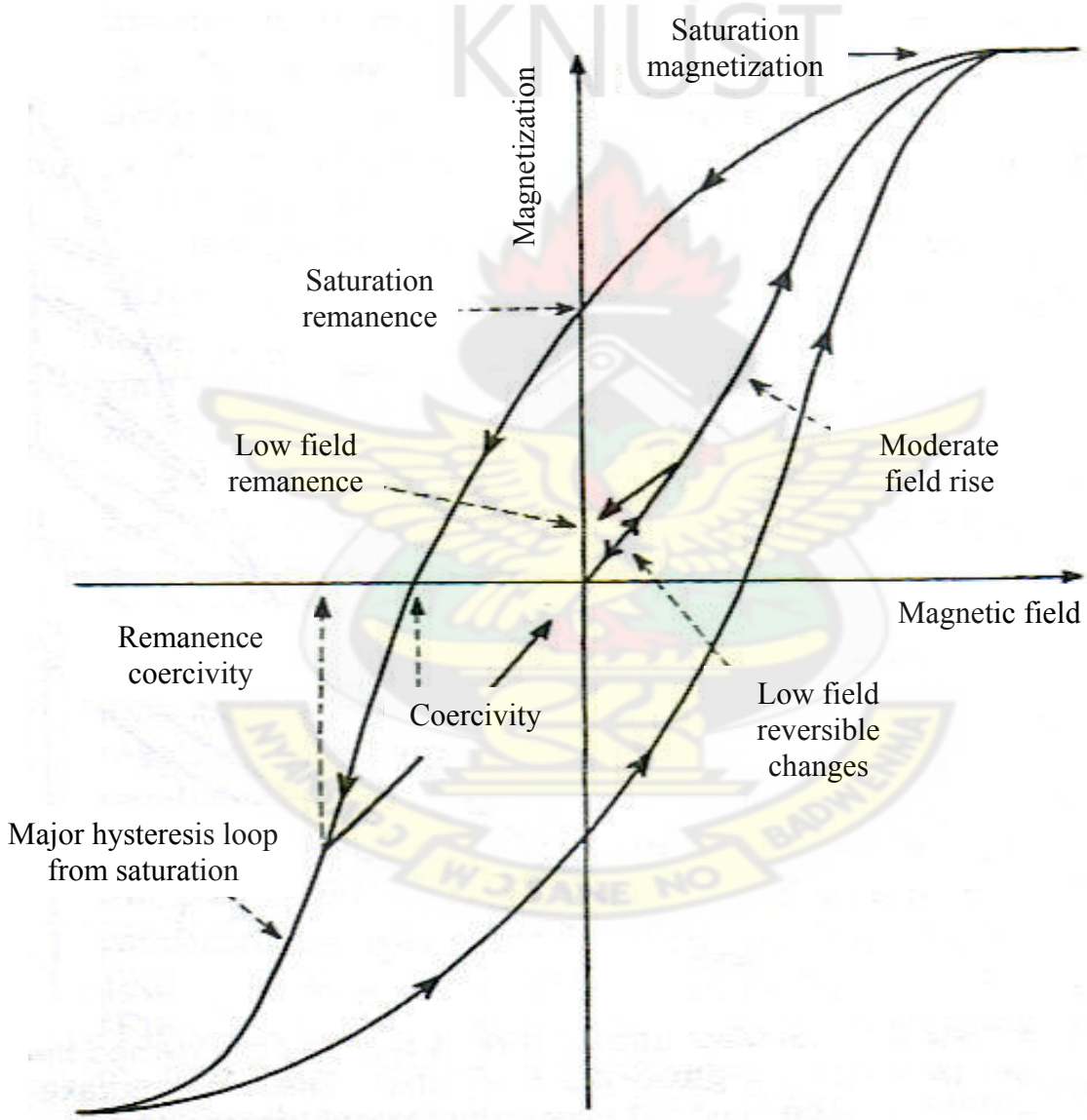

Figure 2.9 Magnetic hysteresis loop and initial magnetization curve showing saturation magnetization, saturation remanences, coercivity, remanences coercivity and low field magnetization changes.

Furthermore, it was noticed that on removal of the field (i.e. zero field), the iron no longer remains unmagnetized but has remanent magnetization (Fuller, 1987). It was realized also that magnetization rises sharply at low fields with an increasing field attaining saturation at still higher fields causing the curve to be flattened.

2.7.1 DEFINITION OF SOME HYSTERETIC PARAMETERS

Saturation magnetization, M_s: It is the magnetization induced in the presence of a large (> 1 T) magnetic field. This magnetization does not decrease completely to zero upon removal of the field. The remaining magnetization is called **saturation remanent magnetization, M_{rs}**.

By the application of a field in the opposite direction, to the first field used, the induced magnetization can be reduced to zero. This reverse field is called the **saturation coercivity, H_c**. The reverse field needed to leave no remanent magnetization after its subsequent withdrawal is called the **coercivity of remanences, H_r**. The **initial susceptibility (χ_o) is** given by the gradient of the magnetization curve at the origin (Thompson & Oldfield, 1986).

Hysteretic magnetization determination has been employed in many studies, an example being in the determination of the magnetic composition of pozzolana cements (The IRM Quarterly, Fall 2003). The hysteresis measurement showed a saturation magnetization around 0.6 to 0.7 Am^2kg^{-1}, equivalent to a magnetite/maghemite content of near 1 % by mass. There is also an indication of the dominance of pseudo-single domain state by the saturation remanence magnetization to saturation magnetization ratio of about 0.3 (The IRM Quarterly, Fall 2003).

2.7.2 MAGNETIC SUSCEPTIBILITY

Susceptibility is the measure of the ease with which a material can be magnetized. Initial susceptibility is measured using low AC or DC fields (< ~1 mT) and is defined as the ratio of magnetization to the applied magnetic field, M/H (Collinson, 1983). This is due to reversible displacements of mobile domain walls in MD particles or moment rotation in SD particles. In the latter, low fields are not very effective in rotating SD moments and therefore, susceptibilities of SD and PSD particles or grains are usually lower than that in MD grains.

Suppose a suitable material is placed in a uniform magnetic field (H) and thereby acquires a magnetization per unit volume of M. It's magnetic susceptibility *(k)* is defined as the ratio of magnetization acquired per unit field to the applied field,

$$\kappa = M/H \text{ -----} (2.1)$$

This is dimensionless. To obtain the mass susceptibility, the volume susceptibility is divided with the density (ρ),

$$\chi = \kappa/\rho \text{ -----} (2.2)$$

Because κ is dimensionless, the χ has a units of reciprocal density, m^3kg^{-1} (Michael, & Heller, 2003).

However, what is usually measured in the laboratories are the apparent susceptibility, Π_o, and not the intrinsic susceptibility, Π_i. This difference is due to the effects of self–demagnetization.

i.e. if the magnitude of the demagnetizing field is NM,

then,

$H_i = H - NM$,

$M = \Pi_i H_i$, where H is the applied field.

The observed susceptibility is the ratio of M to the applied field

$\Pi_o = M/H = \Pi_i/[1+N\Pi_i]$

For strongly magnetic minerals, like magnetite,

$N\Pi_i > 1$ and

$\Pi_o \approx 1/N$ (Moskowitz, 1991).

2.8 EFFECTS OF CRYSTAL SIZE, SHAPE AND STRUCTURE ON THE MAGNETIC PROPERTIES

2.8.1 MAGNETIC ANISOTROPY

Anisotropy of magnetic susceptibility in materials, i.e. dependence of susceptibility on the direction along which it is measured in a sample, arises from either fundamental anisotropy in the crystal structure (which is a property of all the common magnetic minerals), or from non-sphericity of shape of mineral particles (Collinson, 1983).

Magnetic properties of crystals are therefore modified and controlled by anisotropy but generally, any specimen will be magnetically anisotropic, that is to say, will have varying magnetic properties with direction (Thompson & Oldfield, 1986).

2.8.2 FORMS OF MAGNETIC ANISOTROPY

There are three forms of anisotropy (Thompson & Oldfield, 1986);

1. The one arising from the internal geometry of crystals (i.e. lattice property) and is referred to as ***magnetocrystalline*** anisotropy and defined as the energy necessary to deflect the magnetic moment in a single crystal from the easy to the hard direction. The easy and hard directions arise from the interaction of the spin magnetic moment with the crystal lattice (spin–orbit coupling) (Moskowitz, 1991). This is so because the various axes of the crystals have different magnetic properties. This property is considerably very important with minerals like

goethite and haematite (the imperfect antiferromagnets with their low spontaneous magnetizations) in that it leads to very high coercive forces. It also leads to characteristic low temperature magnetic behavior because of extreme sensitivity to temperature.

This is unique because magnetocrystalline anisotropy, along with spontaneous magnetization and Curie temperature, is an important intrinsic magnetic property depending only on crystal structure and composition.

2. The second form of anisotropy is linked with shape of the bodies. Example being the fact that a magnetic compass needle is invariably magnetized parallel with its long axis serving as the easy direction of magnetization (Moskowitz, 1991; Thompson & Oldfield, 1986). An example is ferrite and magnetite in natural minerals in which shape anisotropy is of great importance.

3. The third form of magnetic anisotropy is referred to as strain-anisotropy; an effect related to spin–orbit coupling, which may be induced by mechanical stress through the phenomenon of ***magnetostriction***. This phenomenon results from the attraction of the size of magnetic specimen when it is subjected to a magnetic field (Thompson & Oldfield, 1986).

2.9 MAGNETIC DOMAINS AND DOMAIN WALLS

The properties mentioned under hysteresis, of ferromagnets are largely related to the arrangements of magnetic domains. Consequently, the magnetic domains play an important role along with anisotropy, in controlling the magnetic properties of natural magnetic materials (Dunlop, 1981). However, the reason why magnetic domains form is that they produce a state of lower total energy, a stage that is achieved by the establishment of a balance between various competing energies of which the most advantageous balance is reached by domains of size about one micrometer. The thickness

of this domain walls establishes however as a compromise between the opposing influences (Thompson & Oldfield, 1986).

Supposing a grain is uniformly magnetized, and hence a single domain. Surface charges will form on the ends due to the magnetization and are themselves a second source of a magnetic field (the demagnetizing field). The energy associated with the surface charge distribution is called the magnetostatic energy, e_m (Banerjee, 1989), which is the volume integral of the field over all space. This magnetostatic energy is the energy required to maintain the distribution of the magnetic dipoles on a material in the absence of an external field (Piper, 1987). Figure 2.10 below show types of magnetic mineral domain.

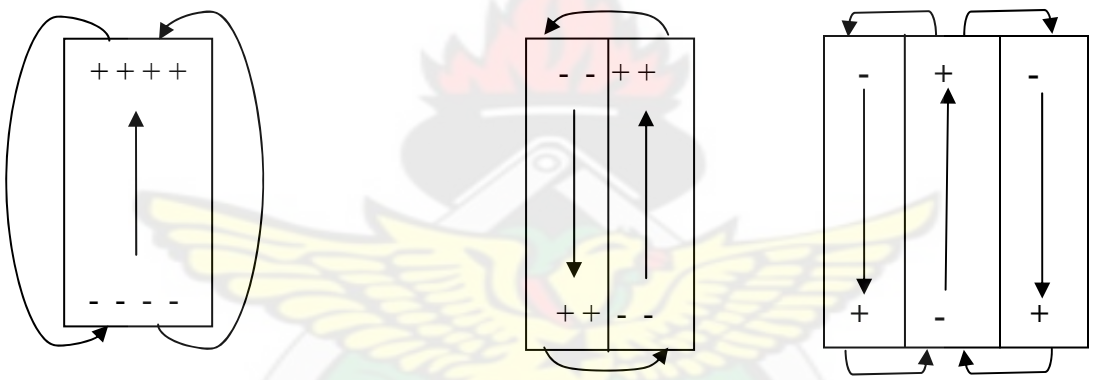

Single Domain **Multi-Domain**

Figure 2.10 Diagram showing basic types of magnetic domain (Moskowitz, 1991)

The magnetostatic energy of the grain can be halved when the magnetization splits into two equal domains magnetized in opposite directions. This brings (+) and (-) charges closer together, thus decreasing the spatial extent of the demagnetizing field.

The subdivision into more and more domains however can not continue indefinitely since the transition zones referred to as domain walls (which are interfaces between regions in which magnetization has different directions) needs energy (wall energy) to form (Moskowitz, 1991). Based on the magnetic behavior of minerals, magnetic mineral grain

sizes can be subdivided into: Superparamagnetic (SPM), Single Domain (SD), Pseudo – single Domain (PSD) and Multi –Domain (MD) grain sizes.

2.9.1 SUPERPARAMGNETIC (SPM) GRAINS

When ferromagnetic or ferrimagnetic grains are extremely small, about 0.001 – 0.01μm in diameter, have thermal vibrations at room temperature which have energies of the same order of magnitude as the magnetic energies. i.e., the grain size decreases in the single domain range until a critical size (the threshold) where both the remanence and the coercivity go to zero (Moskowitz, 1991).

As a result of this equivalence of energies, these ultrafine–grained magnetic materials do not have a stable remanent magnetization and therefore do not exhibit hysteresis as their magnetization is continually undergoing thermal reorientation. In the presence of applied field, they do have however, an overall magnetic alignment (i.e. an apparent magnetization), which is as a result of an SD particle containing 10^5 atoms and not that from a single atom (Thompson & Oldfield, 1986).

This behavior exhibited by these ultrafine grains is termed superparamagnetic (Néel 1955, Creer 1959, Vlasov et al. 1967). This is similar to but much stronger than paramagnetic behavior and strongly depends on temperature, in that for superparamagnetic particles, the net magnetic moment in a zero field and at $T > 0$ K, will average to zero.

2.9.2 SINGLE DOMAIN (SD) GRAINS

With decreasing grain size, the number of magnetic domains in the particle decreases. As the grain size decreases, a critical size is reached when it no longer accommodate a wall. Below this critical size, the grain is said to contain a single domain (SD) (Banerjee, 1989).

The magnetic properties of single domain grains are quite different from multi-domain grains since motion of domain walls does not play any role in their magnetization and therefore they uniformly magnetizes to their saturation magnetization. Their magnetic remanences are therefore much higher and more stable than that of the multi-domain grain assemblages and there are also clear differences in their hysteresis properties.

The absence of domain walls leads to a characteristic, single-domain hysteresis loops with shapes depending on the orientation of the grain with respect to the applied field. The only way to change the magnetization of an SD grain is to rotate the magnetization, which is energetically a difficult process. SD grains are therefore said to be magnetically hard with high coercivity and remanences values (Thompson & Oldfield, 1986).

2.9.3 PSEUDO – SINGLE DOMAIN (PSD) GRAINS

The distinction between SD and MD is straightforward. However, small MD grains exhibit a mixture of SD – like (high remanences) and a MD – like (low coercivity) behavior. For magnetite, this behavior occurs in the size range between 0.1 – 20:m. The importance of PSD behavior in magnetite is that the grain size range for PSD behavior covers that range in sizes that most commonly occur in natural samples.

They can also exhibit significant coercivity and time stability of remanent magnetism. Grain-size distributions of many igneous and sedimentary rocks peak within the magnetite PSD field but have only a small percentage of particles within the true SD field (Banerjee, 1989).

2.9.4 MULTI - DOMAIN (MD) GRAINS

To change the magnetization of a multi-domain (MD) grain, needs the change of the domain wall, which is an energetically easy process which can be accomplished in relatively a low field. Thus, MD grains are magnetically soft with low values of coercivities and remanences (Moskowitz, 1991).

2.10 MAGNETIZATION TECHNIQUES

The purpose of demagnetization is to remove the components of magnetization with short relaxation times, which may contribute to secondary magnetizations that obscure the primary signal. It is also useful for characterizing the coercivity of distribution. There are two main methods:

2.10.1 ALTERNATING FIELD (AF) DEMAGNETIZATION

The fundamental AF demagnetization procedure is to expose a specimen to an alternating magnetic field. The waveform of the alternating magnetic field is a sinusoid with a linear decrease in magnitude with time. The frequency of the sinusoidal waveform is commonly 400 Hz, and the time for the decay of the field from maximum value to zero is ~ 1 minute (Butler, 1992). A sample is subjected to alternating field that is smoothly reduced to zero from some peak value. The AF demagnetization curve is measured by exposing the sample to a series of increasing AF peak values (5, 10…100 mT).

The remaining remanence is then measured after each step. Remanence in grains with low coercivities is eased first (Fig. 2.11). Remanence carried by grains with higher coercivities remains unaltered.

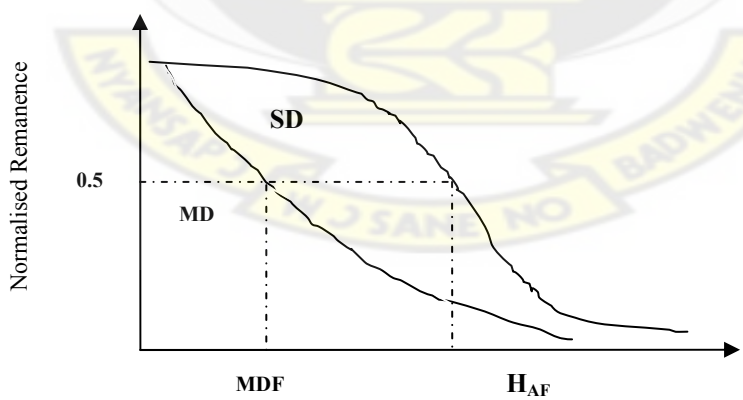

Figure 2.11 Illustration of the easiness with which domain particles give off their remanence on demagnetizing (MDF = mean destructive field and H_{AF} = alternating demagnetizing field) (Moskowitz, 1991).

The AF value needed to reduce the initial remanence by one-half is called the **median destructive field** (**MDF**) (Moskowitz, 1991).

2.11 GRAIN SIZE

Grain size is studied for a variety of reasons. First, it is a fundamental descriptive measure of sedimentary rock. It is also important in understanding the mechanisms operating during transportation and deposition, as well as the distance of sediment transport. Grain size is commonly related to other properties (e.g. permeability) which have major economic implications.

These reasons have made and continue to make size analysis an important aspect of sedimentologic research.

2.11.1 CLASSIFICATION OF GRAIN SIZE

There are two main classification types, which are;

1) **Size grades**: - this is defined as the sizes intermediate between two defined points on a scale. It is based on a geometric scale in which class limits increase from the base of 1 mm by a factor of 2 or decrease by a factor of 0.5.
2) **Phi (ϕ) notation: -** this is a negative logarithm to the base 2 of a particle diameter in millimeters.

i.e. $\phi = -\log_2 X$, where X is the particle diameter.

This notation simplifies calculations used to derive grain – size parameters (e.g. mean size and standard deviation).

2.11.2 TREATMENT OF GRAIN – SIZE DATA

The statistical measures of size distributions used by sedimentologists are most commonly based on quartile measures (Trask, 1932), phi notation (Inman, 1952; Folk &

Ward, 1957), or the methods of moments (Kane & Hubert, 1962; Folk, 1974; Sawyer, 1977).

Three mathematical measures of average grain size are therefore in common use;
The **mode,** which is the most frequently occurring particle size in a population of grains.
The **median**, which is the midpoint of the grain size distribution and
The **mean** size, which is the arithmetic average of the entire particle, sizes in a sample.

The sorting is mathematically given as the **standard deviation**, which is the measure of the range of grain sizes present and the magnitude of the spread or scatter, of these sizes around the mean size.

However, grain- size statistical parameters can be calculated directly without reference to graphical plots, by use of the mathematical **method of moments.** The formulae for computing the various parameters are as shown below.

Mean, $x_\phi = \sum \frac{fm}{n}$ ---------- ***(2.3)***

Standard Deviation, $\sigma_\phi = \sqrt{\frac{\Sigma f (m - x_\phi)^2}{100}}$ ---------- ***(2.4)***

Skewness, $Sk_\phi = \frac{\Sigma f (m - x_\phi)^3}{100 \sigma_\phi^3}$ ---------- ***(2.5)***

Kurtosis, $k_\phi = \frac{\Sigma f (m - x_\phi)^4}{100 \sigma_\phi^4}$ ---------- ***(2.6)***

where,
f = weight percent (frequency) in each grain size grade present.
m = midpoint of each grain – size grade in phi value.
n = total number in sample; 100, when f is in percent

(Boggs, 1987).

2.11.3 USE AND INTERPRETATION OF GRAIN – SIZE DATA

Because grain – size is a fundamental physical property of sedimentary rocks and for that matter a useful descriptive property, study of grain – size data has commonly been assumed to be a useful tool for interpreting the depositional environments of ancient sedimentary rocks because the size and sorting of sediment grains may reflect sedimentation mechanism and depositional conditions.

2.11.4 BASIS FOR ENVIRONMENTAL INTERPRETATION

It is this assumption that grain – size characteristics reflect conditions of the depositional environment that has sparked most of the interest in grain size analyses.

Studies also have shown that fluvial sediments have generally coarser grains than sediments deposited in beach or dune environments. In addition, fluvial sediments appear to be more poorly sorted than the latter two. Unlike grain – size, sorting tends to reflect the persistence of the depositional process to a greater degree than it reflects the actual energy of the environment. Fluvial sediments may be positively skewed owing to the large amount of clay and silt commonly carried by rivers causing excess fine sediment to be trapped among coarser particles during deposition (Boggs, 1987).

CHAPTER THREE

EXPERIMENTAL METHODS

3.1 FIELD PROCEDURE AND DATA COLLECTION

3.1.1 STUDY SITE

Lake Bosumtwi is located 35 km southeast of Kumasi, the capital city of the Ashanti region in central Ghana. Kumasi is at about 6.5° N, 150 km from the Coast, and has an elevation of 310 m. Other nearby towns include Konongo (elevation 233 m), 30 km to the northeast of the lake, and Bekwai (elevation 230 m), 20 km to the southwest (Turner et al., 1995). Lake Bosumtwi, located along 6° 30' N and 1° 25' W (Fig. 3.1 a), occupies a 1.07 ± 0.05 million years old meteorite impact crater (Koeberl et al., 1997) in the tropical forest zone of southern Ghana. The crater has a diameter of 11 km, and the circular lake, which currently has no surface outlet, is 8 km across. Maximum depth is 75 m.

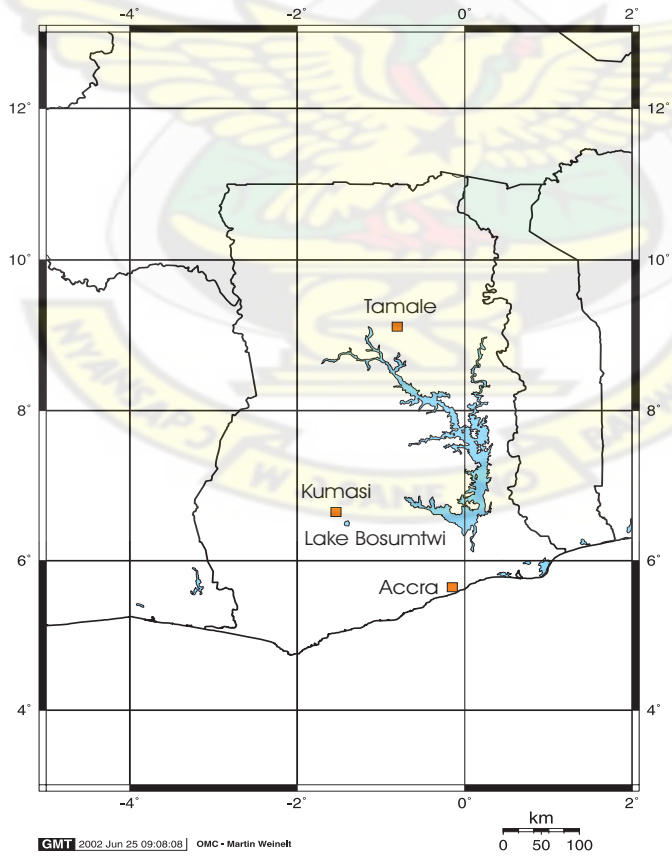

Figure 3.1a The location of the lake Bosumtwi on the map of Ghana.

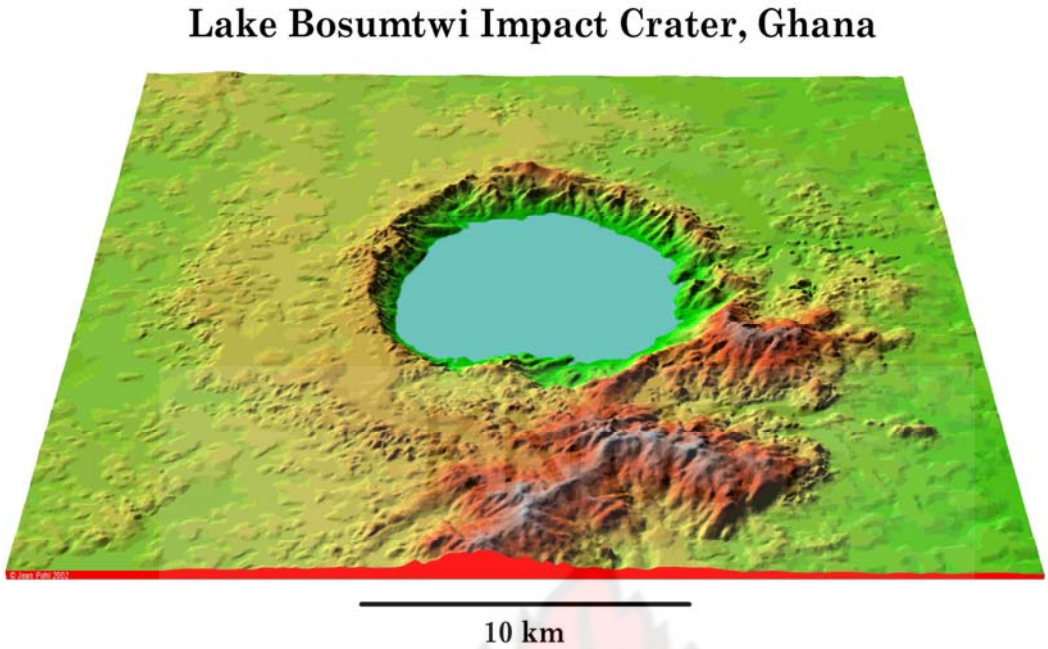

Figure 3.1b The morphology of Lake Bosumtwi (Danuor, 2004).

Surface waters are of pH 9.1 – 9.6, and vary seasonally in temperature between about 27.5 and 32.5 °C (Junner, 1937).

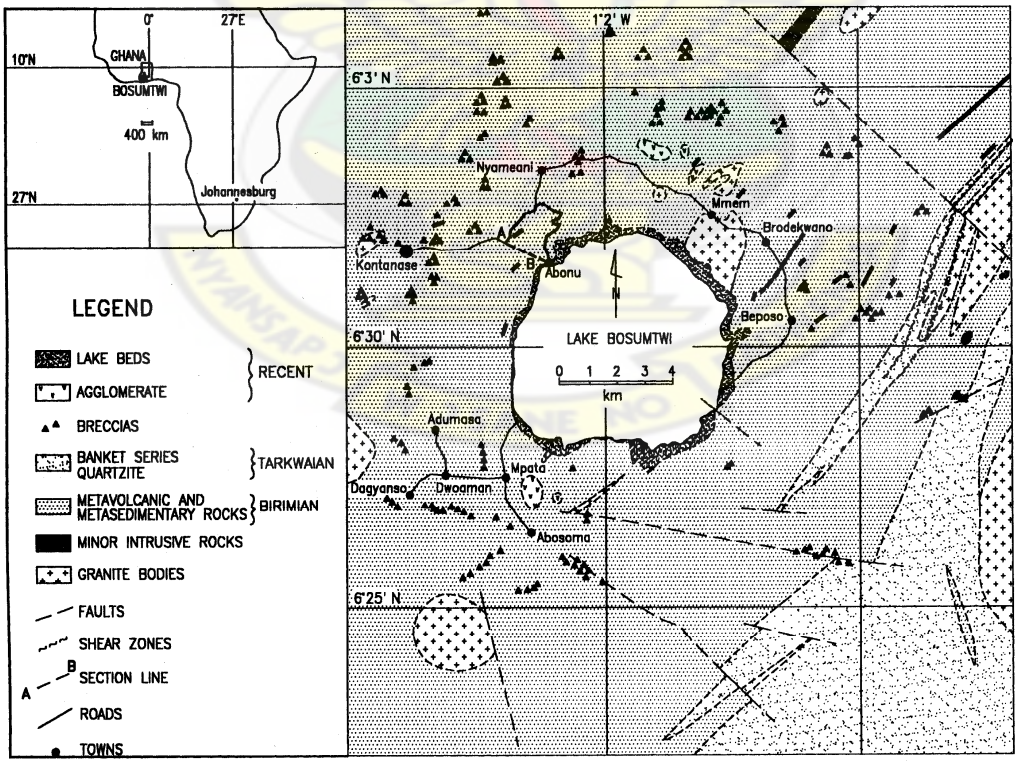

Figure 3.2 Geological map of Lake Bosumtwi area (after Jones et. al. 1981).

The modern lake has a surface area of about 50 km^2 with the maximum depth near the center of the basin (shown in Fig. 3.2). Lake Bosumtwi is hydrologically closed, and is maintained by direct precipitation, groundwater, and numerous small streams. Lake Bosumtwi is also affected by two major air masses: the West African monsoon off the Atlantic Ocean, which brings precipitation to the region during much of the year, and dry, northeasterly flow (harmattan winds) that penetrates into West Africa. Annual rainfall in the region averages 1380 m, with a monthly maximum in June and a secondary peak in October. Both rainfall and lake levels are variable from year to year, and appear highly correlated to regional rainfall (Talbot et al., 1984; Nicholson, 1986). Together, these facts have made Lake Bosumtwi the premier study site for monitoring past changes in the African monsoon. Figure 3.3, shows a shot of the sample site (lake Bosumtwi) as viewed from the northwest.

Figure 3.3 Photo showing Lake Bosumtwi.

3.1.2 DATA COLLECTION

3.1.2.1 INTRODUCTION

Samples were collected from the entire lake surface between July 15, 2004 and August 28, 2004. During these periods, the weather was sunny with a lot of wind. This induced strong wind coupled with heavy and stormy rains. Positioning the speedboat was a bit of a problem because of the roughness of the weather.

3.1.2.2 EQUIPMENT USED

1. The Global Position System (GPS)
2. The Speed Boat
3. The Ekman Dredge.

3.1.2.3 The Ekman Dredge

The Ekman dredge is designed for sampling in soft, finely divided bottoms that are free from vegetation and other coarse debris. Each sampler features machined jaws and hinged overlapping lids that open easily during descent to let water pass through and close during retrieval to reduce sample washout.

The patented Two-Pin release mechanism has few moving parts and is very reliable. Each sampler is constructed of 316 stainless steel, including the springs, cables and fasteners. The sampler measures 150 mm x 150 mm x 150 mm. All parts are made of heavy-gauge, stainless steel, sheet metal, carefully fitted to ensure uninterrupted operations even under adverse field conditions. The hinged, extra-strong, closure jaws are machined and fitted so that they close completely to prevent leakage of sediment; they cannot readily be dented or bent, should they strike hard objects or rocks on the bottom.

The finger-lifts, formed from the jaws themselves, facilitate easy opening and avoid possible hand injury should the jaws accidentally be released while the device is being

cocked. The jaws are held open by flexible stranded wires, which fasten to the release holding pins at the top of the framework as shown in the labeled Fig. 3.4 below. These are freed when a messenger, dropped down the line, strikes the release bar; external coil springs snap the jaws shut, trapping the sediment within. There are no spring-lever cocking devices to malfunction after a short time period or flimsy brass sheet to easily deform in use.

Overlapping cover plates, loosely hinged at the top of the box, permit outflow of water during descent and close snugly on the upward haul to prevent wash-out of collected material. This is the most practical and reliable device of its type and it is unconditionally guaranteed for workmanship and quality of materials. A reliable, detachable messenger is supplied with each dredge. Figure 3.4 shows a labeled Ekman dredge.

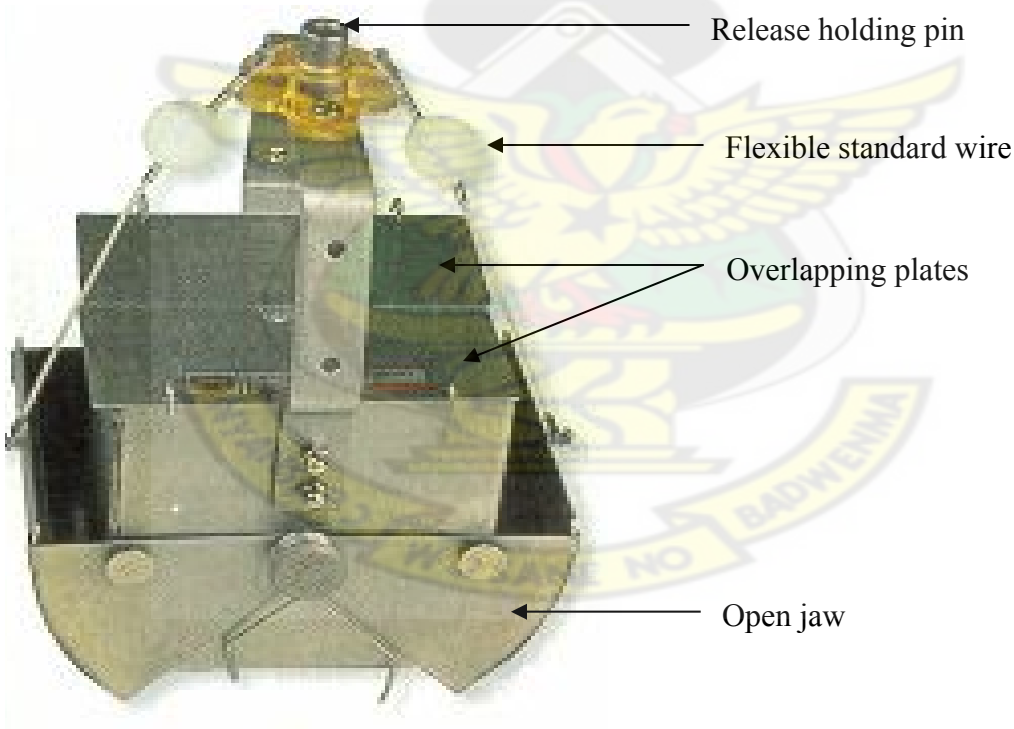

Figure 3.4 Picture of the Ekman Dredge. The equipment show jaws open and ready for sampling.

3.1.2.4 SAMPLING METHOD USED

The speedboat was positioned at a specific location which is to be sampled on the lake. This position is noted by taking its longitude and latitude readings from the global position system (GPS).

The Ekman dredge was lowered then to the bottom of the lake. Efforts were made to keep the boat as stable as possible, as it does not work well if the rope is not vertical. The messenger was held in the left hand (over the side of the boat) and the rope was let out with the right hand. When the dredge reaches the bottom, it was lifted slightly to get the rope vertical. The messenger was then released. The corer was lifted to the surface and allowed the water content to drain slowly. The sediment was not disturbed. The uppermost sediment (i.e. 2 cm – 8 cm), was scooped into a plastic bag and then labeled with the site number and name of the location that was sampled (say GR – 1A), which shows the first sampled position on the GR transect.

This procedure was repeated for all the 134 samples collected.

Table 3.1 in (Appendix F) shows the tabulated field data. Figure 3.5 below shows the corresponding spatial plot on the field data.

Figure 3.5 A spatial map of the sample sites, bathymetry, rivers and villages surrounding the lake.

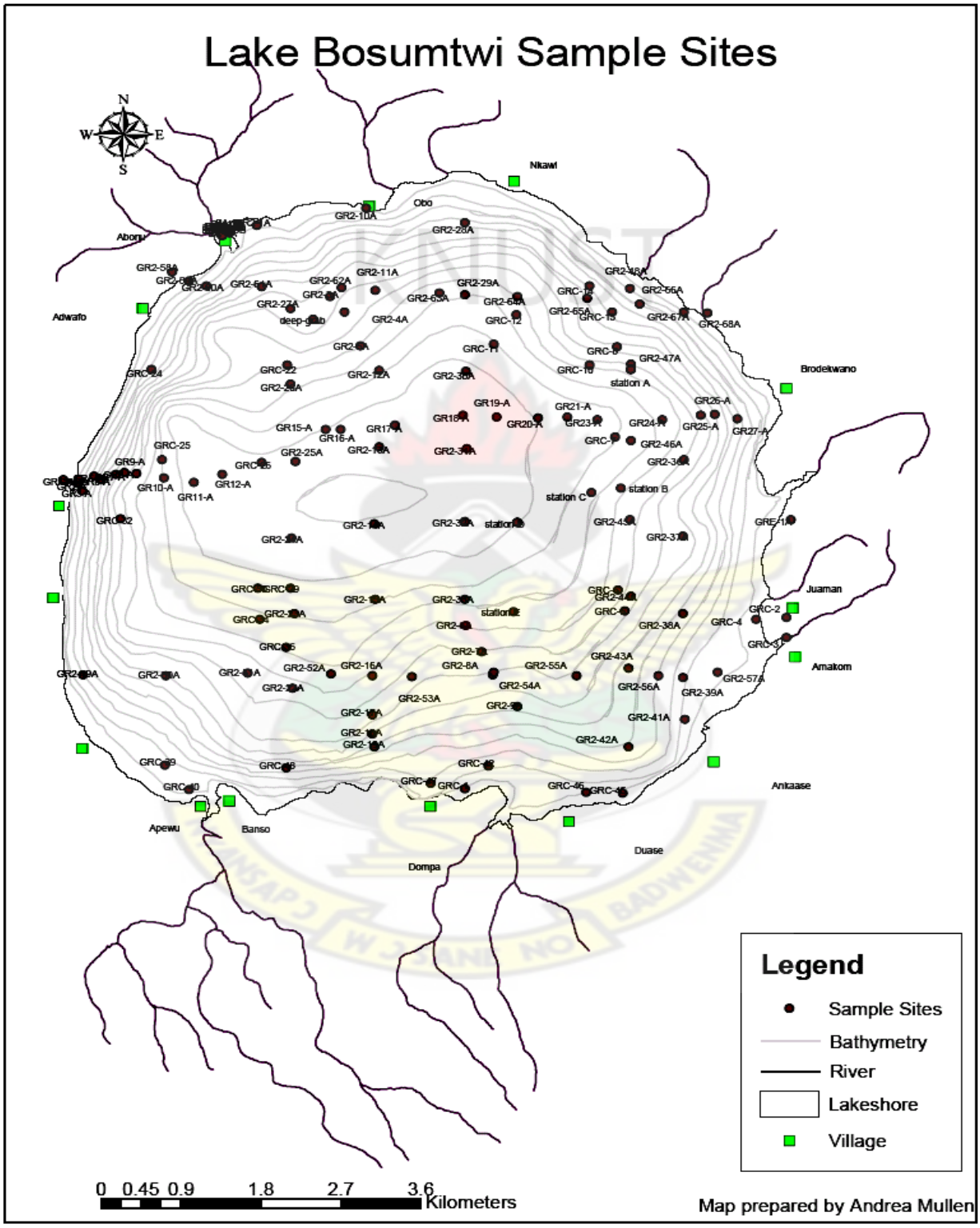

3.2 LOSS-ON-IGNITION METHOD

3.2.1 INTRODUCTION

Determination of organic content in geologic material by using the loss-on-ignition method is not a new technique. It has appeared in most standard texts on quantitative inorganic analysis (e.g., Kolthoff & Sandell, 1946), and has been used to determine the amount of carbon dioxide (CO_2) in the carbonate rocks (e.g., Galle & Runnels, 1960; Waugh & Hill, 1960) and in recent sediments (e.g., Konrad, Chesters, & Keeney, 1970). The method employed here is a modification of the old one, which is fast and requires basic equipment found in most laboratories (Dean, 1974).

3.2.2 THEORY

Differential thermal analysis (DTA) thermograms show that when a dried sample containing organic material and calcium carbonate is heated in a muffle furnace, the organic material begins to ignite at about 200° C and is, completely ignited by the time the furnace temperature has reached approximately 550° C (Dean, 1974).

Evolution of CO_2 from the calcium carbonate will begin at about 800° C and proceed rapidly so that most of the CO_2 present has been evolved by the time the furnace temperature reaches 850° C. If any dolomite exists in the sample, it will evolve CO_2 at a lower temperature than calcite (700 - 750° C). Based on this theory, several different techniques have been used to measure organic and carbonate carbon evolved on ignition. The weight loss of the sample can be determined by weighing the sample before and after ignition and determining the weight percent loss by difference.

3.2.3 METHODOLOGY

(a) The weight of a wet sample of known volume is determined by weighing the sample in a crucible with a known weight and the weight difference calculated.

Figure 3.6 Picture showing bagged and labeled samples from the field.

(b) The sample contained in the crucible, was then dried in an oven at a temperature of 60° C for 24 hours. After cooling to room temperature in a desiccator, the sample and the crucible were weighed. This gives the dry weight of the sample, which is the basis for all weight loss calculation.

(c) The sample and crucible are then placed in a muffle furnace and heated to 550° C for two and half hours. The crucibles and their contents were then removed and allowed to cool. After cooling to room temperature, the sample is again weighed. The difference between this weight and the dry weight is the amount of organic carbon ignited (Dean, 1974).

Figure 3.7 Picture showing samples in crucibles after heating at 550 º C.

The measured and computered results of water depth, wet sample weight, percentage water content of sample, dry bulk density and percentage organic matter content of samples are tabulated in Table 3.2 (Appendix G). Figure 3.8 shows plot of the determined loss on ignition parameters on a spatial map.

3.2.4 SPATIAL PLOTS OF 'LOSS ON IGNITION' PARAMETERS DETERMINED.

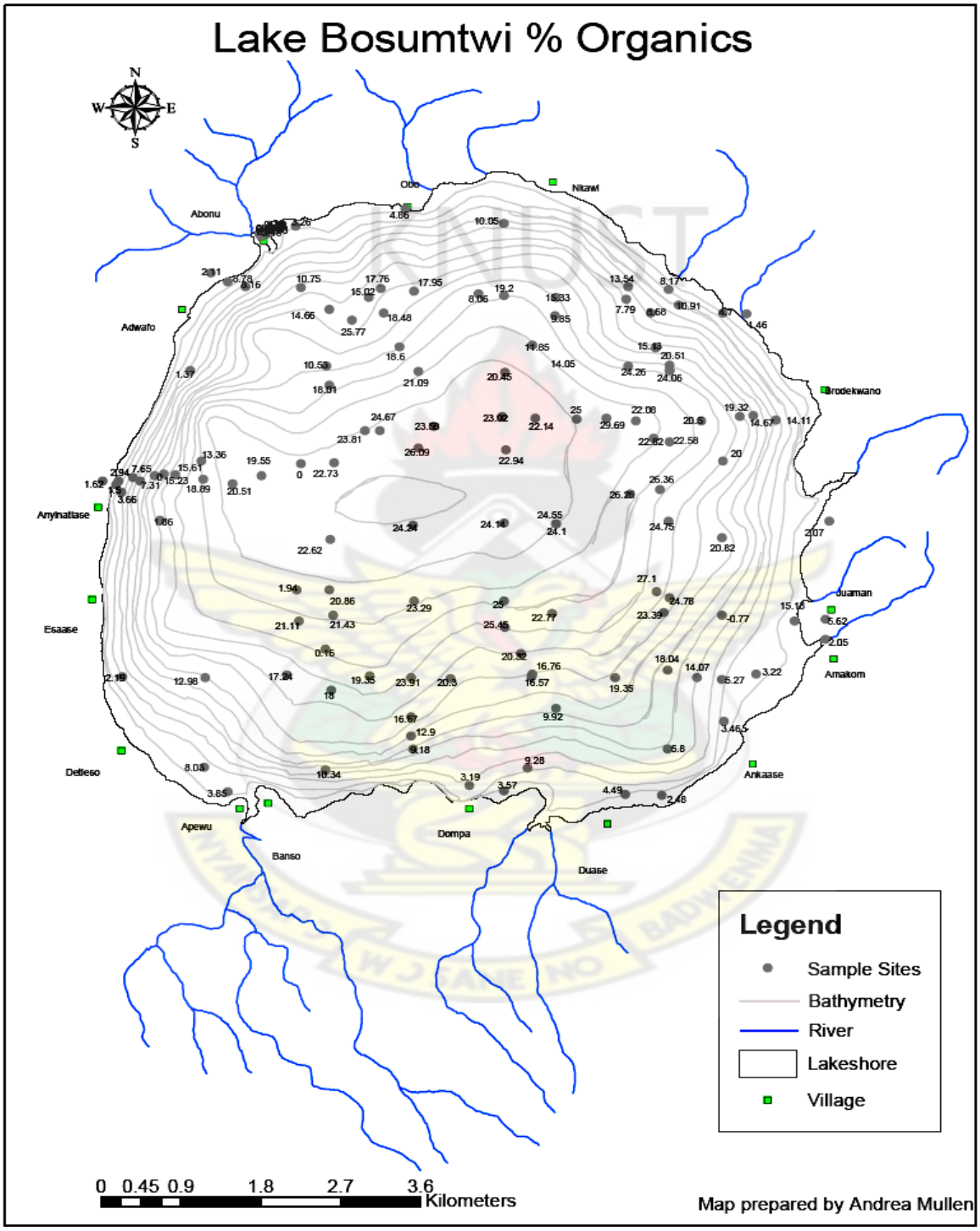

Figure 3.8 (a) Map showing the distribution of percentage organic content of samples.

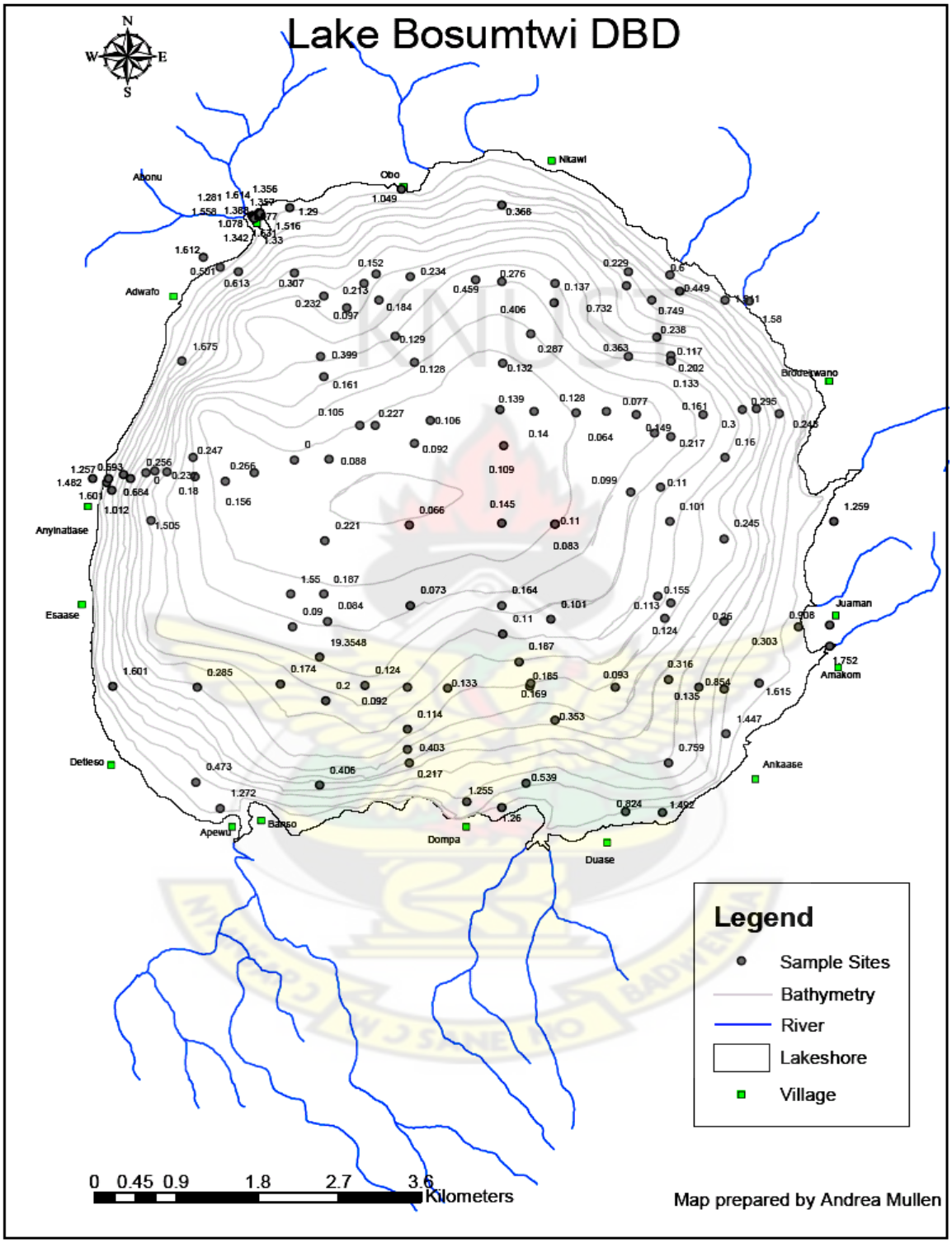

Figure 3.8 (b) Map showing the distribution of dry bulk density content of samples.

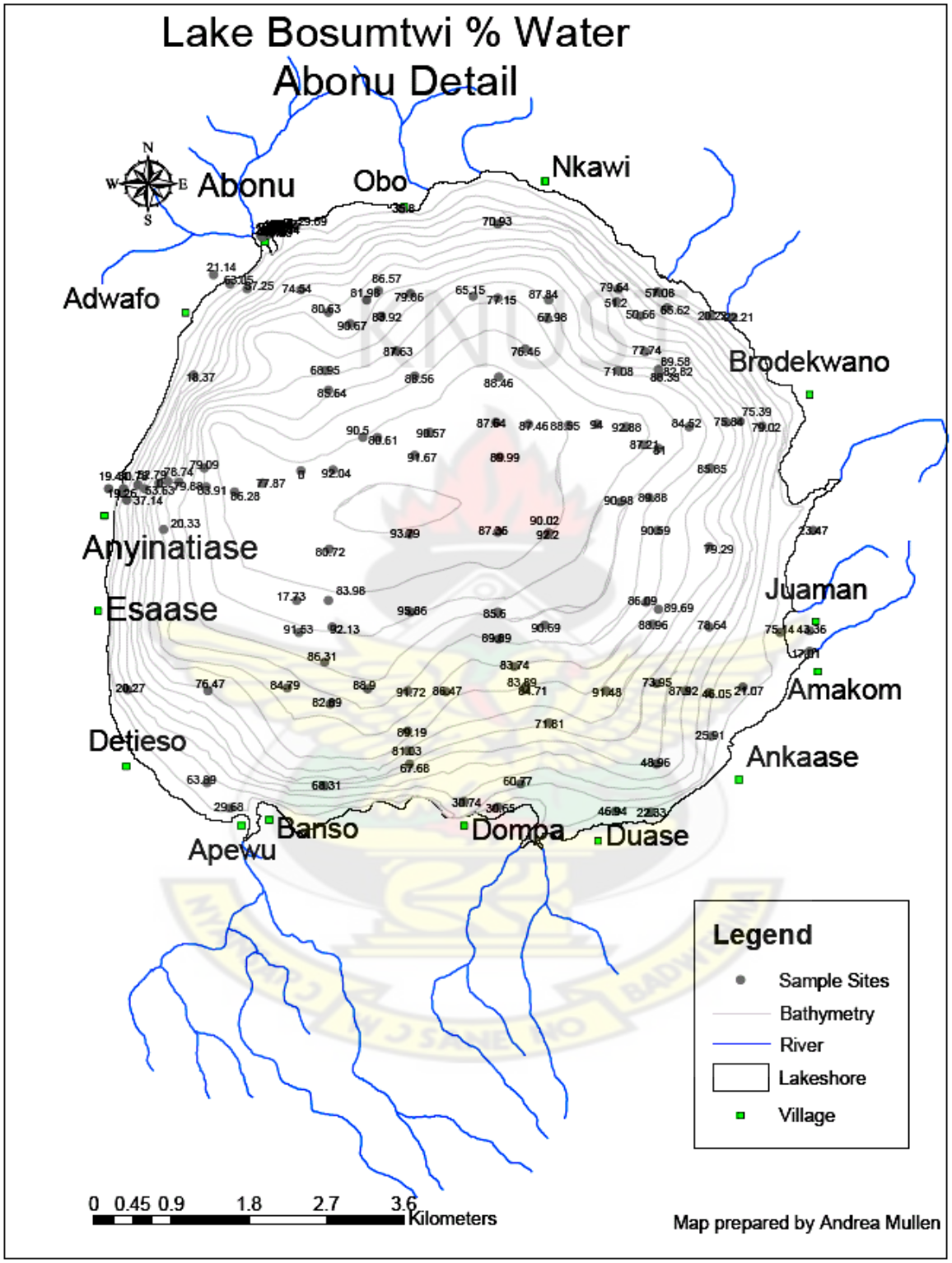

Figure 3.8 (c) Map showing the distribution of percentage water content of samples.

3.3 MEASUREMENT OF MAGNETIC PARAMETERS ON SAMPLES

3.3.1 SUSCEPTIBILITY MEASUREMENT

3.3.1.1 INTRODUCTION

A magnetic field is caused by the movement of electric charges. At an atomic level, it can result both from the spin of the electrons about their axes, (this produces a spin dipole moment) and by motion of the electrons in their orbits about the atomic nuclei, (this produces orbital dipole moment). In the absence of an external influence, these magnets would normally be randomly oriented. However, they respond to an external field in a way that depends on the configuration and the atomic structure of the substance. All materials acquire a magnetic moment when placed in a magnetic field, and this is their *magnetic susceptibility*. Magnetic susceptibility therefore measures how magnetic an object becomes under the influence of a magnetic field (Maher & Thompson, 1999).

3.3.1.2 SAMPLE PREPARATION

Sizeable volumes of the samples taken from the field were poured into clean-labeled cup with the sample names and then air dried in a fine hood. The sample after air-dried, was packed into a square plastic box and sealed after it has been crushed softly in a crucible so that the grains are released. The boxes were then labeled and arranged, allowing to attain room temperature as shown below (Fig. 3.9), ready for measurement. The packing was made full to avoid physical movement of grains.

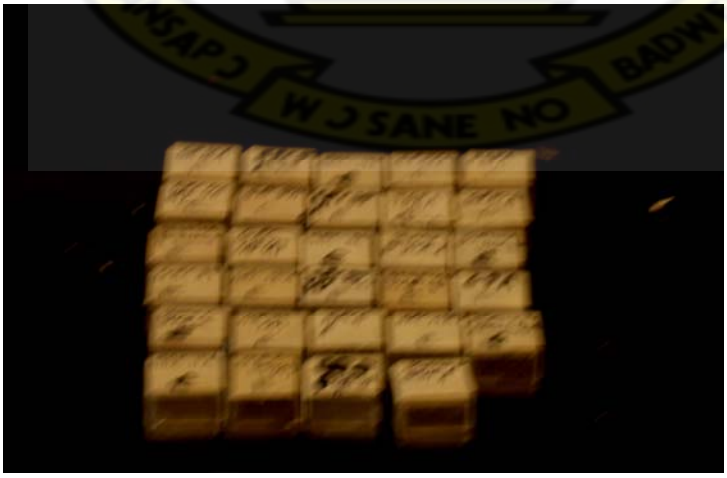

Figure 3.9 Picture of samples prepared for susceptibility measurement.

3.3.1.3 INSTRUMENT USED

The **Bartington *MS2B* sensor** was used to measure the susceptibility. It contains a single simple dual frequency sensor, which accepts 10 cm^3 sample in plastic pots supplied by Bartington Instruments. It has the facility of making measurements at two different frequencies. This dual frequency facility allows the detection of an important category of very fine ferrimagnetic minerals, described as superparamagnetic, found commonly in soils and in some rocks (Dearing, 1999). The Multisus Software, which the instrument contains, is a purpose-designed software for interfacing the *MS2* susceptibility system with a personal computer running Windows. Figure 3.10 below shows a shot of the Bartington *MS2B* sensor. It allows measurements on single samples and whole cores to be recorded and stored on file. The software is able to compensate for:

- Equipment drift
- Container susceptibility
- Core diameter

The software can also calculate:

- Volume and mass specific susceptibility
- Frequency dependent susceptibility
- Average value and standard deviation for a single sample (Bartington Instruments). **[www.bartington.com/multisus.htm]**

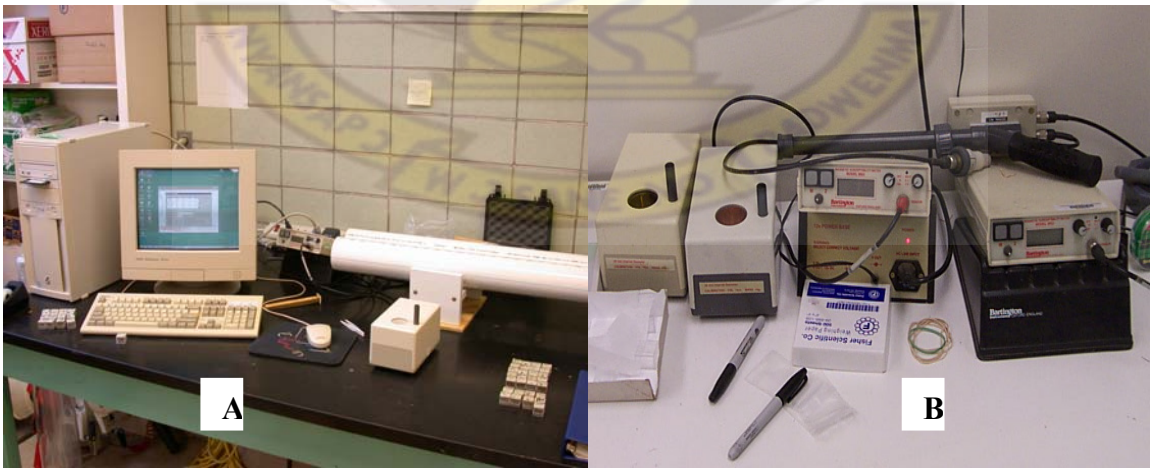

Figure 3.10 Picture showing; (A) the set up of Bartington *MS2B* sensor connected to the computer interface (B) the disconnected components of the instrument.

3.3.1.4 EXPERIMENTAL PROCEDURE

The MS2B sensor was connected to the meter and the computer as shown in the diagram making sure that connections were not overtightened. The right-hand range of the multiplier switch was turned to the BATT point, which was followed with the toggling of the on/off switch to SI mark. The turning of the MS2B sensor knob to low frequency (LF) preceded the choosing of the range value 1.0 on the range multiplier switch. The system was then left to 'warm up' for ten minutes.

The equipment was calibrated by lifting the handle of the insertion mechanism on the sensor and then placing the calibrated sample on it. The measuring button was then pushed to begin with the measurement after the insertion handle has been lowered with the calibrating sample back to its original position. Time was made for the instrument to measure the susceptibility of the sample. The set-up automatically saves the measured susceptibility value on the computer. The completion of this process was signaled with a beep from the setup.

Figure 3.11 Picture showing the author taking some susceptibility values using the Bartington *MS2B* sensor.

The calibrating sample in the sensor was then replaced with a prepared sample and the procedure repeated to determine its susceptibility at low frequency. This was repeated until measurement on the entire samples was done.

The MS2B sensor knob was flipped to the high frequency (HF), and the procedure above repeated for the corresponding susceptibility measurements at HF. The measured susceptibility values as well as ratios of measured susceptibility parameters are shown in Table 3.3 and Table 3.4 (Appendix H).

3.3.2 ANHYSTERETIC REMANENT MAGNETIZATION (ARM)

3.3.2.1 THE SPINNER MAGNETOMETER

The Spinner Magnetometer is an advanced feature instrument to measure remanent magnetization in rock specimens or sediment samples.

The Spinner Magnetometer uses therefore special holders that allow automatic orientation of specimens. All functions are microprocessor-controlled.

The microprocessor controls measurements, carries out digital filtration of the signal, controls and tests the speed of specimen rotation orientation, and automatically executes tests for erroneous conditions with its automatic, software driven feature. Individual specimens are measured three to four times.

3.3.2.2 PROCEDURE FOR MEASURING

The computer, the battery charger and the spinner magnetometer (LED readout should be 31), were turned on in the sequential order. The electronics (the whole set up), was left to stand and warm up for between ten – fifteen minutes. The attenuator and lever, were set to 1 and short spin respectively on the spinner.

For (ARM, IRM) measurements, the software used for the measurement was opened by clicking a shortcut, **SPIN1C** placed on the computer desktop. A standard sample was placed in the holder with the perfect orientation and the spin option on the computer chosen to begin the measurement. This process calibrates the magnetometer to a standard for use.

A prepared sample whose magnetization was to be measured was then put in the spinner holder in position. The click knob of the software panel on the computer screen was clicked. The spinner magnetometer automatically measures the magnetization of the sample and gives the value on the computer.

Figure 3.12 A shot of the author operating the spinner magnetometer.

3.3.3 THE D–2000 A.F. DEMAGNETIZER

3.3.3.1 STARTUP PROCEDURE

The powers of the computer and the surge suppressor were turned on in succession, which displays the D – 2000 software automatically on the computer.

The crest power of the amplifier was turned to the left (-80 db) and the amplifier switched on. The front panel "channel A" control of the crest amplifier was turned fully clockwise to "0 db". Likewise, the same step was repeated for the front panel "channel B" control.

Figure 3.13 A set up of the D–2000 A.F. Demagnetizer made ready for measurement.

3.3.3.2 USING THE DEMAGNETIZER

The D – 2000 software on the computer was clicked open and **class.set** file was selected. The peak field strength to be used (100 mT) was selected with the decay rate as 0.0075.

Four samples were fed into the demagnetizer using the holder. With the indicator **"ARM off"** activated in the window of the software, the command ***Run Demag*** was issued to start with the demagnetizing process. The positions (orientations) of the sample boxes in the holder were changed and the demagnetizing process followed. This procedure was followed until the samples were demagnetized in the x, y, and z directions.

In giving the samples Anhysteretic Remanent Magnetization (ARM), the indicator **"ARM off"** shown in the software control window, was toggled, making the option "**ARM on"** rather active**.** The samples were then fed into the demagnetizer and then the **"run ARM"** button in the control window was selected. The demagnetizer through this process imparts **ARM** to the samples.

The sample was then taken out of the demagnetizer and the magnetization imparted measured with the spinner magnetometer as described above. The value measured from the spinner magnetometer was then recorded. The imparted magnetization measured values are shown in Table 3.3 (Appendix H).

Figures 3.15 and 3.16 below, however, shows the spatial plot of the magnetic susceptibility values measured as well as the frequency dependent magnetization measured respectively.

Figure 3.14 A shot of the author carrying out a demagnetizing function on the samples using the D–2000 A.F. Demagnetizer.

Figure 3.15 Spatial map showing the distribution of low frequency susceptibility values of the samples.

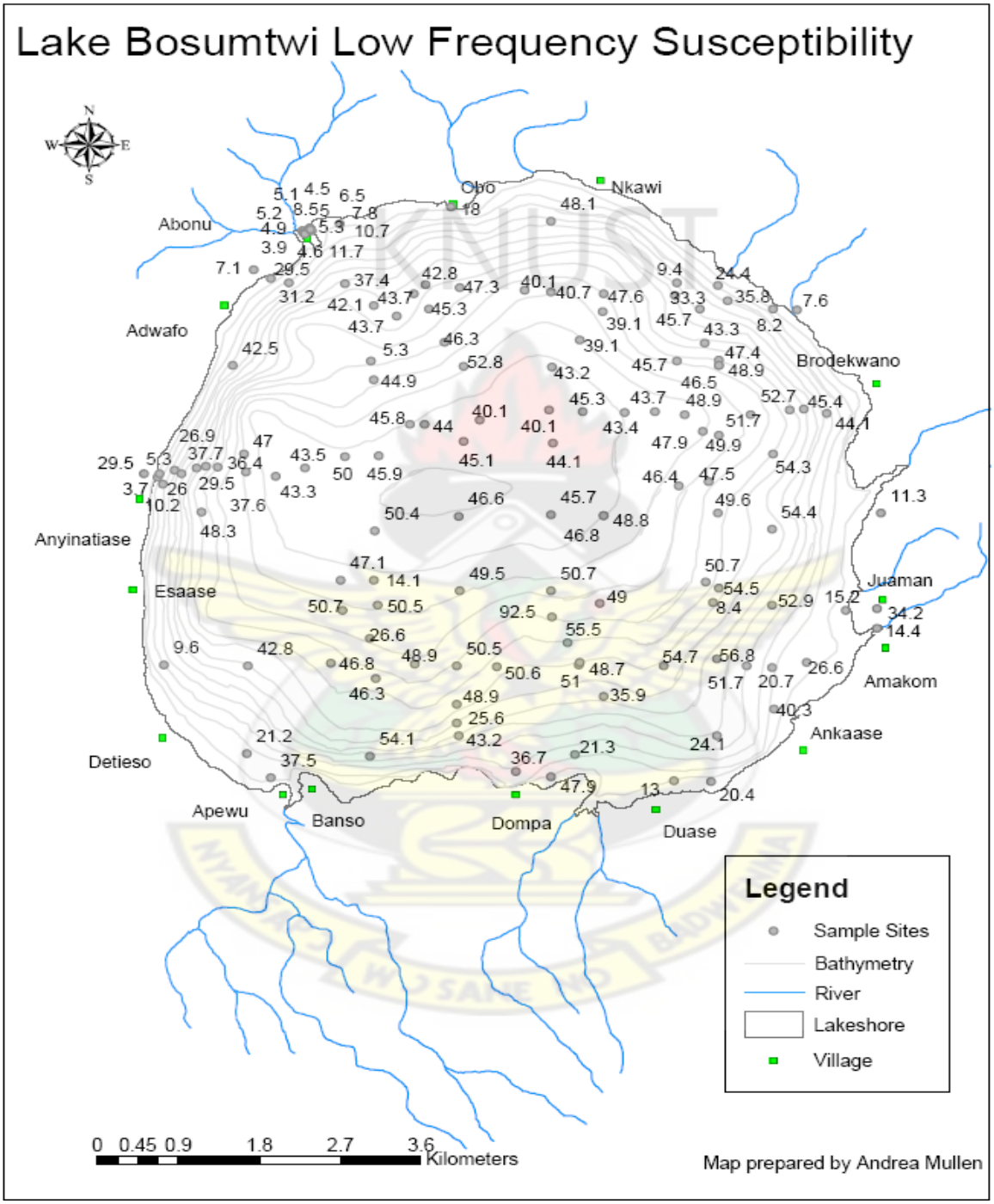

Figure 3.16 Spatial map showing the distribution of frequency dependence values of samples.

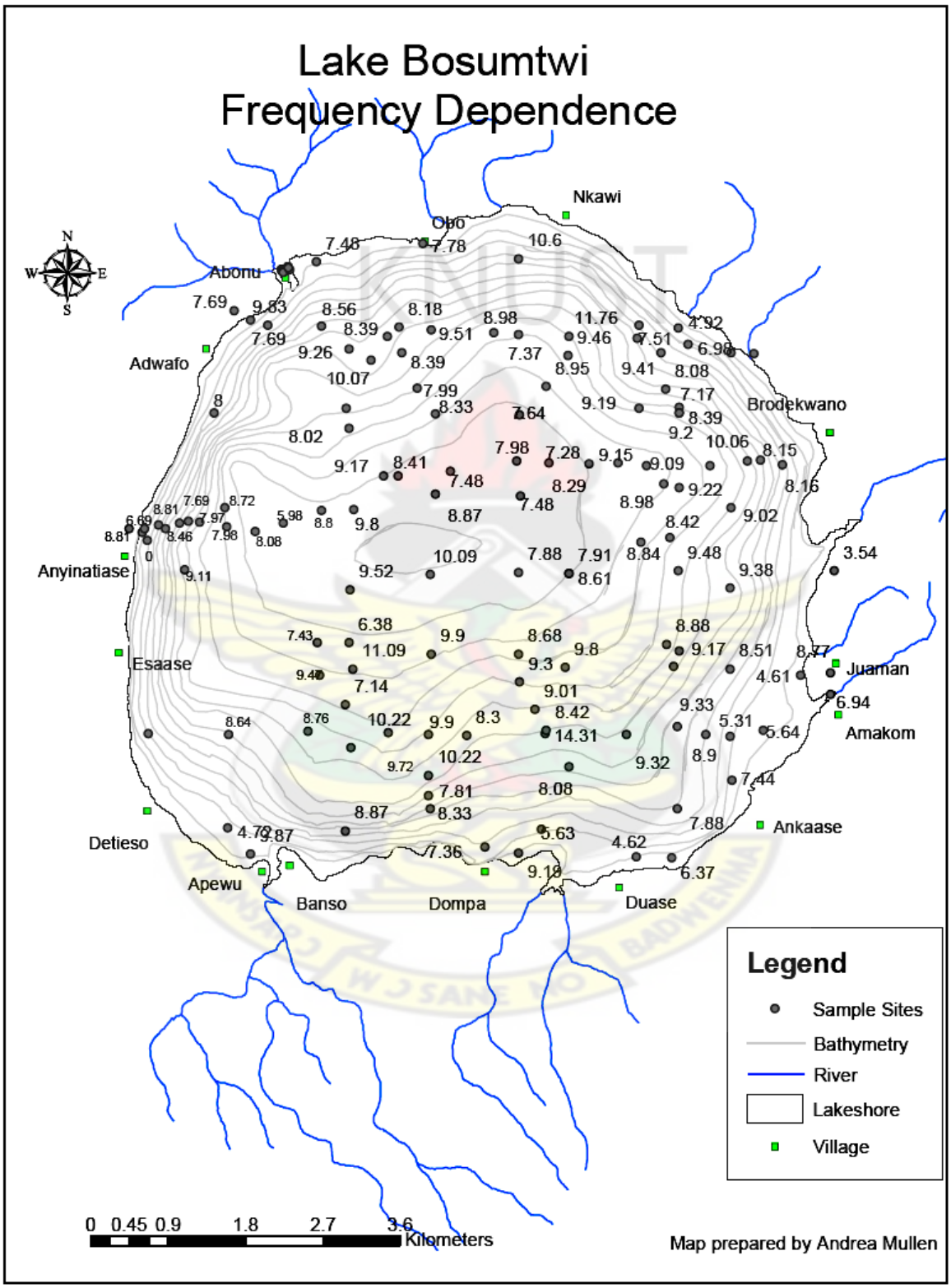

3.3.4 DEMAGNETIZING THE ARM MOMENT

3.3.4.1 INTRODUCTION

This technique of alternating field demagnetization has been successfully employed by many workers (As & Zijderveld, 1958; Khan, 1960 and Irving et al., 1961a) to remove secondary components of magnetization from igneous rocks, (Creer, 1959; Opdyke, 1964) and sedimentary rocks.

This measurement was performed on eight (8) selected samples shown below.

Table 3.5 Table of samples used for the demagnetization process and their respective water depth.

Sample Name	GR-2A	GR-4A	GR-5A	GRC-45	GR-12A	GR-17A	GR-20A	GR-25A
Water depth	10.60	13.00	26.60	4.90	74.60	74.00	74.00	39.50

3.3.4.2 EXPERIMENTAL PROCEDURE

The **"ARM off"** knob showing in the software control window on the computer was turned on. The alternating frequency peak field, 2.5 mT was selected as the first demagnetizing peak field strength in this study. The **'Run Demag'** option in the window was then selected by clicking. This option starts the demagnetizing process, which took between two – five minutes to complete demagnetizing the sample placed in the demagnetizer.

The sample was taken out of the demagnetizer and its magnetization, measured on the spinner magnetometer. This procedure was repeated while varying and increasing the alternating frequency peak field (i.e., 5, 7.5, 10… 80, 100 mT) employed for the eight samples selected. A table of the measured ARM values on the samples are shown in Table 3.6 (Appendix I).

3.3.5 ACQUISITION OF ISOTHERMAL REMANENT MAGNETIZATION (IRM) AND SATURATION ISOTHERMAL REMANENT MAGNETIZATION (M_{rs} or SIRM)

3.3.5.1 INTRODUCTION

Isothermal remanent magnetization is imparted using the impulse magnetizer as the instrument.

3.3.5.2 THE IMPULSE MAGNETIZER

It enables a variety of high-field magnetic studies to be conducted on geologic samples without the need for a large electromagnet.

It is ideally suited for IRM and anisotropy of IRM acquisition studies. The instrument comes with a sample holder, which is designed to hold 1" cubic samples in various orientations. The sample cavity is large enough to accommodate cubic samples up to 1.40" (aligned along the coil axis).

The magnetic field is produced by discharge of energy from a capacitor bank through a coil surrounding the sample cavity. The capacitor bank is first charged to the desired voltage (corresponding to the desired field). It is then discharged through the coil very quickly using a high capacity as a switch.

The use of this impulse magnetizer offers the following advantages:

- Better magnetizing results
- Higher current in the magnetization fixture
- Less heating of magnetization fixture
- Longer lifetime of magnetization fixture (www.rockgateco.com).

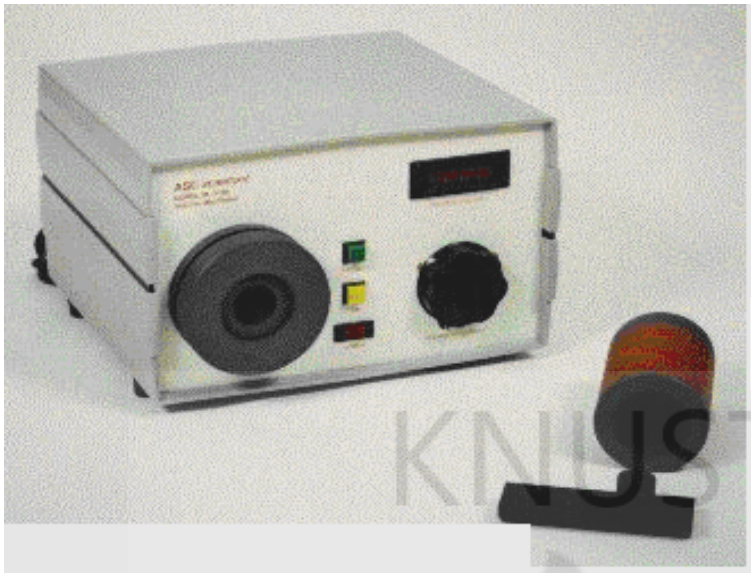

Figure 3.17 The Impulse magnetizer.

(www.ascscientific.com).

3.3.5.3 PROCEDURE FOR MEASUREMENT

The sample was placed in the impulse magnetizer via a plastic slide maintaining the right orientation. The voltage knob was adjusted through a clockwise turn, to build a desire magnetic field strength (the least field that is 5 mT). On realizing the field has been attained, the trigger knob was pushed to release the voltage. The magnetic field generated by the released voltage, magnetizes the sample in the magnetizer.

The sample was then taken out and the magnetization acquired measured using the spinner magnetometer. The sample was magnetized varying the field strength from 5 – 1100 mT and measuring the corresponding magnetization.

This procedure was repeated for the eight selected samples and the measured values recorded. After the eight samples acquired their saturation isothermal remanent magnetization at a field of 1100 mT, they were demagnetized following the demagnetizing process illustrated above in section 3.3.4.2. The measured results are recorded in Table 3.7 (Appendix J).

3.3.6 SATURATION ISOTHERMAL REMANENT MAGNETIZATION IMPARTED

Saturation Isothermal Remanent Magnetization was imparted unto sixty-eight (68) samples at three different field strengths (40 mT, 1100 mT and –300 mT), using the impulse magnetizer and the measured values recorded. Results are tabulated below (Table 3.8).

Table 3.8 Tabulated Saturation Isothermal Remanent Magnetization Values.

Sample Names	40 mT	10^{-6} Am^2k^{g-1}	1100 mT	10^{-6} Am^2k^{g-1}	- 300 mT	10^{-6} Am^2k^{g-1}
GR1-A	177.99	393.70	506.00	1119.22	-480.27	-1062.31
GR2-A	45.57	58.94	104.47	135.13	-97.04	-125.52
GR3-A	182.45	311.30	316.54	540.08	-293.49	-500.75
GR4-A	64.22	91.47	166.06	236.52	-152.65	-217.42
GR5-A	463.94	888.60	880.58	1686.61	-845.8	-1620.00
GR6-A	412.77	820.45	665.34	1322.48	-612.61	-1217.67
GR7-A	460.69	1019.00	758.99	1678.81	-735.33	-1626.48
GR8-A	674.42	1446.94	1235.03	2649.71	-1166.22	-2502.08
GR9-A	612.48	1376.05	1175.79	2641.63	-1110.36	-2494.63
GR10-A	762.48	1646.47	1429.19	3086.14	-1340.82	-2895.31
GR11-A	1062.68	2087.37	1901.08	3734.20	-1826.78	-3588.25
GR12-A	703.32	1583.70	1460.67	3289.06	-1411.91	-3179.26
GR15-A	973.4	2061.85	1761.18	3730.52	-1701.78	-3604.70
GR16-A	959.41	1961.58	1725.86	3528.64	-1700.8	-3477.41
GR17-A	751.56	1832.63	1716.81	4186.32	-1688.57	-4117.46
GR18-A	959.61	1918.84	1797.91	3595.10	-1686.88	-3373.09
GR19-A	1133.06	2208.26	2142.8	4176.18	2067.93	4030.27
GR20-A	738.2	1716.35	1692.78	3935.78	-1687.72	-3924.02
GR21-A	870.34	2148.46	1538.59	3798.05	1472.62	3635.20
GR23-A	1018.23	2187.39	1790.3	3845.97	1686.71	3623.44
GR24-A	969.78	2019.95	1681.47	3502.33	1603.77	3340.49
GR25-A	834.25	1723.30	1460.24	3016.40	-1400.38	-2892.75
GR26-A	550.7	1691.86	843.13	2590.26	-764.51	-2348.73
GR27-A	851.21	1685.23	1341.41	2655.73	-1276.88	-2527.97
GRE-1A	205.31	247.93	344.18	415.63	-322.75	-389.75
GRC-1	316.74	406.55	653.86	839.25	-615.06	-789.45
GRC-2	377.41	624.75	606.86	1004.57	-567.24	-938.98
GRC-3	1043.62	1286.67	1508.65	1860.00	-1407.3	-1735.05
GRC-4	979.56	1982.51	1610.75	3259.97	-1495.74	-3027.20
GRC-5	712.25	2157.68	1312.88	3977.22	-1219.94	-3695.67
GRC-6	996.06	2310.51	1831.08	4247.46	-1745.21	-4048.27

GRC-7	933.68	2150.84	1741.47	4011.68	-1655.83	-3814.40
GRC-8	654.2	1479.76	1021.01	2309.45	-969.46	-2192.85
GRC-10	876.03	1697.40	1345.82	2607.67	-1270.76	-2462.24
GRC-11	792.43	1600.55	1264.16	2553.34	-1183.85	-2391.13
GRC-12	565.78	1291.44	839.86	1917.05	-782.12	-1785.25
GRC-13	579.39	1229.87	829.23	1760.20	-778.46	-1652.43
GRC-14	822.3	1593.30	1257.54	2436.62	-1152.59	-2233.27
GRC-22	481.58	1035.43	756.97	1627.54	-709.4	-1525.26
GRC-24	84.79	108.00	116.94	148.95	-105.5	-134.38
GRC-25	686.48	1451.03	1110.2	2346.65	-1032.48	-2182.37
GRC-26	811.13	1782.31	1455.81	3198.88	-1394.07	-3063.22
GRC-29	958.02	2091.29	1684.43	3676.99	-1571.65	-3430.80
GRC-32	598.43	814.08	703.21	956.62	-685.89	-933.06
GRC-34	930.69	2081.61	1625.63	3635.94	-1534.81	-3432.81
GRC-36	999.01	2129.63	1692.19	3607.31	-1564.6	-3335.32
GRC-39	548.07	1033.90	856.76	1616.22	-793.71	-1497.28
GRC-40	284.77	487.54	648.7	1110.60	-625.36	-1070.64
GRC-41	159.22	442.15	275.58	765.29	-208.2	-578.17
GRC-42	808.47	1513.71	1323.46	2477.93	-1231.75	-2306.22
GRC-45	790.83	1161.11	1464.51	2150.21	-1360.7	-1997.80
GRC-46	455.63	784.08	767.49	1320.75	-689.69	-1186.87
GRC-47	275.61	404.65	431.04	632.86	-407.88	-598.85
GRC-48	658.73	1392.37	1088.03	2299.79	-1021.11	-2158.34
GRC-50	354.47	447.51	489.1	617.47	-438.3	-553.34
station A	1216.93	2438.25	2391.56	4791.75	-2282.19	-4572.61
station B	1150.82	2448.03	2139.52	4551.20	-2017.3	-4291.21
station C	1189.48	2441.96	2270.94	4662.16	-2145.35	-4404.33
station D	1168.32	2428.43	2290.94	4761.88	-2214.76	-4603.53
station E	1031.73	2162.50	1931.75	4048.94	-1734.96	-3636.47
station F	972.39	2179.76	1818.52	4076.49	-1710.21	-3833.69
station G	1095.1	2198.55	1876.54	3767.40	-1737.09	-3487.43
deep-grab	873.7	1786.34	1477.05	3019.93	-1301.87	-2661.77

Figure 3.18 below shows a plot of the SIRM values imparted to the samples collected at magnetizing fields 40 mT, 110 mT and – 300 mT.

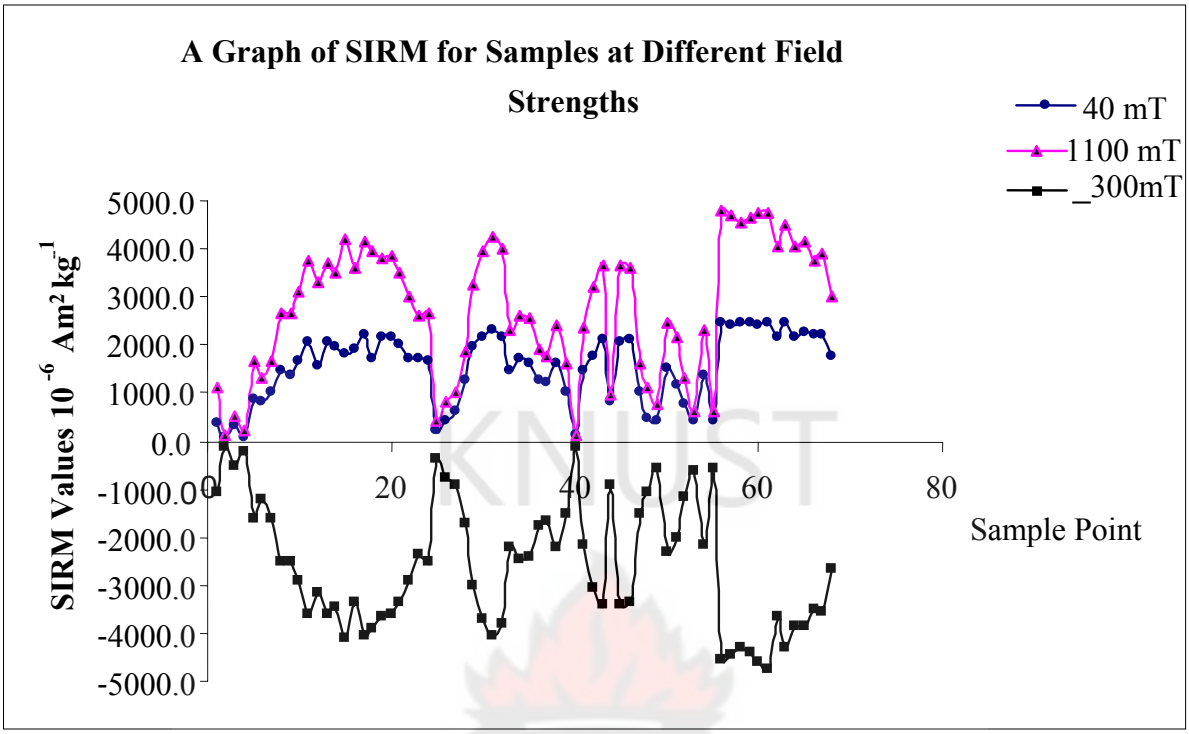

Figure 3.18 A graph showing trend of Saturation Isothermal Remanent Magnetization of samples at 40 mT, 1100 mT and – 300 mT.

3.3.7 DIRECT CURRENT DEMAGNETIZATION OF SIRM

Twenty selected samples were given magnetization (SIRM) at field strength 1100 mT using the impulse magnetizer. They were then demagnetized using the impulse magnetizer. In doing this, the sample orientation was placed in the magnetizer exactly opposite in direction to the orientation used when magnetizing the samples (i.e. applying a backfield to the samples).

The voltage knob was adjusted through a clockwise turn, to build a desire magnetic field strength (with the least field as 5 mT).

On realizing the field desired, the trigger knob was pushed to release the voltage. The magnetic field accompanying the released voltage magnetizes the sample in the magnetizer but this time in the opposite direction to the already existing magnetization thereby reducing the magnitude.

The sample was then taken out and the magnetization remaining measured using the spinner magnetometer. The sample was demagnetized varying the field strength until a negative value was encountered. The results are tabulated in Table 3.9 (Appendix K).

Figure 3.19 below is a graph illustrating the SIRM demagnetization trends for the twenty samples.

Figure 3.19 Graphs of SIRM demagnetization for the twenty samples (sheets 'A' to 'F').

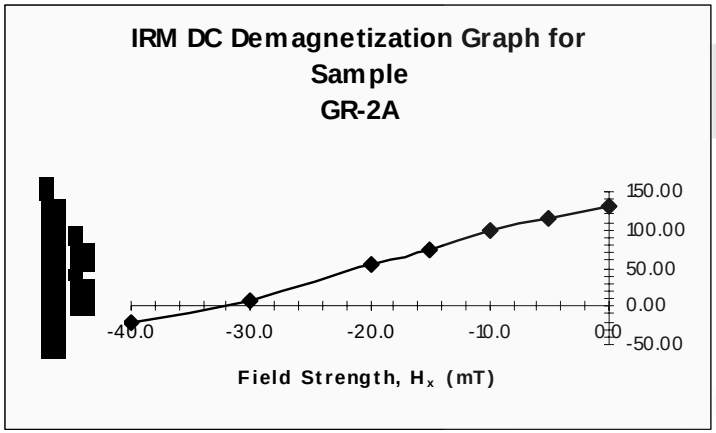

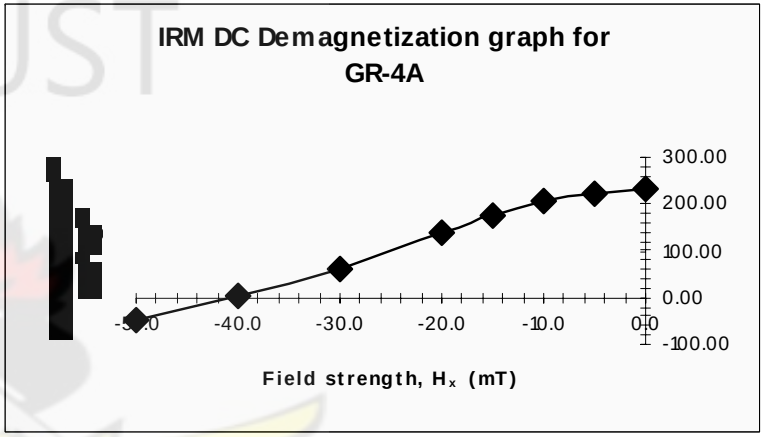

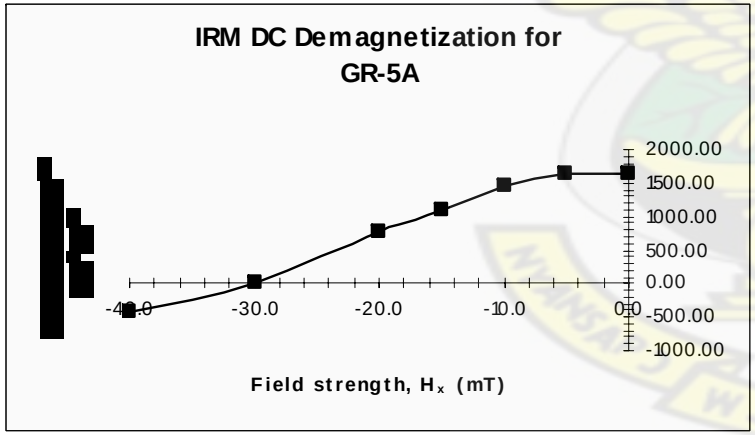

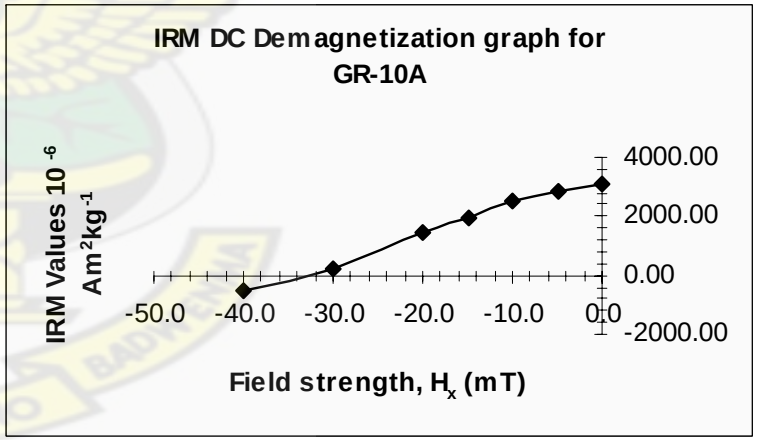

Sheet A

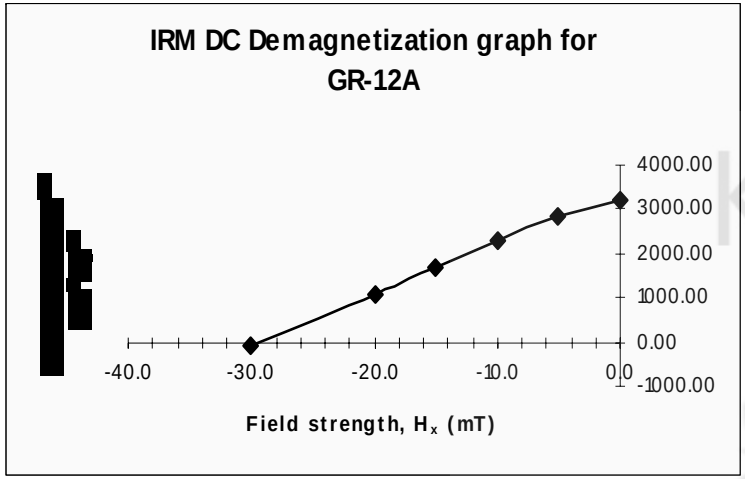
IRM DC Demagnetization graph for
GR-12A
4000.00
3000.00
2000.00
1000.00
0.00
-1000.00
-40.0
-30.0
-20.0
-10.0
0.0
Field strength, Hx (mT)

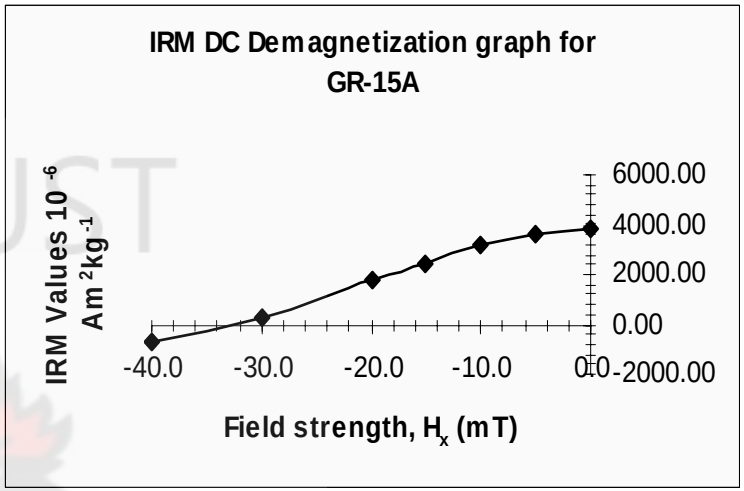
IRM DC Demagnetization graph for
GR-15A
IRM Values 10 -6
Am 2kg -1
6000.00
4000.00
2000.00
0.00
-2000.00
-40.0
-30.0
-20.0
-10.0
0.0
Field strength, Hx (mT)

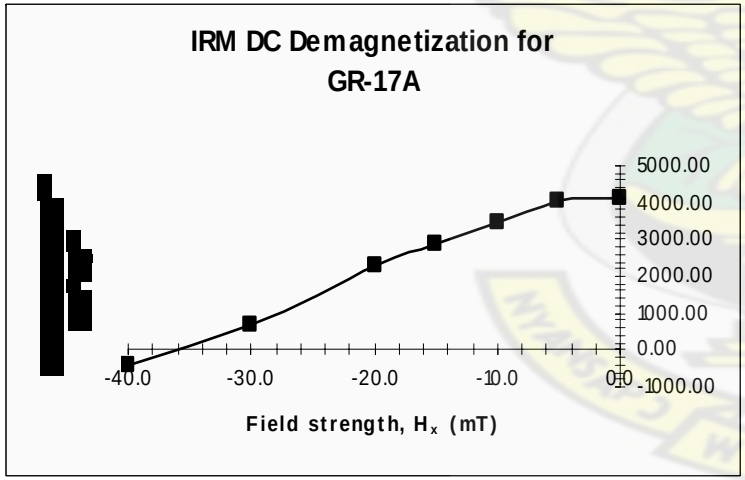
IRM DC Demagnetization for
GR-17A
5000.00
4000.00
3000.00
2000.00
1000.00
0.00
-1000.00
-40.0
-30.0
-20.0
-10.0
0.0
Field strength, Hx (mT)

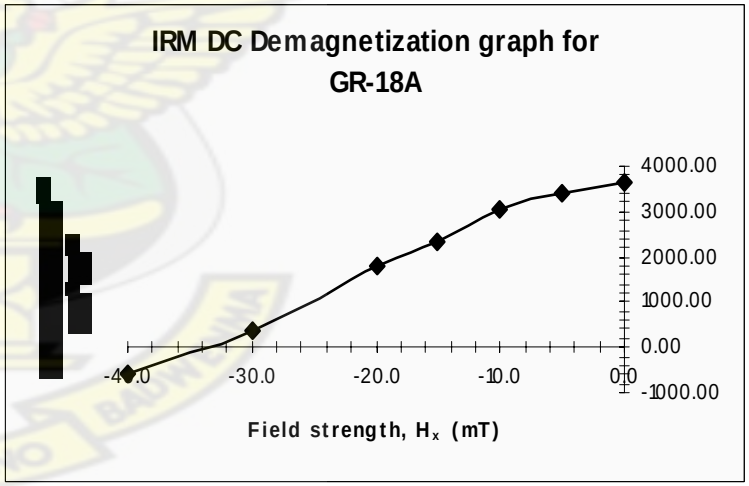
IRM DC Demagnetization graph for
GR-18A
4000.00
3000.00
2000.00
1000.00
0.00
-1000.00
-40.0
-30.0
-20.0
-10.0
0.0
Field strength, Hx (mT)

Sheet B

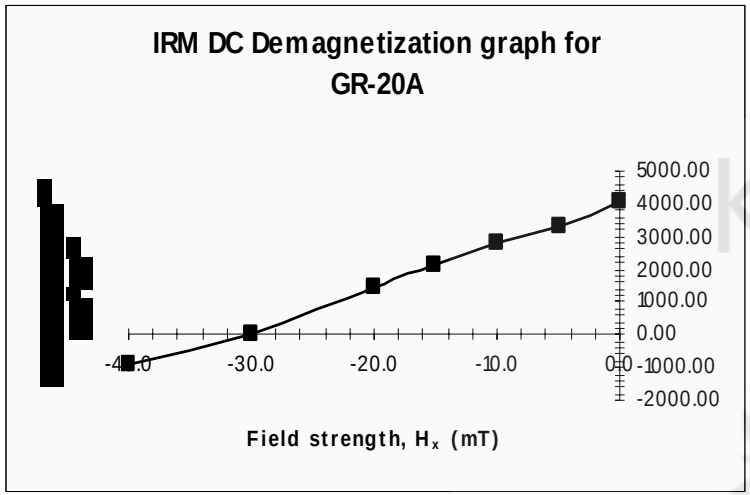
IRM DC Demagnetization graph for GR-20A
5000.00
4000.00
3000.00
2000.00
1000.00
0.00
-1000.00
-2000.00
-40.0
-30.0
-20.0
-10.0
0.0
Field strength, H_x (mT)

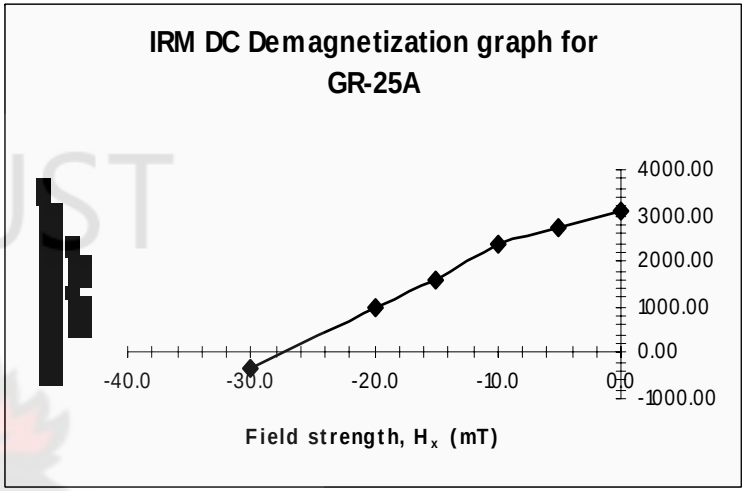
IRM DC Demagnetization graph for GR-25A
4000.00
3000.00
2000.00
1000.00
0.00
-1000.00
-40.0
-30.0
-20.0
-10.0
0.0
Field strength, H_x (mT)

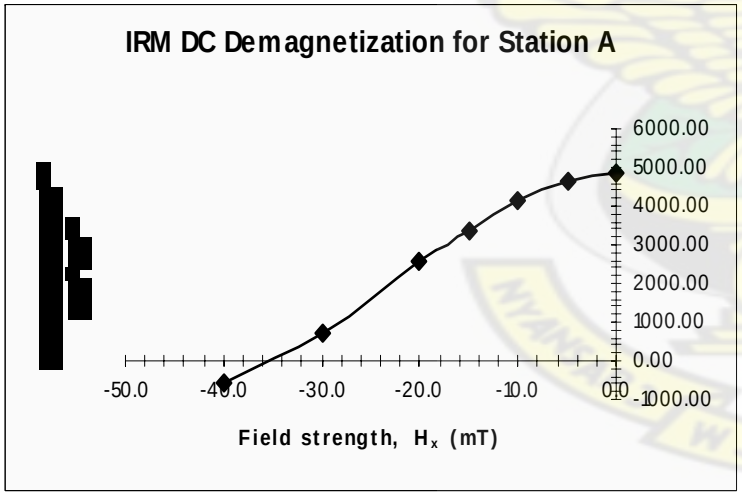
IRM DC Demagnetization for Station A
6000.00
5000.00
4000.00
3000.00
2000.00
1000.00
0.00
-1000.00
-50.0
-40.0
-30.0
-20.0
-10.0
0.0
Field strength, H_x (mT)

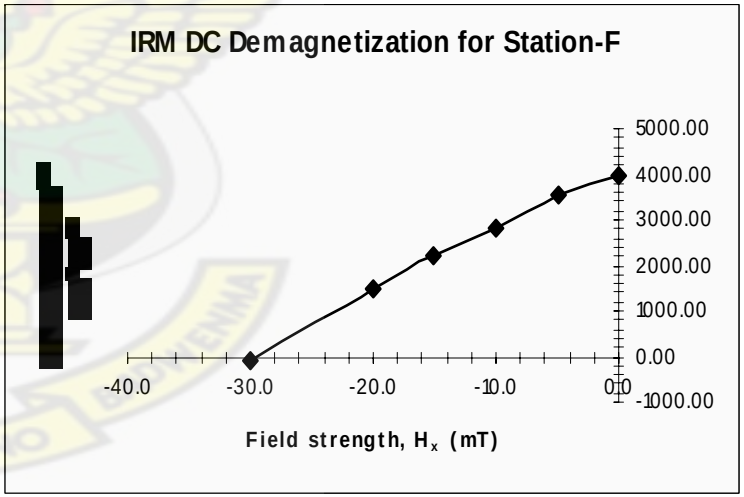
IRM DC Demagnetization for Station-F
5000.00
4000.00
3000.00
2000.00
1000.00
0.00
-1000.00
-40.0
-30.0
-20.0
-10.0
0.0
Field strength, H_x (mT)

Sheet C

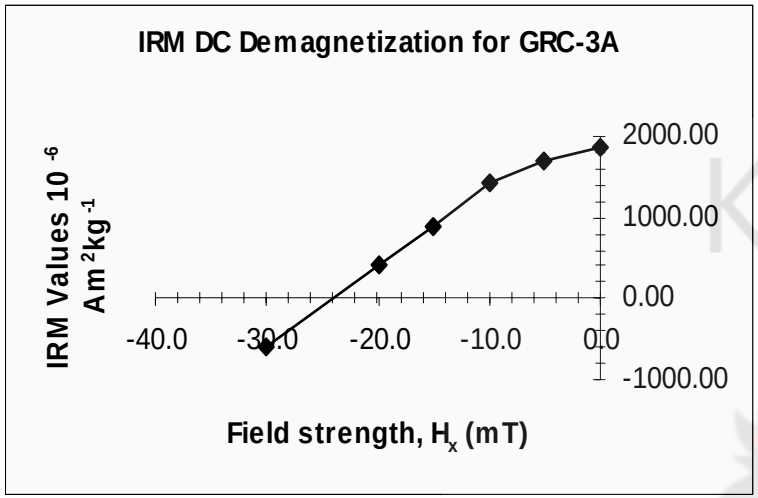
IRM DC Demagnetization for GRC-3A
IRM Values 10 -6 Am 2kg -1
2000.00
1000.00
0.00
-1000.00
-40.0
-30.0
-20.0
-10.0
0.0
Field strength, Hx (mT)

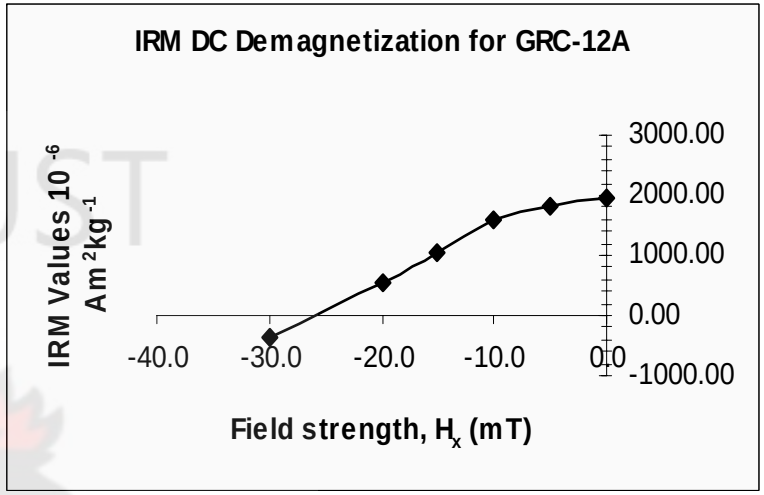
IRM DC Demagnetization for GRC-12A
IRM Values 10 -6 Am 2kg -1
3000.00
2000.00
1000.00
0.00
-1000.00
-40.0
-30.0
-20.0
-10.0
0.0
Field strength, Hx (mT)

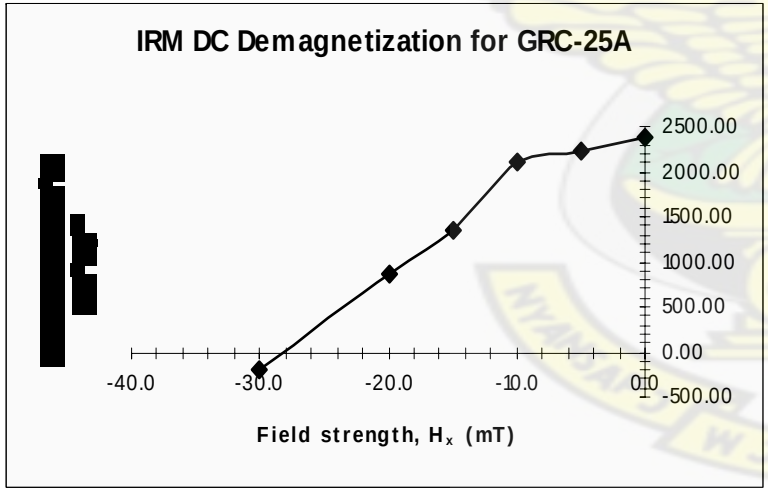
IRM DC Demagnetization for GRC-25A
2500.00
2000.00
1500.00
1000.00
500.00
0.00
-500.00
-40.0
-30.0
-20.0
-10.0
0.0
Field strength, Hx (mT)

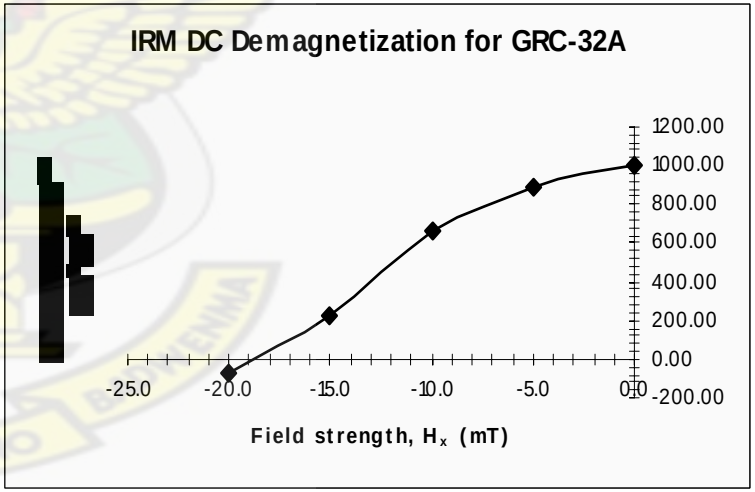
IRM DC Demagnetization for GRC-32A
1200.00
1000.00
800.00
600.00
400.00
200.00
0.00
-200.00
-25.0
-20.0
-15.0
-10.0
-5.0
0.0
Field strength, Hx (mT)

Sheet D

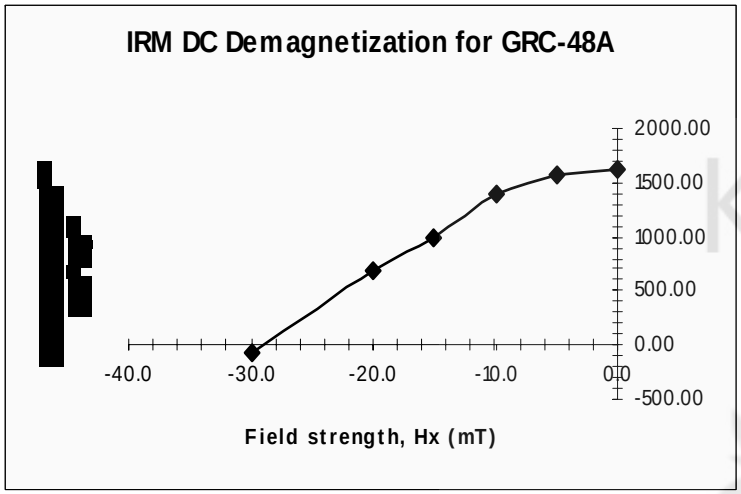
IRM DC Demagnetization for GRC-48A
2000.00
1500.00
1000.00
500.00
0.00
-500.00
-40.0
-30.0
-20.0
-10.0
0.0
Field strength, Hx (mT)

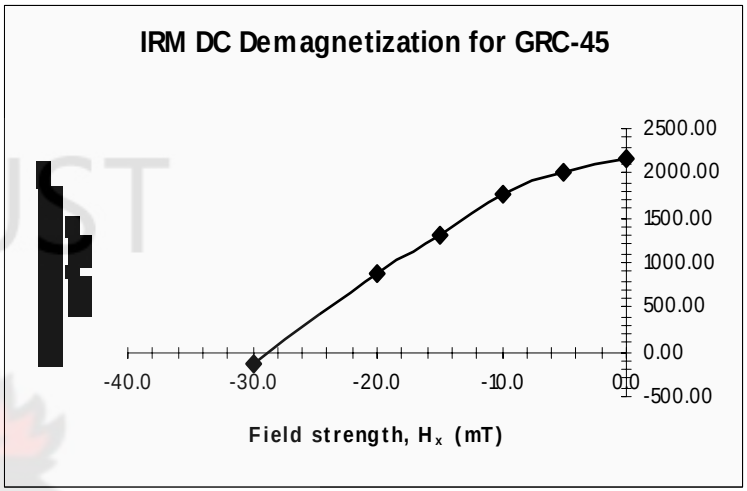
IRM DC Demagnetization for GRC-45
2500.00
2000.00
1500.00
1000.00
500.00
0.00
-500.00
-40.0
-30.0
-20.0
-10.0
0.0
Field strength, Hx (mT)

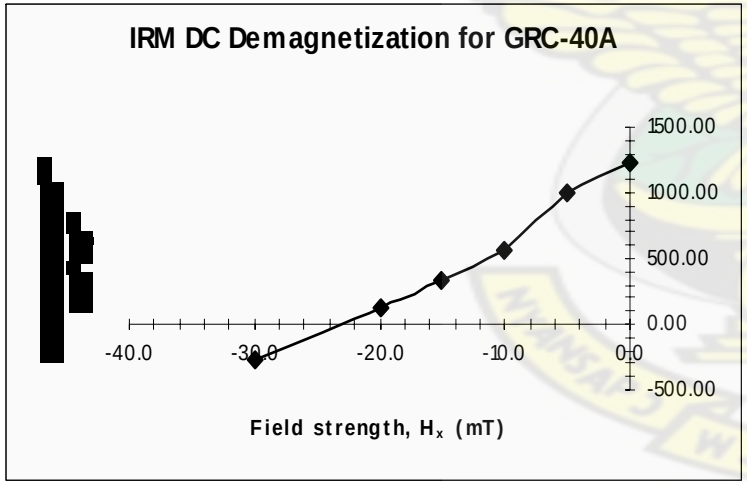
IRM DC Demagnetization for GRC-40A
1500.00
1000.00
500.00
0.00
-500.00
-40.0
-30.0
-20.0
-10.0
0.0
Field strength, Hx (mT)

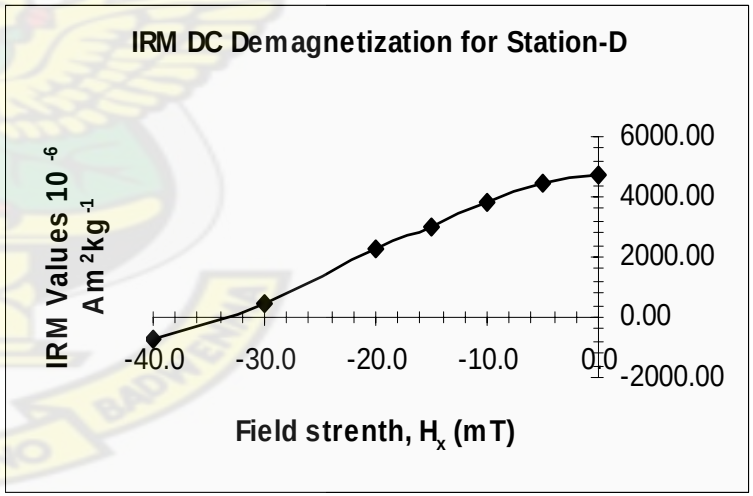
IRM DC Demagnetization for Station-D
IRM Values 10 -6 Am 2kg -1
6000.00
4000.00
2000.00
0.00
-2000.00
-40.0
-30.0
-20.0
-10.0
0.0
Field strenth, Hx (mT)

.

Sheet F

3.3.8 HYSTERESIS MEASUREMENTS USING THE MICROMAG

3.3.8.1 INTRODUCTION

Hysteresis measurements were taken on eight selected samples taken at various lake water depths to represent the various environment across the lake. The samples are as shown below.

Table 3.10 Table showing sample names and the corresponding weights used.

Sample Number	GR–20A	GR–5A	GR–12A	GR – 4A	GRC – 45	GR–25A	GR–15A	GR–6A
Weight (mg)	8.882	16.388	7.063	18.002	17.575	16.317	17.763	6.038
Slide Number	1	2	3	4	5	6	7	8
Water Depth (m)	70.00	26.60	74.60	13.00	4.90	39.50	83.00	32.00

3.3.8.2 EXPERIMENTAL PROCEDURE

The samples were put into a plastic cone shaped tube of about 2 cm^3 of volume. The samples were then air-dried in a desiccator for few days to provide a well-consolidated water free sample. All the dried sediment samples were weighed to ± 0.001mg on a Mettler – Toledo MX5 microbalance and mounted on a 3 mm^2 glass cover slips with a small amount of Dow Corning high vacuum silicone grease. The cover slips and silicone grease were used because these are slightly diamagnetic.

Diamagnetic materials produce only a small negative magnetization in the presence of an applied magnetic field and preserve no remanence (Maher, et al., 1999). The effect of these diamagnetic material on the sediment magnetic measurements is minimal and nearly constant across all samples and measurements in this study. The mineral data were generated using a Princeton Measurements Corporation Micromag 2900-02 alternating gradient magnetometer (AGM), an instrument capable of measuring the full magnetic

hysteresis loop on samples as small as few milligrams. The AGM was used to first demagnetize the samples with decreasing field strengths in both the positive and negative directions. In this study, susceptibility **(Π)** was approximated on the AGM by calculating the slope of a line through the initial few in-field magnetizations. A saturating magnetic field is the positive direction (500 mT) and a subsequent in-field saturation magnetization is measured **(M_s)**.

Repeated magnetizations were measured at decreasing field strengths until the applied is equal to zero, where all sample magnetization is remanent magnetization **(M_r).** Field strengths were then incrementally applied in the negative direction up to – 500 mT, producing measurements of coercivity **(H_c),** which qualifies the in-field strength needed to reduce the sample to zero remanences. Separate isothermal remanent magnetization (IRM) acquisition curves were made on each sample up to 500 mT. Direct current (DC) demagnetization measurements were also conducted on each sample by first saturating the sample at 500mT and then stepwise DC demagnetized in order to determine the reversed field required to reduce the remanent magnetization to zero. A value termed as the coercivity of remanences **(H_{cr})** was obtained.

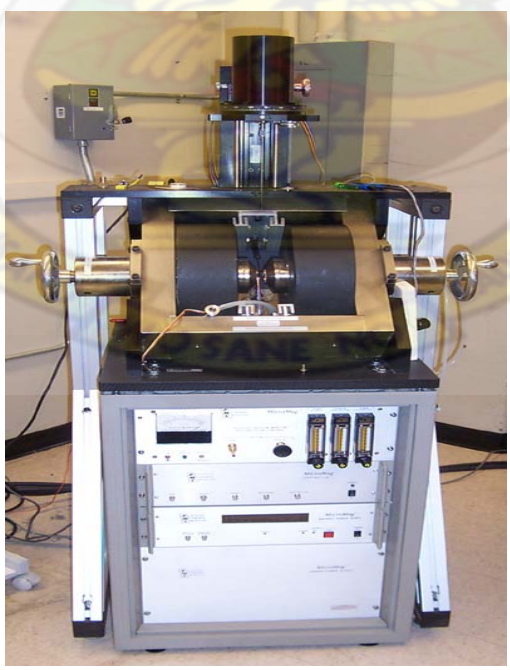

Figure 3.20 Showing a set up of the micromag equipment.

3.3.8.3 TABLE OF RESULTS

Below are tabulated values extracted from the hysteresis measurement performed on the eight samples (Table 3.11) together with their computered stability values in Table 3.12.

Table 3.11 Table of data extracted from magnetic hysteresis measurement and plot (Appendix M) on the eight selected samples.

Sample	Π (mAm^2kg^{-1})	Hcr (mT)	Hc (mT)	Hcr/Hc	Mr (mAm^2kg^{-1})	Ms (mAm^2kg^{-1})	Mr/Ms
GR-4A	9.59	35.27	13.24	2.66	187.100	692.300	0.27
GR-5A	109.90	25.64	9.54	2.69	1.597	6.655	0.24
GR-6A	273.40	28.79	11.12	2.59	4.568	17.980	0.25
GR-12A	212.90	28.79	10.97	2.62	3.492	13.890	0.25
GR-15A	254.10	28.48	10.79	2.64	4.061	16.240	0.25
GR-20A	174.30	36.71	16.33	2.25	4.130	14.200	0.29
GR-25A	260.10	23.03	8.14	2.83	3.252	15.210	0.21
GRC-45	112.20	21.81	9.14	2.39	1.484	6.801	0.22

A table is fitted here showing the eight samples selected for the hysteresis experiment and their corresponding computered magnetic stability ratios.

Table 3.12 Table of values showing samples and their computered stability ratios.

Sample	Water Depth (m)	IRM $_{40\ mT}$	SIRM $_{1100\ mT}$	IRM $_{40\ mT}$/SIRM $_{1100\ mT}$
GRC-45	4.90	1161.11	2150.21	0.54
GR-2A	10.60	58.94	135.52	0.43
GR-4A	13.00	91.47	236.52	0.39
GR-5A	26.60	888.60	1686.61	0.53
GR-25A	39.50	1723.30	3016.40	0.57
GR-20A	70.00	1716.35	3935.78	0.44
GR-17A	74.00	1832.63	4186.32	0.44
GR-12A	74.60	1583.70	3289.06	0.48

3.4 GRAIN SIZE ANALYSIS OF SELECTED SAMPLES FROM IMPORTANT SITES

3.4.1 INTRODUCTION

Catchment – derived sediment particles that enter lakes are transported toward low energy sites of permanent deposition. This process is known as **sediment focusing** when the deposition occurs in the profundal zones of the lake. Sediment distribution in deeper lakes can be conveniently subdivided into three zones by reason of the differences in their potential for resuspension with the two principal zones being the zone of sediment erosion (ZSE), characterized by periodic high turbulence and dominated by coarse – grained inorganic sediments; and the zone of sediment accumulation (ZSA), a zone of low turbulence dominated by fine inorganic particles (fine silt 2 – 32 :m; clays < 2 :m diameter) and organic particles of similar low density. The two zones are separated by the zone of discontinuous sediment accumulation (ZDA) and known as the zone of transportation (Kalff, 2002).

The frictional movement of wind blowing over water sets the water surface into motion, producing a wind drift. The wind also sets the surface into oscillation and produces traveling surface waves. If these waves become large enough to break, their energy flux and dispersion are transferred to the water. Short surface waves cause the surface water particles to move in a path or orbit. In cross section, the path is circular (Fig. 3.21), with very little significant motion other than slow horizontal translocation. Of greater interest than the small horizontal movement of short surface waves, is the influence such periodic oscillations have vertically, although the wave height (h) of the vertical oscillation is attenuated rapidly with increasing depth, shown in Fig. 3.21.

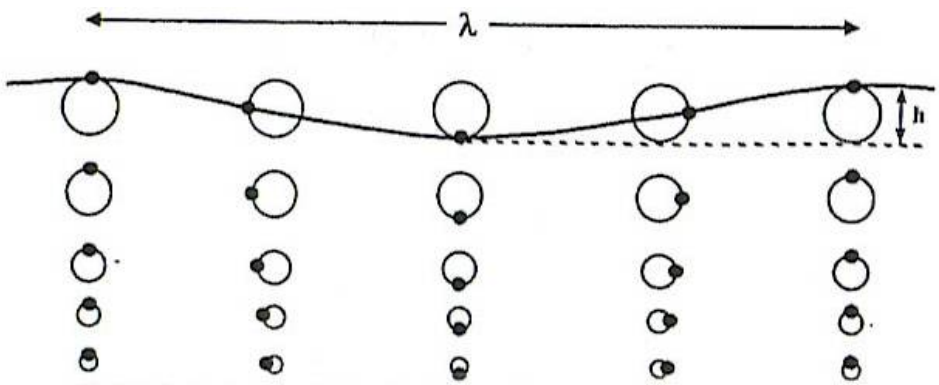

Figure 3.21 Circular motion of fluid particles in a sinusoidal wave of length (λ) traveling from left to right on deep water.

For a given wind speed, wave height appears to become nearly independent of depth in small lakes, but in lakes of greater area, height and length increases with increasing water depth, with the wave height given by;

$$h = 0.105\sqrt{X} \qquad [Eq.\ (3.1)]$$

where,

$h = the\ waveheight\ \ and$

$X = the\ fetch\ distance\ in\ centimeter$

$In\ Fig.\ 6.1, (\lambda) = the\ wavelength\ of\ the\ wave\ \ (Wetzel, 2001).$

Now, as the velocity and shear stress of fluid (e.g. water) moving over a sediment bed increase, a critical point (the threshold) is reached, at which the grains begin to move down current. Commonly, the smallest and lightest grain move first. As shear stress increases, larger grains are put into motion until finally grain motion is common everywhere on the bed. This critical threshold for grain movement is a direct function of several variables, including boundary shear stress, fluid viscosity, particle size, shape and density.

The threshold of a grain movement under orbital wave is observed to be a function of grain diameter, wave period and orbital velocity of the wave. Orbital velocity is in turn a function of wave height, water depth, wave period and wavelength. The relation is shown by the equation;

$$U_t = \frac{\pi d_o}{T} = \frac{\pi H}{T \sinh\left(2\pi h / L\right)} \qquad \text{-------} \quad [Eq.\ (3.2)]$$

where

U_t = the threshold velocity

d_o = the orbital diameter of the wave motion

h = wave height

L = wave length

T = wave period and

H = the water depth (Boggs, 1987).

The waves described above (deep water or short waves), are waves in which wavelengths are much less than water depth. When this condition no longer holds, and wavelengths become more than 20 times the water depth, the wave is transformed into a "shallow water" "long" wave, and the circular motions are transformed into a to-and-fro sloshing, which extends to the bottom of the water column (Fig. 3.22).

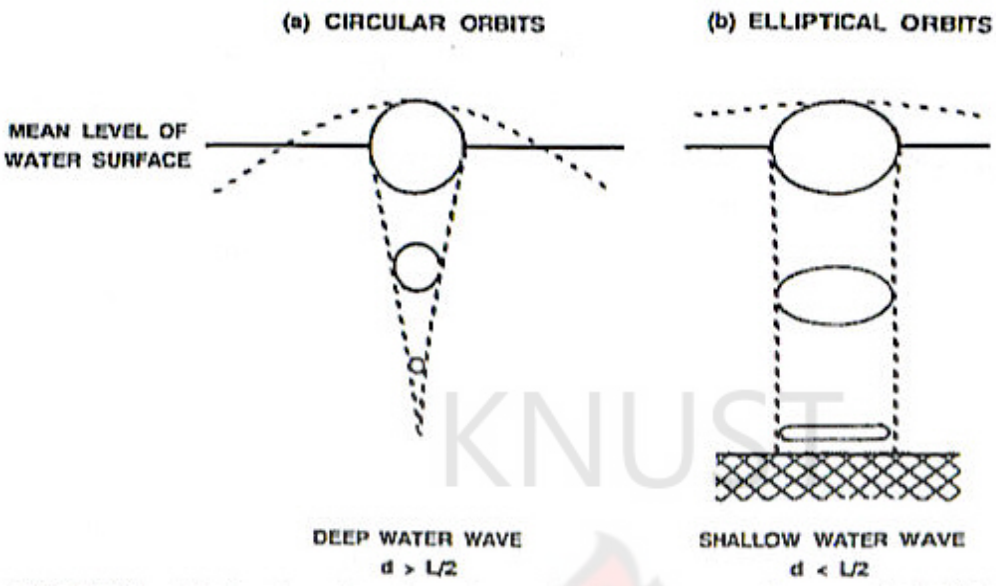

Figure 3.22 Orbital motions of water beneath waves. (a) Deepwater waves where water depth *(d)* is greater than the wavelength $\lambda/2$. (b) Shallow water waves where d < $\lambda/2$ (Wetzel, 2001).

The above factors lead to different transport and depositional processes and thereby generating a wide variety of siliciclastic and nonsiliciclastic sedimentary rocks. These rocks are each characterized by distinctive physical properties, of which the most important are sedimentary textures and structures (i.e., the small-scale features that arise from the size, shape and orientation of individual sediment grains), (Boggs, 1987).

3.4.2 BASIC GRAIN PROPERTIES

Grain size is the most fundamental physical property of sediment as already stated in the beginning of this work. Geologists and sedimentologists use information on sediment grain size to study trends in surface processes related to the dynamic conditions of transportation and deposition while engineers, geochemists and hydrologists use grain size for different purposes (Blatt & others, 1972; McCave & Syvitski, 1991).

3.4.3 TECHNIQUES USED IN GRAIN SIZE ANALYSIS

The techniques used for grain size analysis must be fast, accurate, and yield highly reproducible results (Poppe, et. al., 2000). For many years, the size and distribution of the sand and gravel fractions were determined solely by sieve analyses, and silt and clay fractions were determined by pipette or hydrometer methods. Later, rapid sediment analyzers (RSA; Ziegler & others, 1960; and Schlee, 1966) were used to reduce much of the tedium from grain-size analyses.

In this portion of the write up, the author concentrates on using the sieving method (employing the Ro-tap equipment) for the grain size analysis.

3.4.4 EXPERIMENTAL PROCEDURE

3.3.4.1 INTRODUCTION

Twenty-five samples that represent the general trend of sediment distribution in the lake were selected from among the samples collected from the field. Samples are shown in the Table 3.12 below.

Table 3.13 Selected sample for grain size analysis and their corresponding weights used.

Sample Name	Weight of Empty 500 ml Beaker (g)	Weight of Beaker with Sample (g)	Weight of Sample (g)
BA-1A	79.509	80.877	1.37
BA-1B	81.852	86.216	4.36
BA-2A	79.033	82.287	3.25
BA-2B	79.215	81.68	2.47
BA-3A	81.79	87.754	5.96
BA-3B	94.584	97.553	2.97
BA-4A	78.441	83.04	4.60
BA-4B	79.556	83.966	4.41
BA-5B	81.859	93.11	11.25
BA-6A	79.36	96.667	17.31

BA-6B	78.413	99.348	20.94
GR-1A	81.744	83.178	1.43
GR-2A	81.906	87.589	5.68
GR-4A	78.394	91.058	12.66
GR-20A	81.694	85.538	3.84
GRE-1A	81.971	92.599	10.63
GRC-3A	79.34	85.06	5.72
GRC-32A	79.217	80.911	1.69
GR2-49A	79.043	88.04	9.00
GRC-45	78.404	119.537	41.13
GRC-50A	79.217	79.47	0.25
GR2-57A	97.787	98.03	0.24
GR2-58A	79.225	100.667	21.44
GR2-67A	79.38	81.022	1.64
GR2-68A	78.429	93.708	15.28

3.4.4.2 METHODOLOGY

A volume of the samples selected was poured into an already labeled plastic cup with the sample name. A hydrogen peroxide (H_2O_2) solution was then added to the sample to remove all organics present while the mixture was left to stand for few days.

The weight of an empty 500 ml beaker, labeled with the sample name was determined by weighing on an electronic balance to '3' decimal places (i.e. 0.000 g). The sample with the H_2O_2 solution was then wet sieved, separating the grain sizes less than 63 µm into the 500 ml beaker with the use of a sieve and de-ionized water (**DI - water**).

The grain sizes greater than 63 µm (sand and silt size fractions), were washed into a clean cup and labeled with the sample name and grain size fraction.

Figure 3.23 Picture of the sample preparation process showing samples in labeled bags, data sheet and a measuring balance.

The 500 ml beaker and its content (muddy water), was then put into a fume hood to dry off the water gently. The sandy grain size fraction contained in the cup was then put in an oven to dry off the water (Fig.3.24).

Figure 3.24 Picture showing the arrangement of sample cups with grain sizes fraction greater than 63 μm (sand sizes), drying in an oven.

The method enumerated above was followed for all the twenty-five samples to have dried samples ready for the Ro-tap step.

Each dried sandy sample was then Ro-tap sieved at $\frac{1}{2}\phi$ interval in a Ro-tap machine for five minutes to separate the bulk grains into the composition of grain sizes present (Folk, 1980).

Figure 3.25 Picture showing the author removing a stack pile of sieve from the Ro-tap machine. Here the separation of grain sizes is complete.

The stuck of sieves in the Ro-tap machine were then removed, the contents poured and weighed on a balance to determine the weights of the fractions (Fig 6.4). The results are tabulated in Tables 3.14 and 3.15 (Appendix L).

Figure 3.26 Picture showing the collection of grain size component from sieve for weighing.

Folk 1980, gives a conversion table of phi (N) values into microns. This is the basis for the conversion found in column four of Table 3.15.

CHAPTER FOUR

RESULTS AND DISCUSSION

4.1 THE LOSS-ON-IGNITION METHOD

Figure 4.1 below shows plots of: (a) percentage water content, (b) percentage organic matter content and (c) the dry bulk density of samples with water depth.

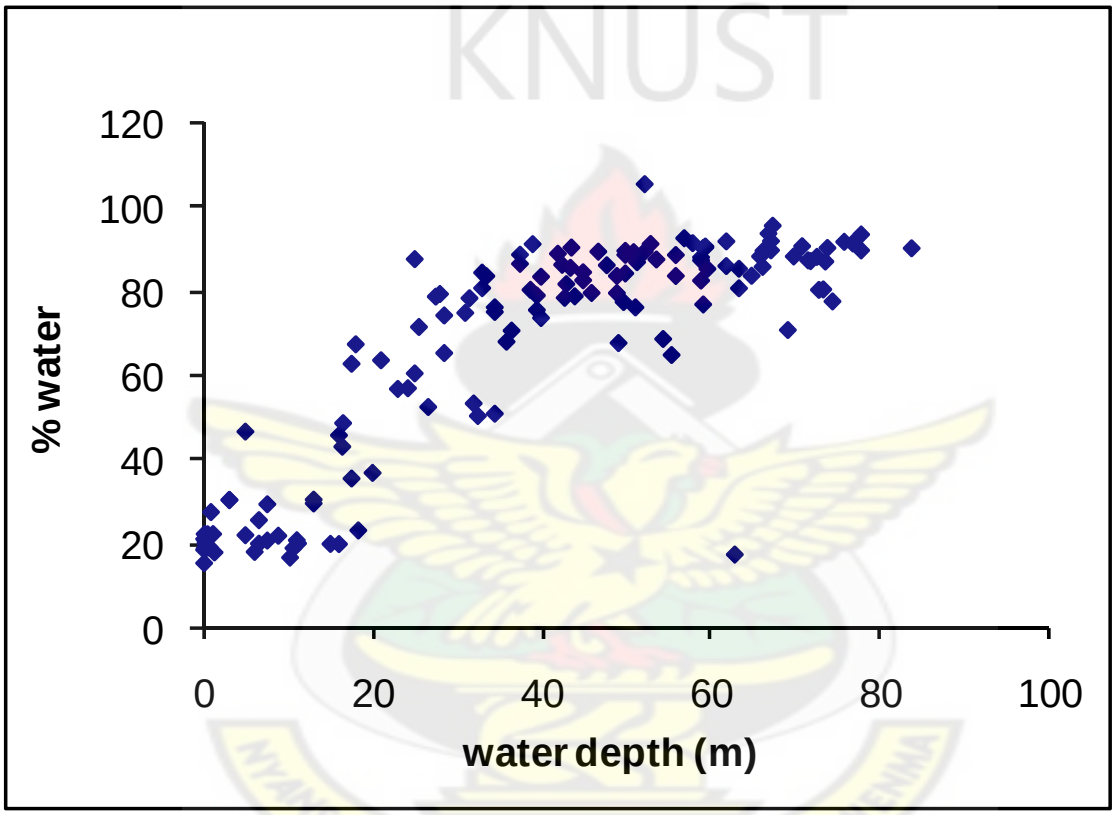

Figure 4.1 a A plot of percentage water content of samples against water depth

The percentage water content of the sample plotted above shows a general increase in trend of values as water depth increases. However, from 0-20 m, the graph shows average percentage water content of about 25 % with an abnormality of 46.9 % at depth of 4.9 m. This follows with a sharp increase in value between 20-40 m. However, beyond 40 m depth on average of about 85 % water content is maintained.

In comparing Fig. 4.1 (a) to the spatial plot (Fig. 3.8 c), there is a general increase in the values of water content as one moves into higher depth of water with the highest values occurring at the mid portions of the lake. At depth of 63 m, the sample registers only 17.73 % of water content, deviating from the general trend shown.

The dry bulk density plot, Fig 4.1 (b), shows nothing different from what will generally be expected as an inference from the behavior of Fig. 4.1 (a). It displays the inverse of the trend shown by the percentage water content plot, in that as water content is low, the dry bulk density of the sample is at its average peak of about 1.5. This value decreases from around 18 m of water depth and takes an average value of about 0.2 at 25.5 m. This average value is maintained throughout to the deepest part of the lake.

At 4.9 m depth, the dry bulk density registers an anomalous value of 0.82, which is a deviation from the normal trend shown by the bulk sample. This behaviour is repeated at the depth of 63 m with a value of 1.55. However, it trends in conformity with the anomalies shown in Fig. 4.1 (a). A critical look at the spatial plot on the dry bulk density reveals highest values resulting from samples taken on the shore of the lake or very close to the shore.

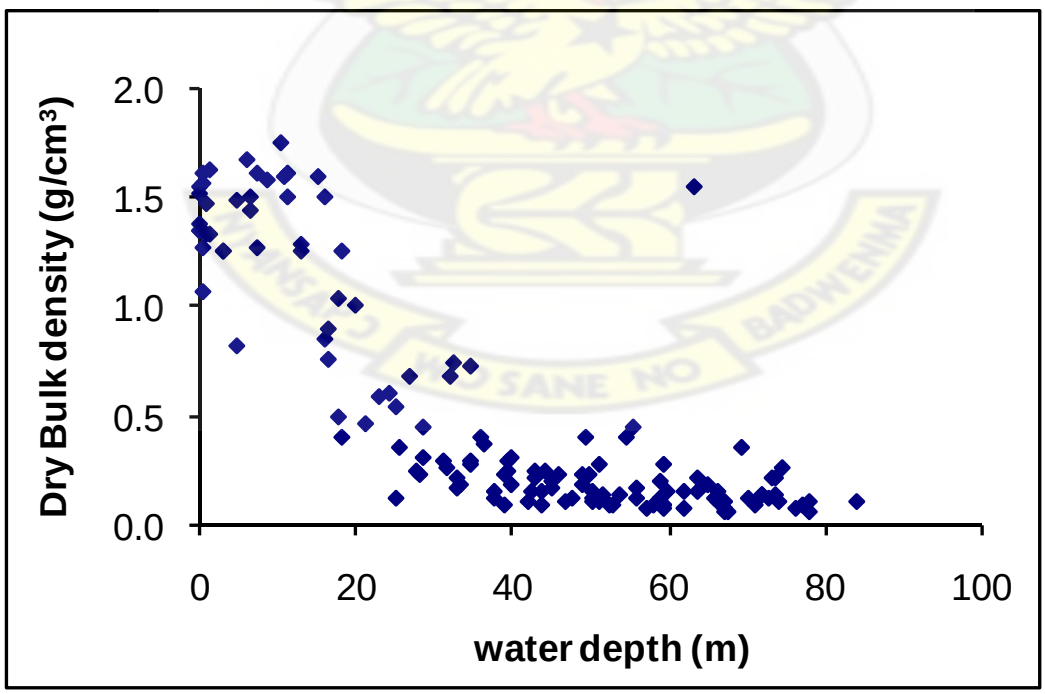

Figure 4.1 b A plot of dry bulk density against water depth

The plot of the percentage organic matter content Fig. 4.1 (c) shows a general increase in values on moving into deeper waters with minor deviations. However, there is a decrease in value from 4.49 % at 4.9 m to 2.05 % at 10.2 m depth of water. This is followed by a rise again in value to 4.86 % at 17.5 m, then to 20.32 % of organic matter at 40.00 m depth and then maintaining an average value of about 24.5 % on the graph.

The percentage organic abnormality values plotted between the water depths of 45 m to 69 m are showing on the spatial plot (Fig. 3.8 a) as samples taken from the same vicinity (i.e. the northeastern part of the lake).

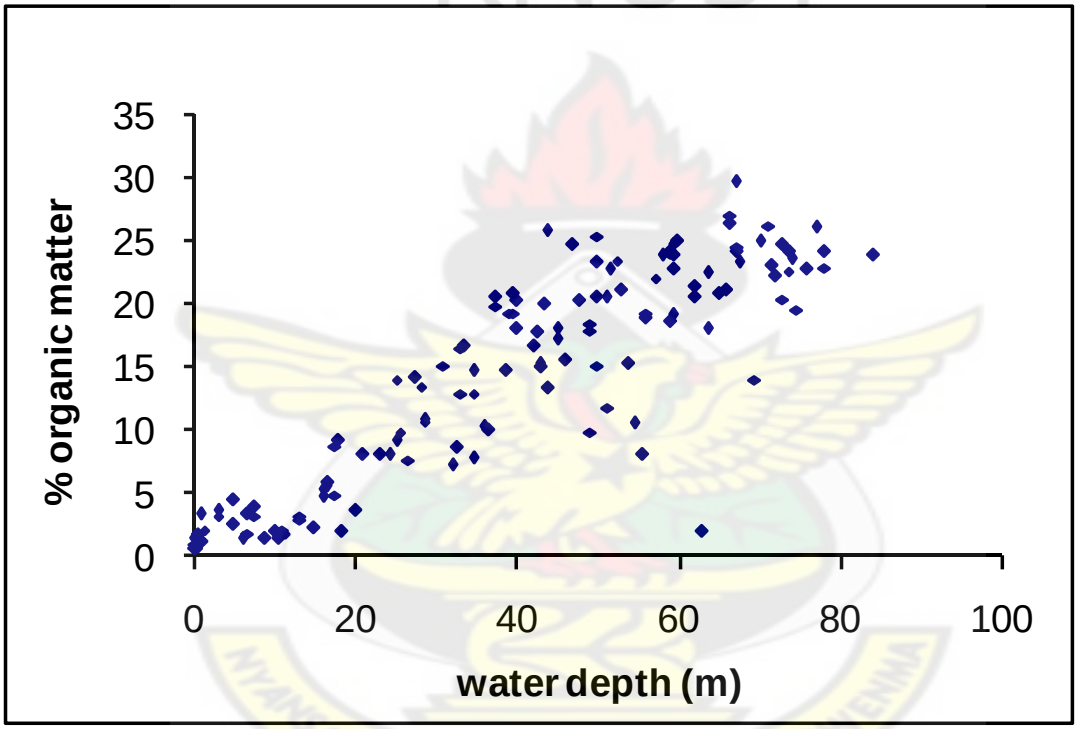

Figure 4.1 c A plot of percentage organic matter against water depth.

The spatial plot (Fig. 3.8 a), however, shows percentage organic matter values increasing with increase in water depth (i.e., a contribution from the slope geometry) in all direction on the lake (NS, SN, EW and WE). In general, the increase in values are concentrated at water depths when moving along the East – West and the Southeast – Northwest transects.

In general, slope geometry, such as slope angle, length and curvature are known to influence runoff, drainage, soil temperature and soil erosion and therefore soil formation (Aandahl,

1948). The difference in soil formation however, along hill-slope in the lake as depth increases will result in significant differences in soil properties (Brubaker et al, 1993), such as nutrients, etc, which significantly affect crop yield (Jones et al, 1989) and therefore organic matter. The amount of water held by soils or sediments at depth, increases because, increasing organic matter content of soils, usually increases total porosity and therefore, decreases bulk density. There is therefore an increase in the water content of the samples collected with increase in water depth because organic matter provides much of the sediments capacity to store nutrients and water. Therefore, as the organic matter content increases with water depth, it is expected that the water content of the samples to also, increase (Hillel, 1980).

Most arable soil which can be likened to the soils in the catchment area of the lake, are known to contain only 2 or 4 % organic matter by weight, yet very little about these soils is not significantly influenced by the organic matter. The higher percentages of organic matter in the deeper water could therefore must have resulted from biogenic activity (from lake algae) in the water (Magdoft & Wiel, 2004).

4.2 THE MAGNETIC PARAMETERS MEASURED

4.2.1 THE SUSCEPTIBILITY, ARM AND SIRM RATIOS

The Figs. 3.15 and 3.16 under section 3.3.3.2, show the spatial plots of the distributions of low frequency susceptibility (χ_{lf}), and percentage frequency dependence (%χ fd), of magnetic concentrations of samples as water depth increases. The χ_{lf} values generally increase with increasing water depth. However, the eastern half of the map gives a considerably higher susceptibility values than the other areas with the low values concentrated at the northwestern portions of the lake around Abonu (shallow water sites). Although, χ_{lf} values are generally low at the shore, it varies with increasing values as one moves southwards along the shore. Figure 3.16 shows no peculiar trend in the %χ fd values as water depth

increases. However, there is a general concentration of higher values in the eastern section and then to the south-southeast section of the map, giving values like 10.22, 14.31 etc.

Susceptibility values generally increase with increase in water depth to about a depth of 48 m and then reach a saturating value as shown by the figure below (Fig. 4.2 a). There occur two abnormal susceptibility signal values of 92.5 and 8.4 at depths of 50 m and 63 m corresponding to samples GR2-6A and GRC-30A respectively.

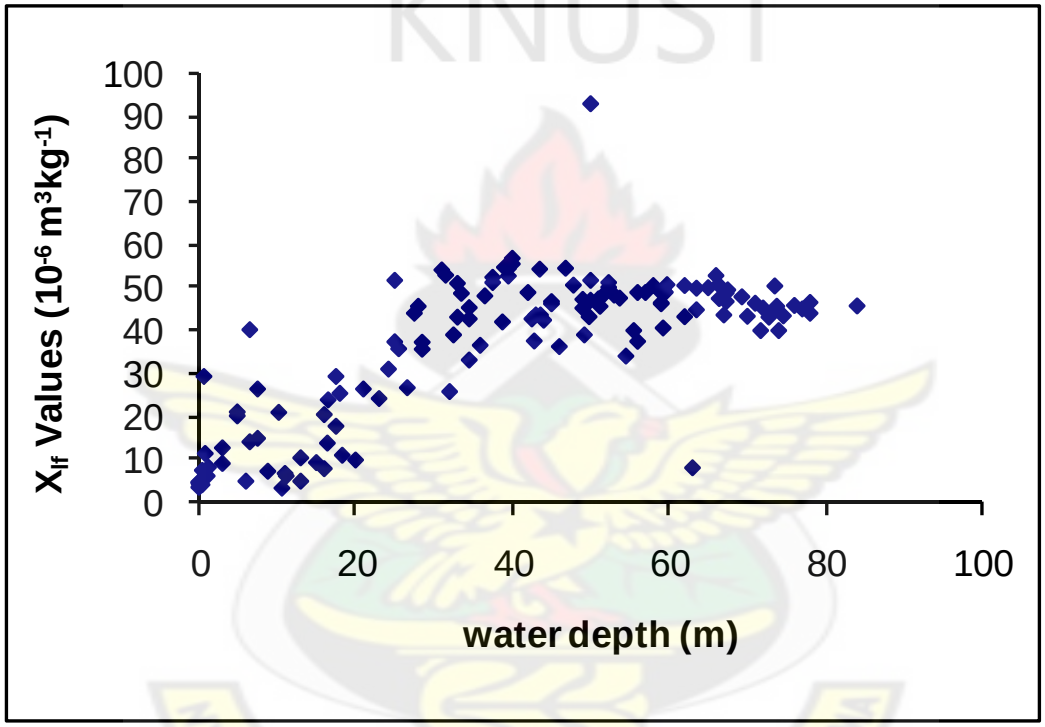

Figure 4.2 a A plot of low frequency susceptibility against water depth.

These susceptibility values therefore suggest that, the grain size fractions of the sample are evident with more multi-domain grain sizes or show the presence of super-paramagnetic mixture grain size fractions as water depth increases (Banerjee, 1989). It can be inferred from the graph that, sample GR2-6A has the highest multi-domain or super-paramagnetic mixture grain size fraction whilst GRC-30A has very low multi-domain or super-paramagnetic mixture grains at deep waters.

Figure 4.2 b, shows the variation in the percentage frequency dependence of the susceptibility measured on samples. It is observed from the plot that there is a decrease in value at water depth of 15 m. This is followed by a gradual increase, with all values measured concentrated around 9.5 as water depth increases beyond 27 m. However, there occur four points with wild frequency dependence values. These points and their coordinates are as follows: BA-1B (0, 12), BA-4B (0.17, 28), GR2-67A (16.00, 1.22) and GR2-54A (33.00, 14.31). The low χ values with corresponding high χfd values are of no importance because measurement is influenced heavily by machine error.

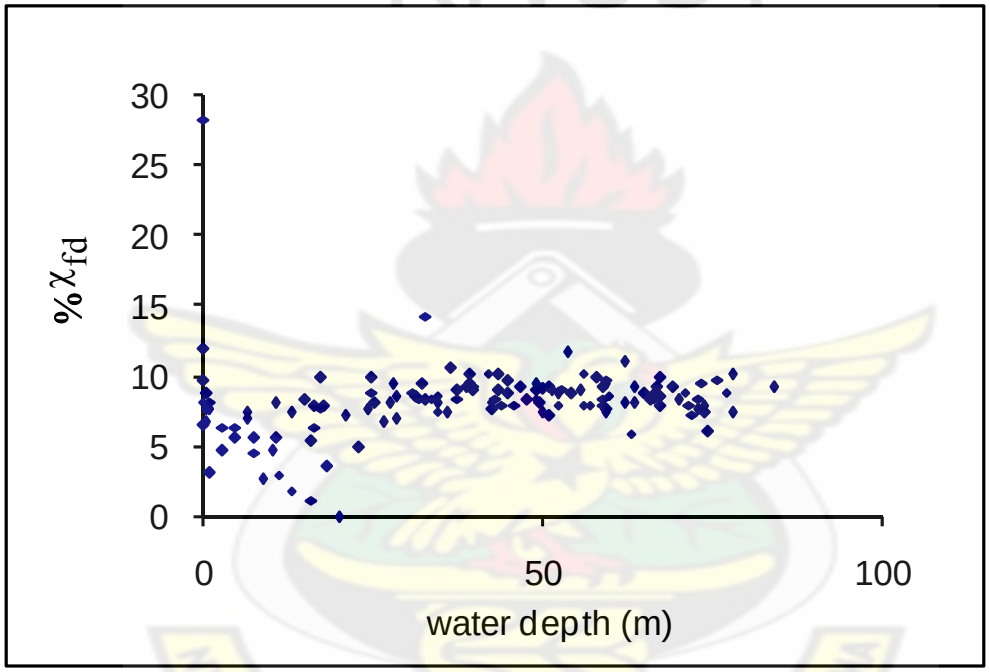

Figure 4.2 b A plot of percentage frequency dependence measurement on samples against corresponding water depth.

The ARM values measured on the samples are shown in Figure 4.2 c. This shows a general increase in values with increase in water depth. Up to 20 m of water depth, the plot shows ARM values between the ranges of 9.69×10^{-6} Am^2kg^{-1} to 196.44×10^{-6} Am^2kg^{-1}. The limits increase from 130.23×10^{-6} Am^2kg^{-1} to 691.83×10^{-6} Am^2kg^{-1} as water depth varies from 21 m

to 71 m. The graph reveals an abnormality in the measured values at 50 m and 63 m with values 871.71×10^{-6} Am^2kg^{-1} and 29.34×10^{-6} Am^2kg^{-1}

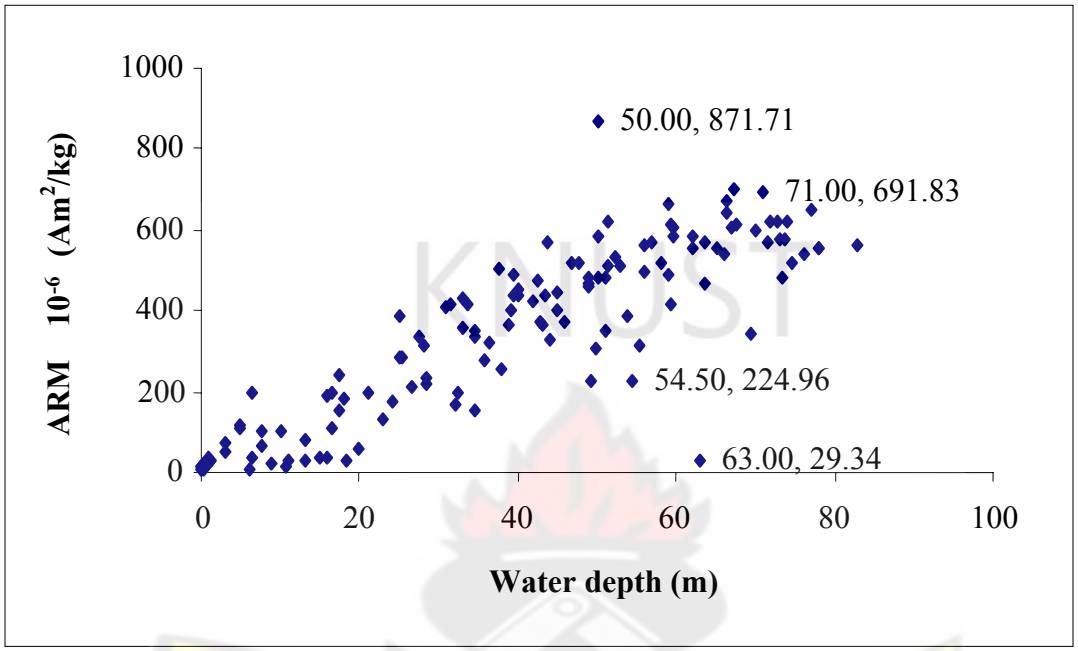

Figure 4.2 c A plot of ARM (10^{-6} Am^2/kg) against water depth

Deductions from the graph are that, there is a mixture of grain size (its being single, pseudo-single and multi-domain) fractions at shallow waters, depth up to 20.00 meters. The grains size then starts decreasing with increase in water depth since increase in ARM value, is an indication of the presence of pseudo-single domain to single domain grain size assemblage (Banerjee, 1989; Michael, et. al., 2003).

The graph of χ_{arm} in Fig. 4.2 d shows the same trend as described under Fig. 4.2 c.

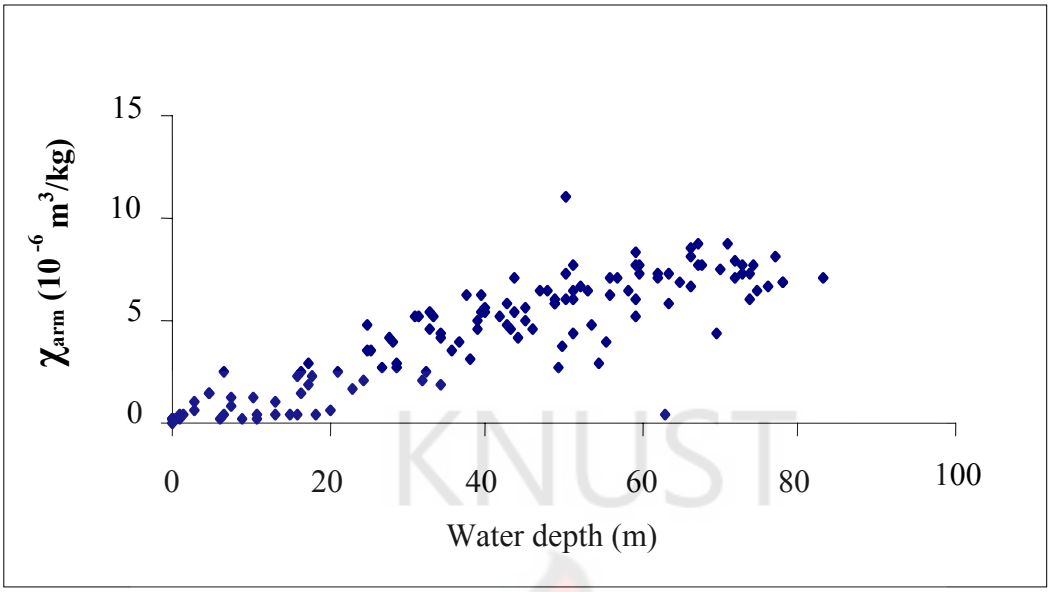

Figure 4.2 d A plot of χ_{arm} (10^{-6} m^3/kg) against water depth

The plot below (Fig.4.3 a), shows a general increase in the value of the ratio $\chi_{arm}/_{SIRM}$ computered with water depth. The higher values with increase in water depth are suggestive of the presence of super-paramagnetic mineral grain size fractions on the increase, along with increasing water depth because $\chi_{arm}/_{SIRM}$ is a grain size indicator for super-paramagnetic minerals (Banerjee, 1989).

Figure 4.3 Plots of (a) χ_{arm}/SIRM, (b) bIRM/SIRM, (c) ARM/SIRM and (d) HIRM computered from the experimental results on samples against water depth.

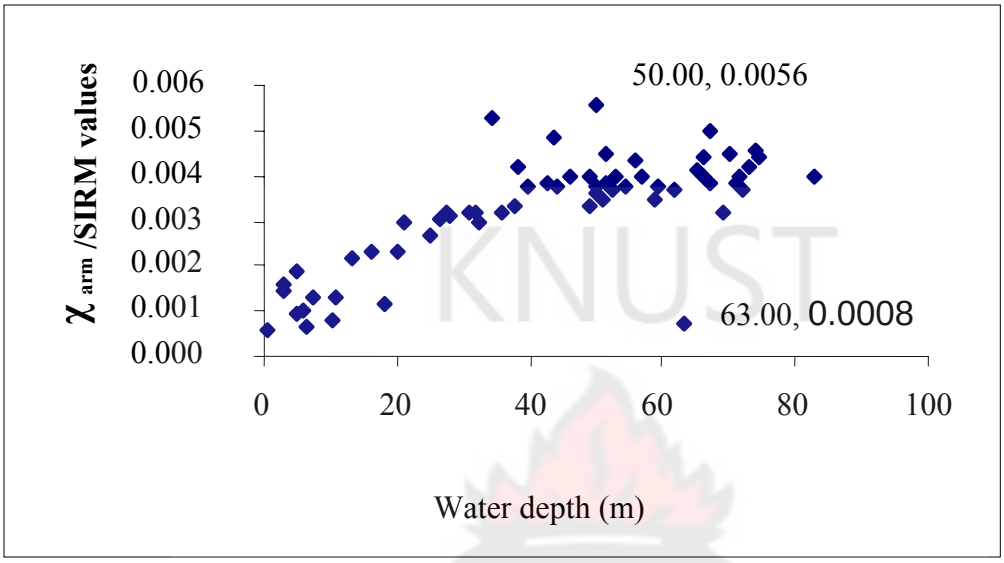

Figure 4.3 a A plot of χ_{arm}/SIRM against water depth

The highest value of the ratio occurs at 50 m depth as 0.0056 with the lowest at 63 m water depth, labeled on the plot (Fig. 4.3 a).

From (Michael, et. al., 2003), the S – ratio given by IRM $_{40\ mT}$/IRM $_{1100\ mT}$, measures the relative amounts of high-coercivity ("hard") remanence to low-coercivity ("soft") remanence.

The plot of S – ratio values against variation in water depth is as shown in Fig. 4.3 b below.

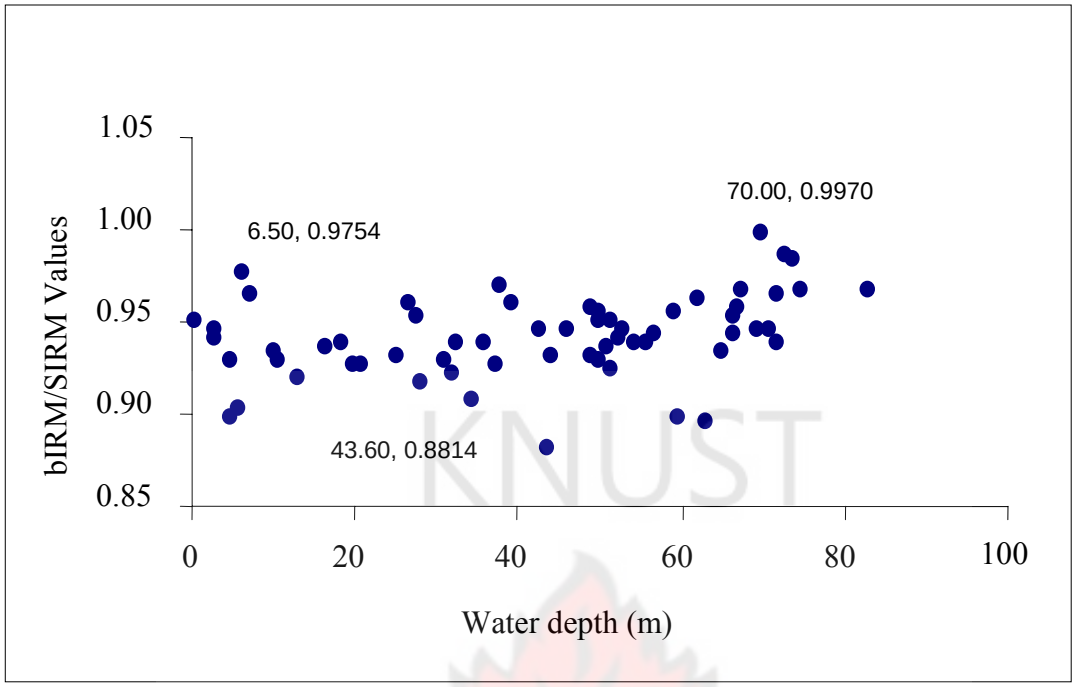

Figure 4.3 b A plot of back IRM/SIRM against water depth.

The S – ratio values plot between 0.8814 at 43.60 m depth and through 0.9754 to 0.9970 at 70.00 m depth. Inference can therefore be made that the samples have remanence dominated by soft ferrimagnetic minerals (e.g., magnetite), since S – ratios plot very close to unity (Michael, et. al, 2003).

The graph (Fig. 4.3 c), shows a general increase in values for the anhysteretic remanent magnetization to saturation isothermal remanent magnetization ratio (ARM/SIRM), computered on the samples with increasing water depth. At 63.00 m depth, the sample taken, registers a relatively low value of the ratio as 0.048, which reveals an abnormality in comparison to the general trend of the measured values in the same region.

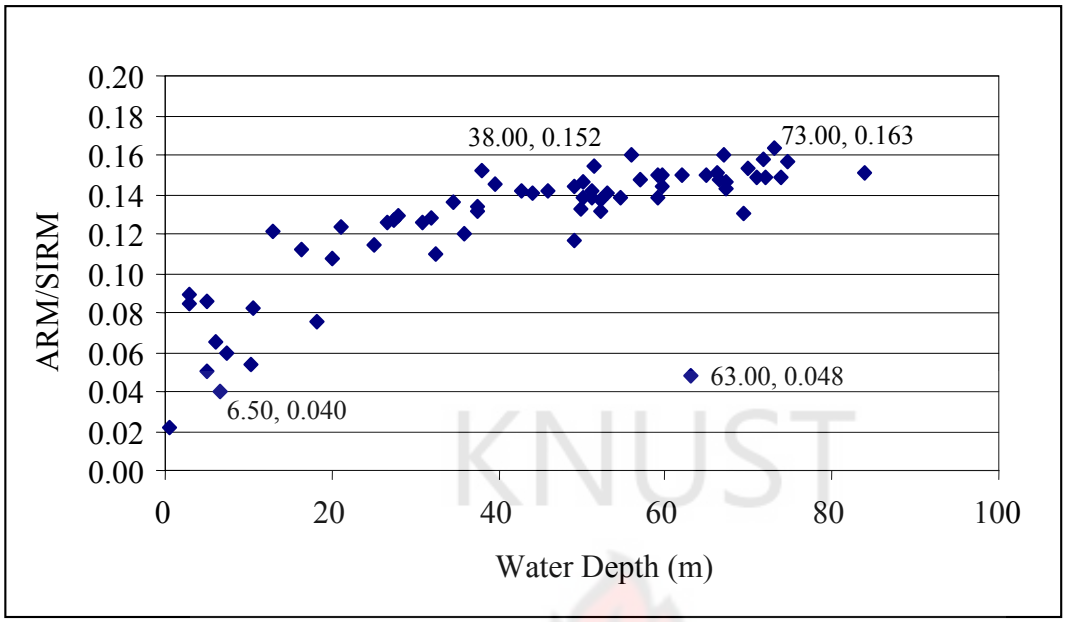

Figure 4.3 c A graph of ARM/SIRM ratio against water depth

Magnetic grain size fractions are coarser (multi-domain) at shallow depths of water (from graph, between water depths of, 0 – 20 m), while water depth increases with higher fraction of single domain (SD) to pseudo-single domain (PSD) particles. The sample GRC – 50A, however will have higher fraction of multi-domain (MD) grains than SD or PSD grain size fractions (Michael et al., 2003).

The plot of the HIRM values shows no peculiar variation with water depth. At both deep and shallow waters, the graph shows high and low values with the highest HIRM value of 206.24×10^{-6} Am^2kg^{-1}. However, values are generally high and concentrated between water depth of 30 m and 74 m (Fig. 4.3 d).

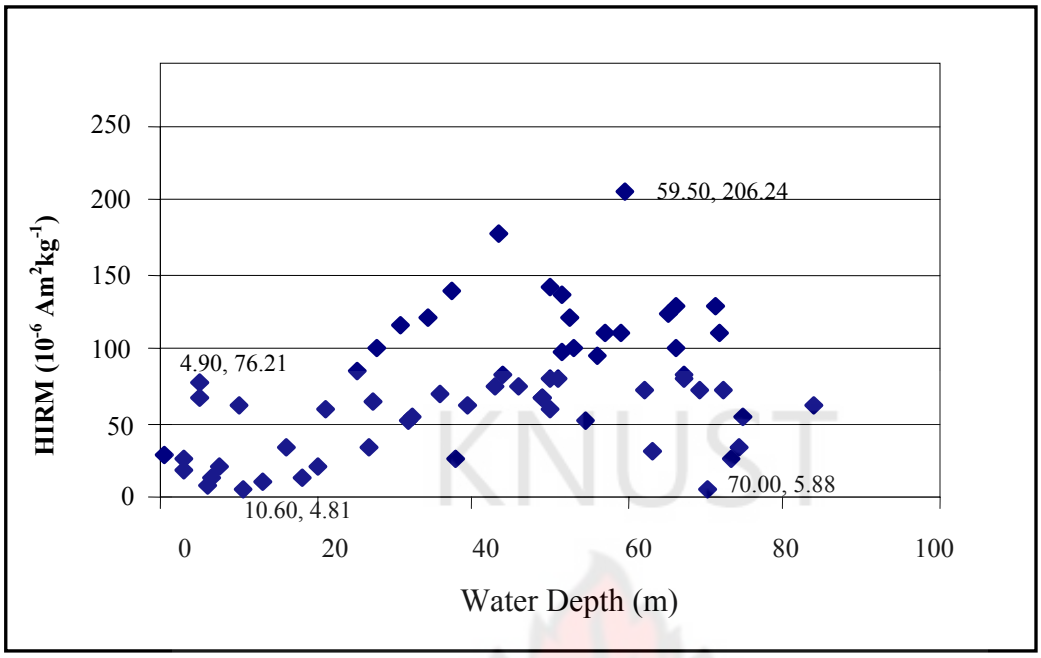

Figure 4.3 d A plot of HIRM values against water depth.

4.2.2 THE DEMAGNETIZED ANHYSTERETIC REMANENT MAGNETIZATION

Figure 4.4 below is the graph of AF demagnetizing values against the demagnetizing field for eight samples. It is observed from the graph that all the samples demagnetized, almost gives off their remamence at the peak field of 100 mT. The rates at which the remanence is given off from the graph is suggestive of the presence of increasing magnetic mineral grain fractions with low coercivity with increasing water depth. Sample GR-2A, which was sampled from a very shallow water depth, appears to ease off its remanence with difficulty than a comparable sample from relatively deeper depth of water, i.e., sample GR-20A.

The deduction here is that, the samples from shallow waters could possess higher fractions of magnetic particles with higher coercivity and this coercivity, decreases with increase in water depth.

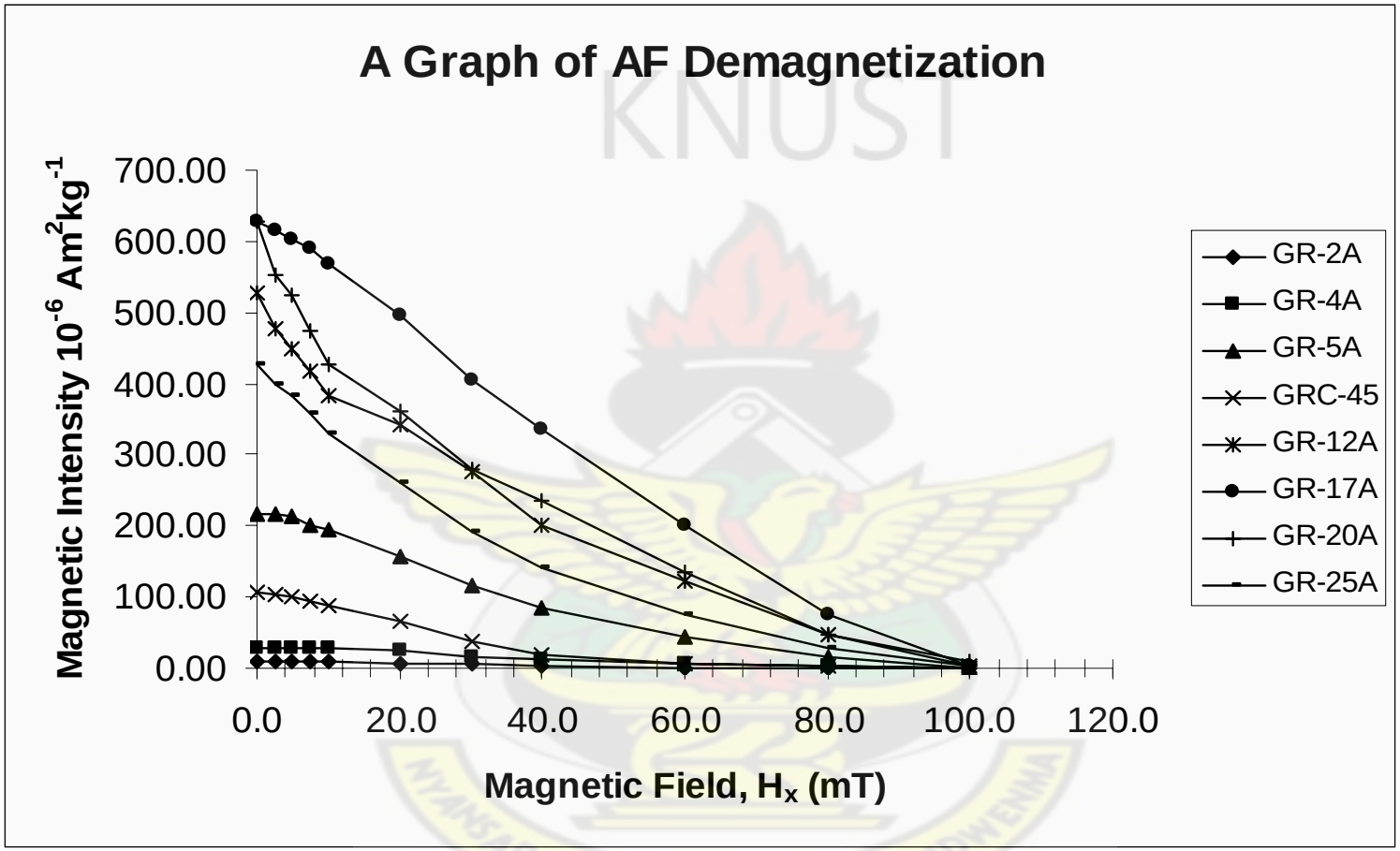

Figure 4.4 A graph showing how the Anhysteretic Remanent Magnetization AF Demagnetization of samples trends

4.2.3 ACQUISITION AND DEMAGNETIZATION OF IRM MOMENT.

Figures 4.5 'A' and 'B', show the graphs of the acquisition of isothermal remanent magnetization (IRM), imparted and the corresponding demagnetization of the imparted IRM of the samples respectively.

From Fig. 4.5 A, it is observed that samples at higher depth of water acquire remanence with difficulty reaching a saturation with the largest value at 4186.3204 * 10^{-6} Am^2kg^{-1} at 74.00 m, followed by 3016.4016 * 10^{-6} Am^2kg^{-1} when water depth drops to 39.50 m. At the shallowest water depth of 10.60 meters, the saturated value of 135.1313 * 10^{-6} Am^2kg^{-1} was reached. The demagnetization plot (Fig. 4.5 B), on the other hand, shows the same trend with samples at deeper depths easily giving off their remanence as compared to samples taken from shallow depth (values from Table 3.7 B).

This observation suggest the presence of higher fraction of multi-domain grain size magnetic minerals in samples taking from deeper water depths than those sampled from the shallow water depths.

Figure 4.5 (A) The trend shown in samples acquiring isothermal remanent magnetization when subjected to the same magnetic field strengths at ambient temperature.

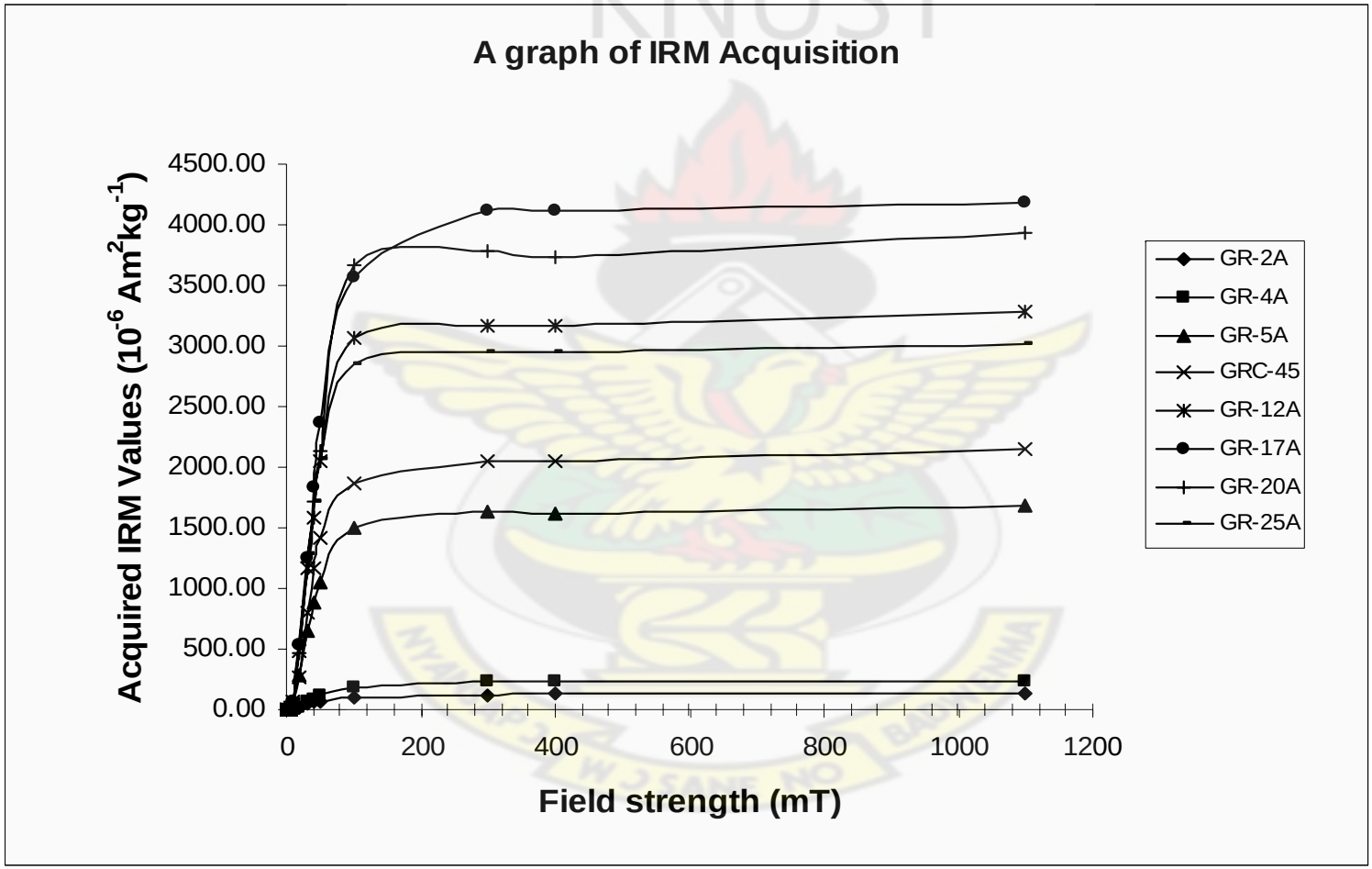

Figure 4.5 (B) A graph showing how the Isothermal Remanent Magnetization AF Demagnetization process of samples.

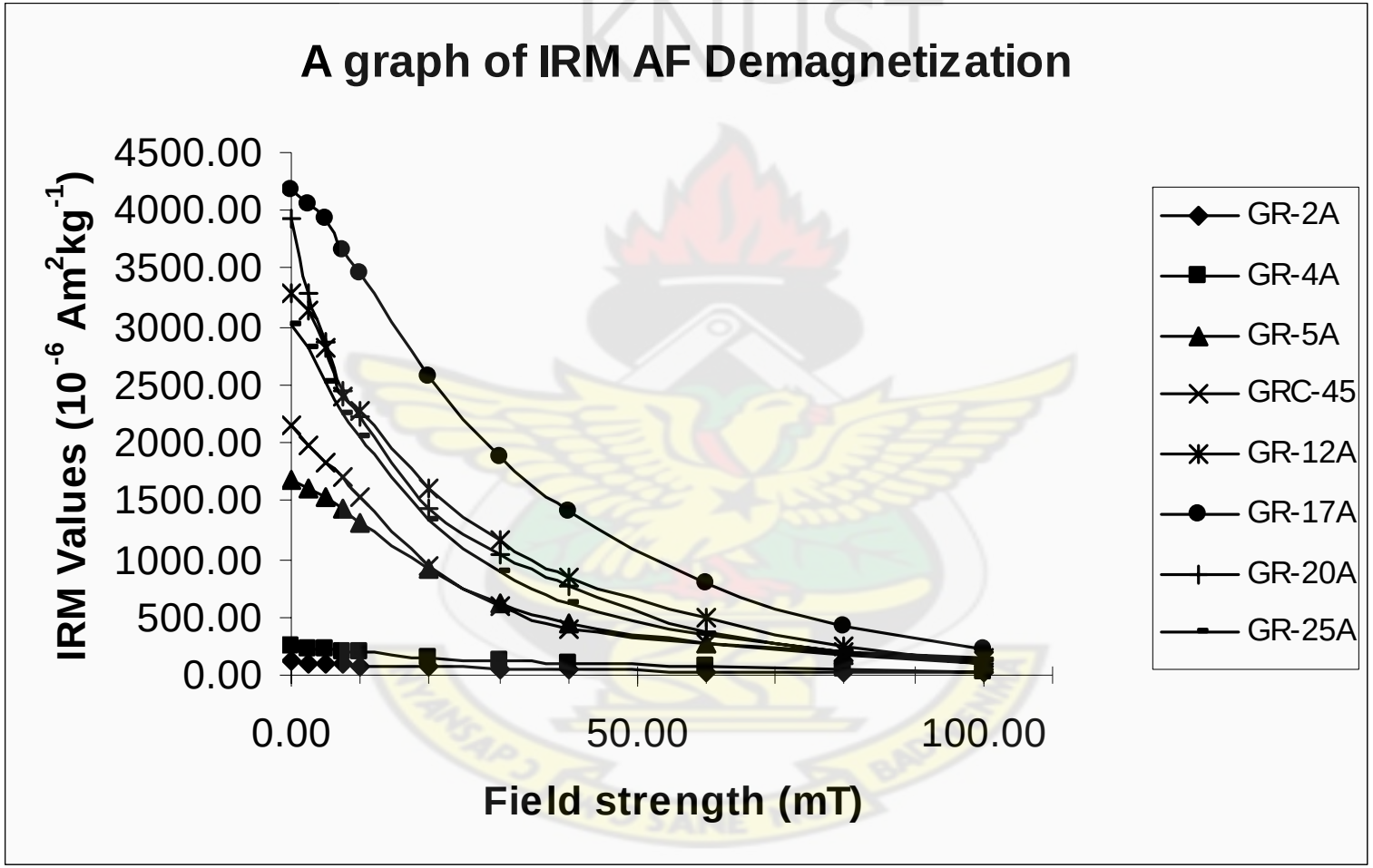

4.2.4 IMPARTED SIRM AND DIRECT CURRENT DEMAGNETIZATION OF THE SIRM MOMENT

Figure 3.18 shows a graph of saturation isothermal remanent magnetization (SIRM) for all 68 samples. It is observed that the samples acquire more remanence as and when the field strength was increased from 40 mT to 1100 mT. However, on applying a backfield (i.e., -300 mT), the magnetization deflects in the opposite direction with the higher peaked values now reading the least.

Figure 3.19, shows a graph of SIRM demagnetization for twenty of the samples from amongst the sixty-eight magnetized. It is realized also from Fig 3.19 that, the sample at depth 13.0 m gives off remanence relatively with difficulty than those samples from deeper depths of water. Table 4.1, gives a summary of the extracted values of remanence coercivities (H_{cr}) from the graphs in Fig. 3.19.

Table 4.1 Showing the Remanence Coercivity (H_{cr}) values extracted from the plotted graphs.

Sample	Water depth (m)	H_{cr} Values (mT)
GRC-45	4.90	28.50
GRC-32	6.50	19.50
GRC-40	7.50	22.50
GRC-3	10.20	23.50
GR-2	10.60	32.00
GR-4	13.00	40.05
GR-5	26.60	30.00
GRC-48	35.90	29.00
GR-25	39.50	27.00
GRC-25	44.00	29.50
GRC-12	49.20	26.00
station F	52.30	30.00
GR-10	56.00	33.00
station A	59.00	35.50
station D	67.30	34.00
GR-20	70.00	30.10
GR-18	71.70	33.00
GR-17	74.00	36.00
GR-12	74.60	30.00
GR-15	84.00	32.00

It is shown from the table that, the samples have remanence coercivity values ranging from -19.50 to – 40.05 mT.

These values (i.e., H_{cr} extracted) of the samples when plotted, showed that, the remanence coercivity values varies with depth of water variation (Fig. 4.6).

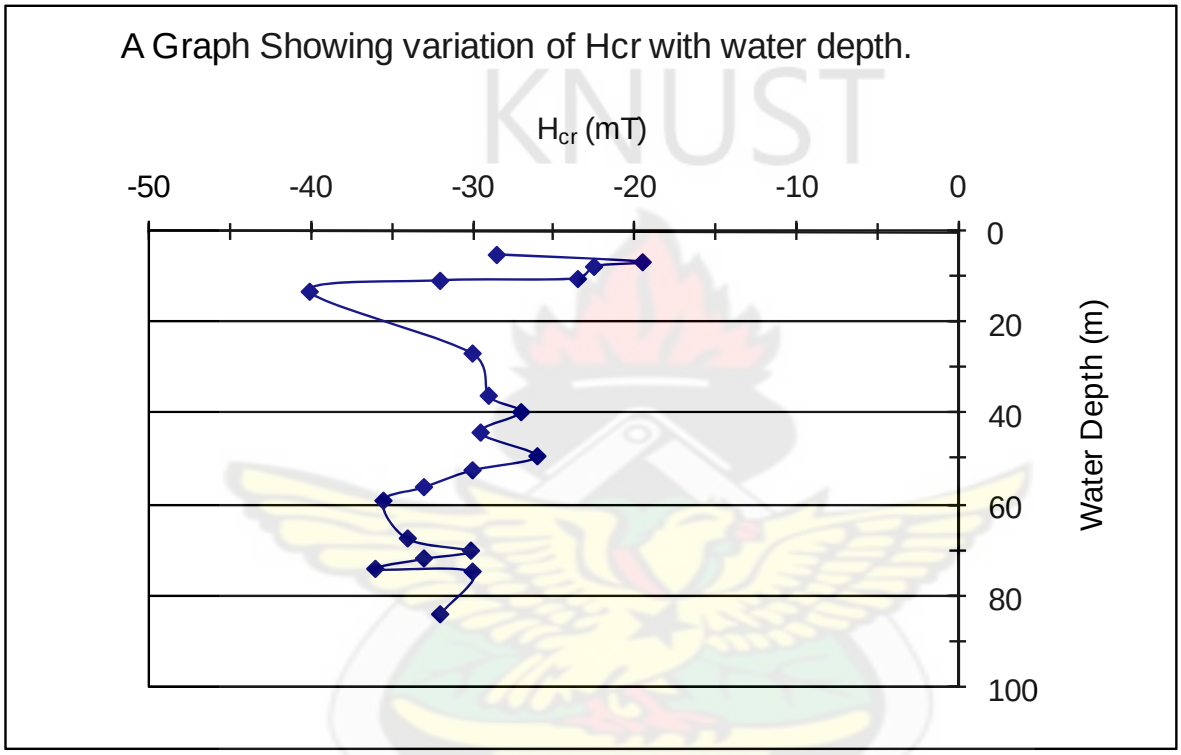

Figure 4.6 Magnetic remanences coercivity variation with water depth for the twenty samples demagnetized.

It is observed from this graph a general increase in the coercivity value of the samples with water depth. However, there occurred a high peak at depth 13.00 m, which corresponds to sample GR – 4A. This high peaked value could result from accumulation of a strong magnetic mineral grain. This value although appears abnormal and distorting the general trend of increase in the values with water depth, does not fall out of range of values within which magnetite for instance could plot, since coercivity of magnetite plots within the range of 10 mT (for multi-domain) to 100 mT (for small grains) (Thompson & Oldfield, 1986).

The trend of increasing remanence coercivity values with increase in water depth shows that magnetic mineral grain sizes generally decreases from coarse grain sizes at shallow water depth to finer grain sizes at deeper water depth.

4.3 HYSTERESIS MEASUREMENT

Table 3.11 under section 3.3.8.3 shows extracted values from the hysteresis experiment performed on the selected samples. The table has in columns five and eight, the calculated values of;

I. The coercivity ratio of coercivity of remanence to saturation coercivity Hcr/Hc and
II. The magnetization ratio of saturation remanence to saturation magnetization Mr/Ms respectively.

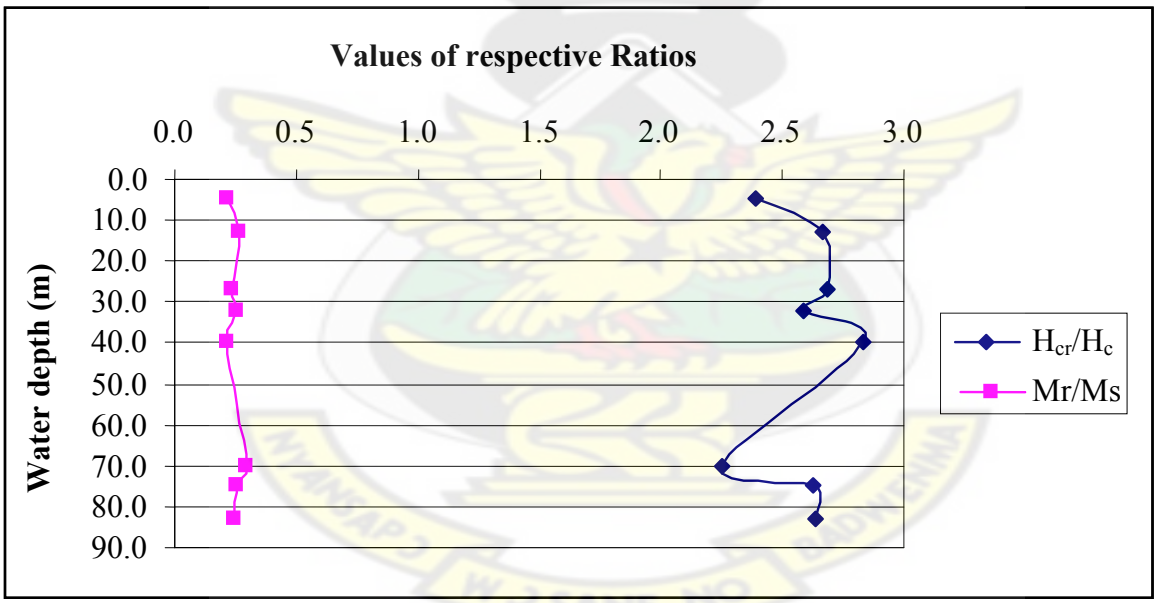

Figure 4.7 The variation of Coercivity and Magnetization ratios with water depth.

Figure 4.7 consequently shows the variation of the ratios with water depth. From this graph, an increase in both the magnetization ratio and coercivity ratio are shown with the variation being prominent in the coercivity ratio. However, there is a sharp decline in coercivity ratio from 2.83 to 2.25 at depth of 70 m of water, which is very relevant in that the lower value (i.e., 2.25) resulted from the sample GR – 20A that was taken from the 70 m water depth at

the eastern portion of the lake. Further at 39.5 m water depth, the coercivity ratio value was as high as 2.62 for the sample GR – 12A. The magnetization ratio however shows a corresponding increase in value as the coercivity ratio falls at the 70 m depth, which suggests for the presence of pseudo-single domain grains.

The relatively small coercivity values suggest the presence of coarser magnetic mineral grain fractions since multi-domain magnetite grains plot around the value 10 mT (Thompson & Oldfield, 1986). To ascertain the true nature of the magnetic mineral grain sizes present in the samples, the magnetization ratio was plotted against the coercivity ratio (after Day et al., 1977) in Fig. 4.8 shown below.

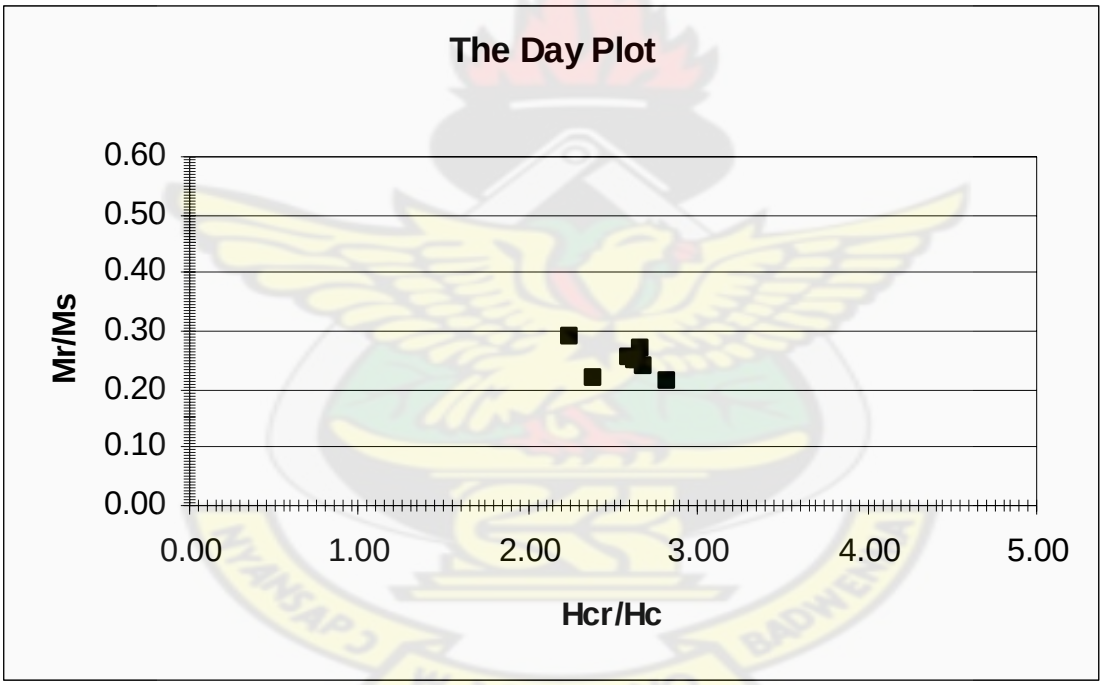

Figure 4.8 Day plot (after Day et al., 1977) on the selected samples from the lake.

The samples plot in the pseudo-single domain region of the graph (i.e., 1.5 – 4.0 for H_{cr}/H_c and 1.0 – 5.0 for M_r/M_s) (Thompson & Oldfield, 1986; Michael & Heller, 2003; The IRM Quarterly Fall, 2003).

The suspicion therefore of the presence of multi-domain grain size fraction in the sample is eliminated by the Day plot.

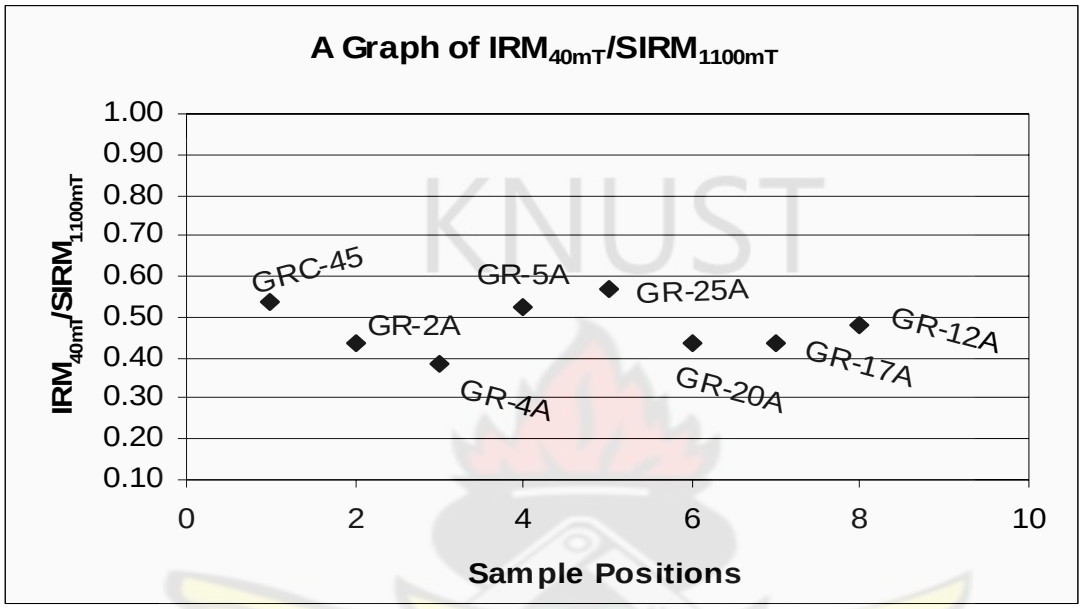

Figure 4.9 The distribution of eight samples of different magnetic stabilities.

Considering the plot of stability ($IRM_{40\ mT}/SIRM_{1100\ mT}$) values computered on the samples in Figs. 4.9 and 4.10, it is realized that, all eight samples plot within the range 0.39 – 0.57. The deduction is that, the lake magnetic materials have hardness of which suggest the presence of mineral types like greigite and magnetite. However, the harder materials are shown concentrated around the 13.00 m water depth.

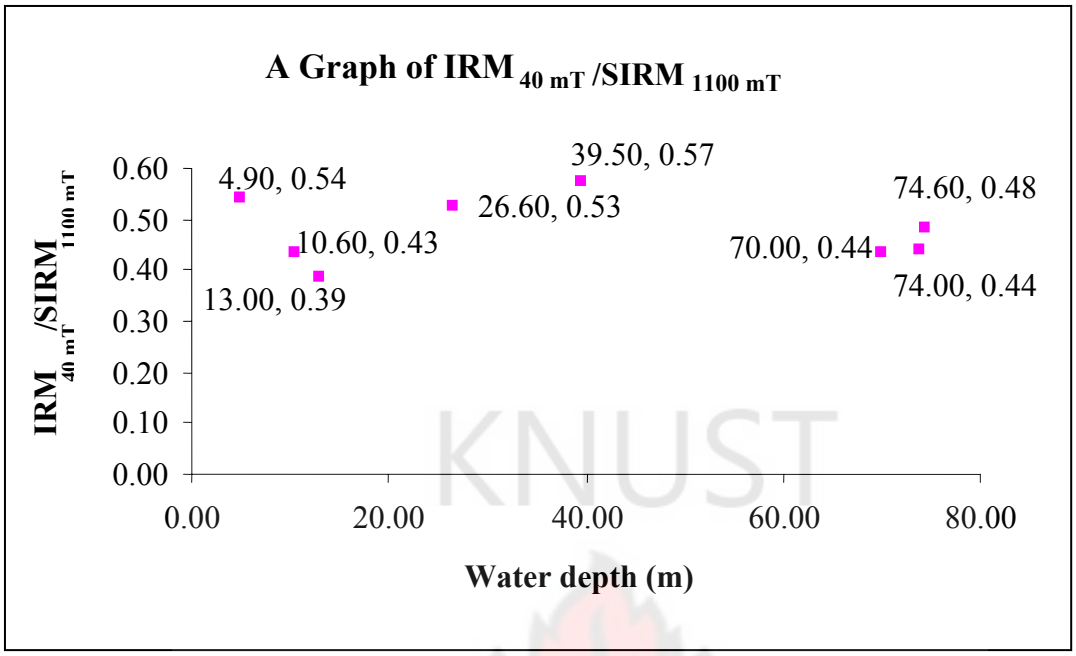

Figure 4.10 Plot of values from Table 3.12 showing the distribution of samples magnetic stability against water depth.

Comparing the plots of sample GR – 4A and GRC – 45 from Figs. 4.9 and 4.10, it is noticed that, samples from the western side of the lake along the GR transect contain higher fractions of magnetically hard materials than those sampled from the southern portion of the lake along the GRC transect (e.g. GRC – 45) at shallow water depth.

4.4 GRAIN SIZE ANALYSIS

Table 3.14 (Appendix L), tabulates results from the grain-size analysis performed on sample BA – 2A. This shows the measured and calculated results from the Ro-tap on this sample out of the twenty–five samples selected.

Table 3.15 (Appendix L), on the other hand, tabulates the values of the calculated statistical parameters on all the twenty-five samples, containing the sample names, water depth, mean grain size values, standard deviation and skewness in the columns 2, 3 & 4, 5, and 6 respectively.

The plot of statistical parameters with water depth is shown in Fig. 4.11 below. The mean grain size values show no trend of interest in the beach samples where water depth is zero. Mean grain size values range between 177 – 350 µm with the beach samples. However, values then drop from 210 µm at water depth 0.07 m at the shore to a value of 44 µm at depth of 0.81 m, shown by sample BA – 6B in Table 3.15. The values then take an increasing trend while water depth increases to the center of the lake (detail plot shown in Fig. 4.12 a).

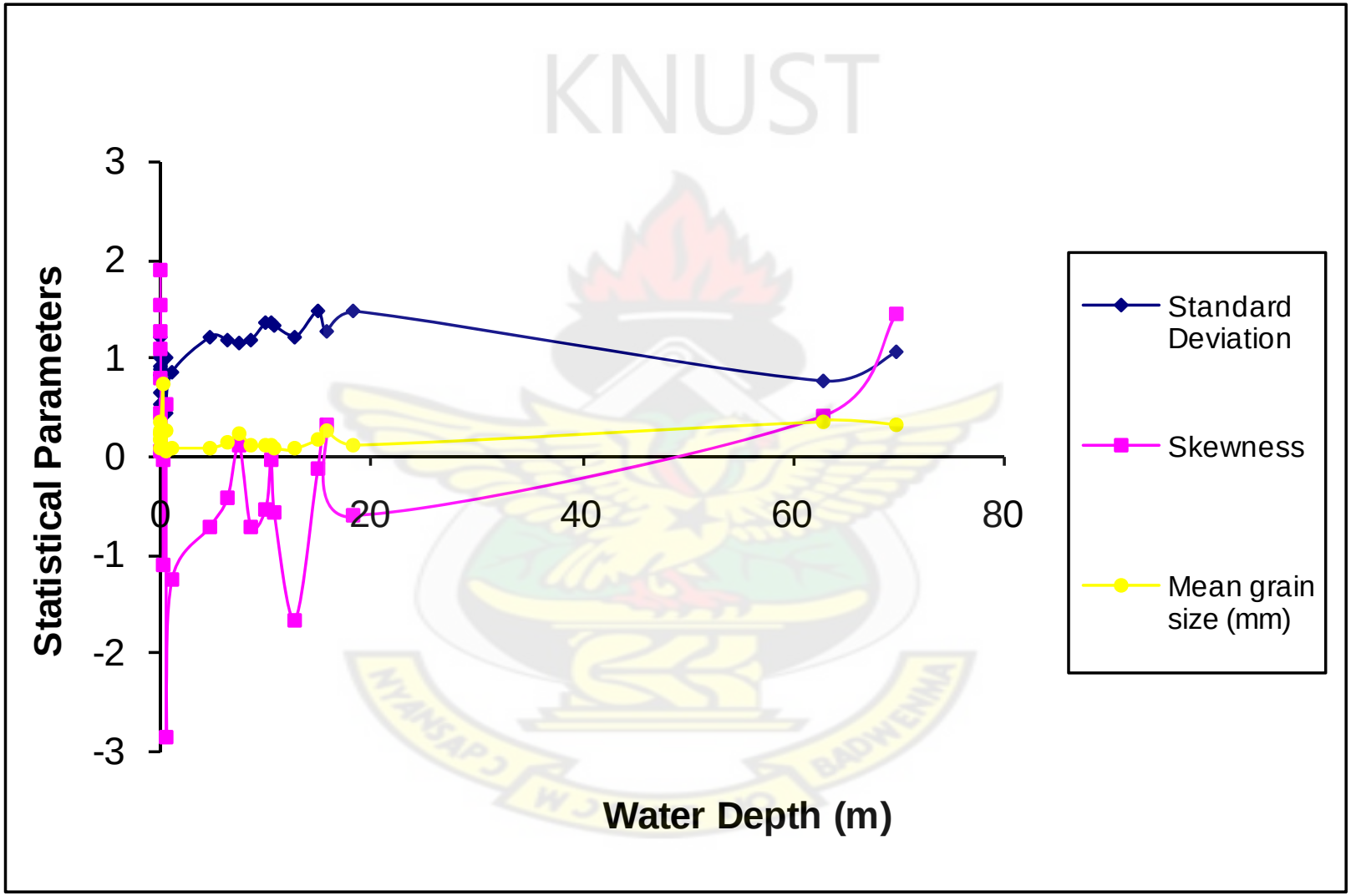

Figure 4.11 A plot of the computered statistical parameters from the twenty-five samples.

Figure 4.12 a Detail plot of mean grain size values (in µm) along the BA, GR, GR2 and GRC transect.

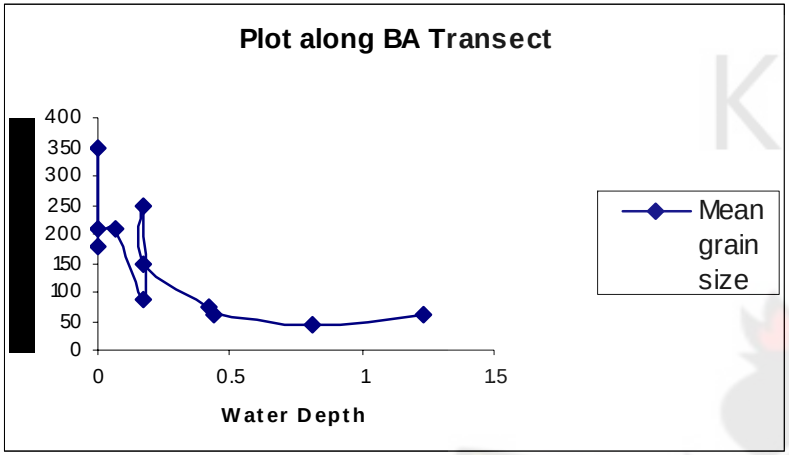

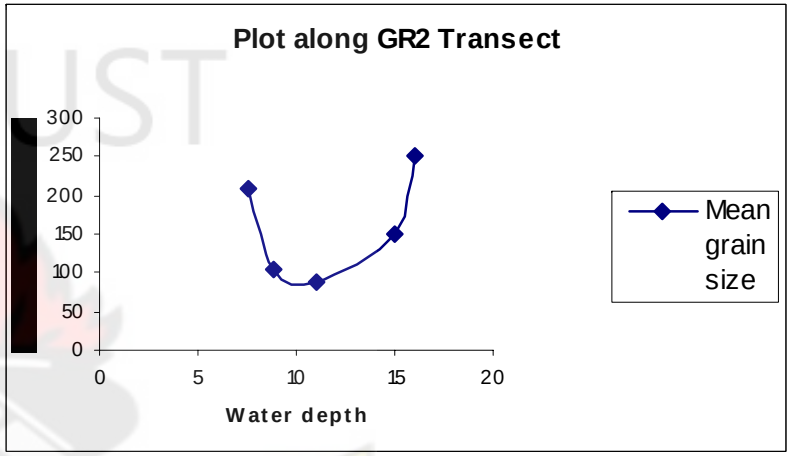

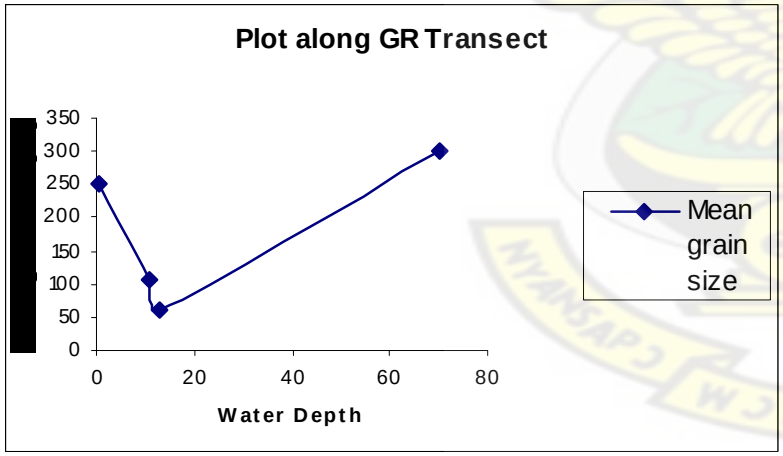

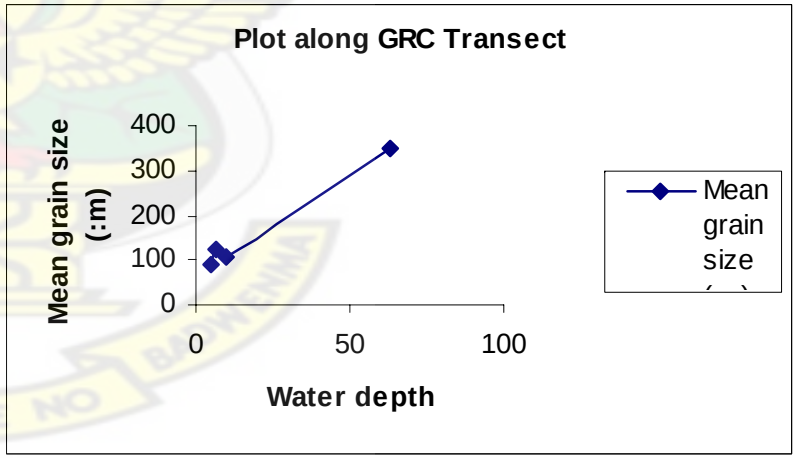

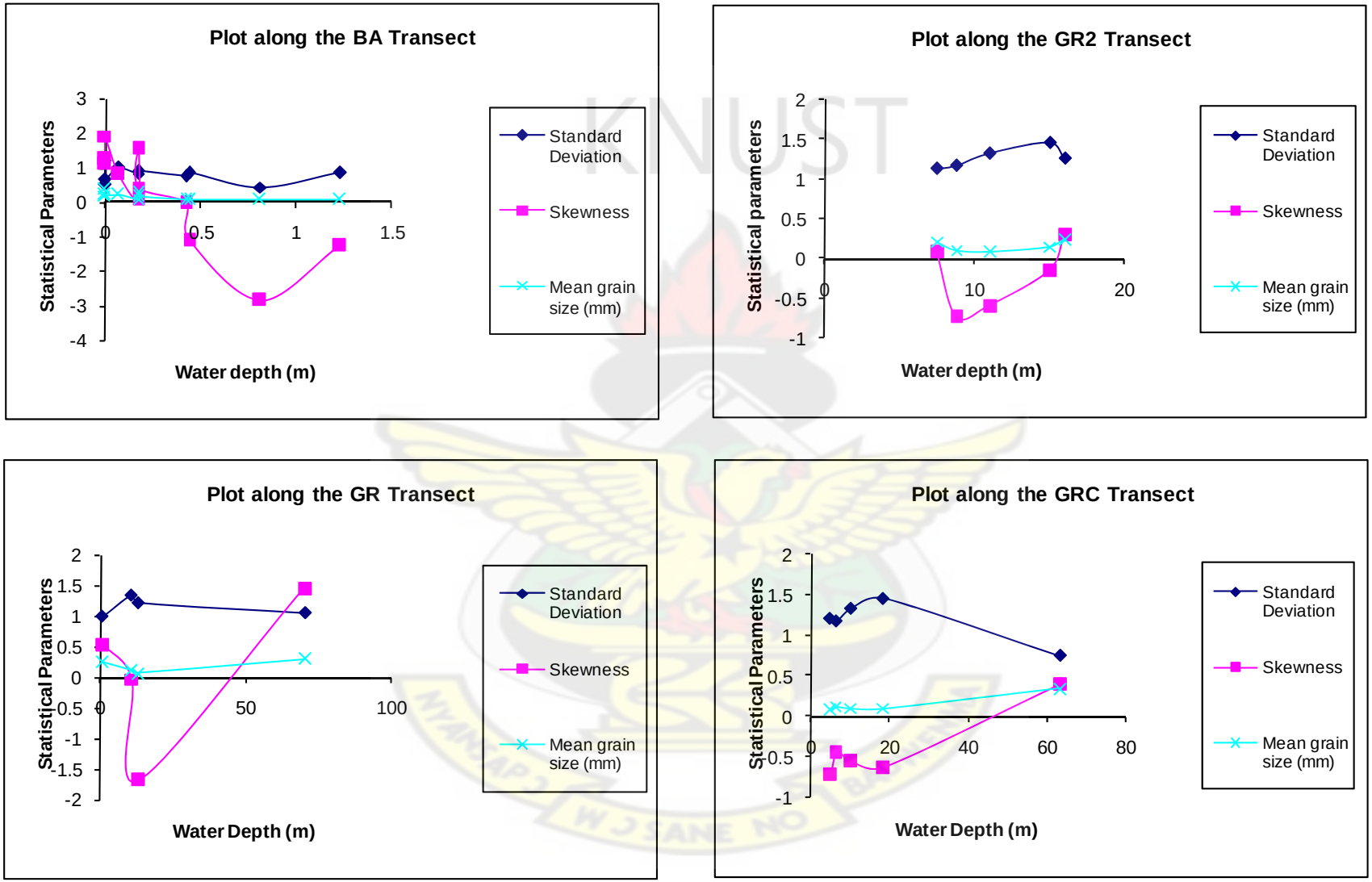

Figure 4.12 b Detail plot of statistical parameter computered on samples showing the trends along the BA, GR, GR2 and GRC transects.

The standard deviation values from the general distribution of grain sizes shows high values when the mean grain size values are low. As mean grain size begins to increase, the deviation values trend in the opposite by decreasing (Fig. 4.11). This variation however, is with increasing water depth. These values (Table 4.1) below, show that, sediments from Lake Bosumtwi are moderately well sorted at shallow water depth, through moderate sorting to poorly sorted at deeper water depths as summarized below (Boggs, 1987).

Table 4.2 Table showing sampling along transect, water depth and the sorting type (Boggs, 1987).

Sampling along Transect	Water depth (m)	Sorting Type
Beach	0.00	Moderately well sorted to Poorly sorted
BA	0.07 - 1.23	Moderately sorted
GR	0.65	Moderately sorted
	10.60 - 70.00	Poorly sorted
GR2	7.50 - 16.00	Poorly sorted
GRC	4.90 - 18.30	Poorly sorted
	63.00	Moderately sorted

The samples are negatively skewed at shallow water depth, which is shown by the plot of skewness values falling below the negative line in Fig. 4.12 b along all transects. The deeper depths show a positive skewness, skewness increasing with depth of water (Fig. 4.12 b).

Considering the lake with a fetch of 8 km (i.e., the diameter of the lake), this will result in a wave height given by;

$$h = 0.105 \times \sqrt{8\ km} \qquad (from\ Eq.3.1)$$
$$= 0.105 \times \sqrt{(8000 \times 100)\ cm}$$
$$= 93.9149\ cm$$
$$= 0.93\ m$$

The lake on the average will have therefore a wave height (h) of 1 m. The wave orbital motion will therefore erode sediment in Lake down to water depth of about 12 m, transporting sediment 12 – 15 m distance and accumulation will be greater than 16 m deep.

4.5 SUMMARY OF DISCUSSION

The co – variations in the magnetic parameters, χ, SIRM, and χ_{arm} on the bulk sediment with water depth for the samples are shown in Fig. 4.2. The generally high values of χ and SIRM suggest that the original detrital magnetic assemblage in the sediment is dominated by ferrimagnetic mineral grains larger than the threshold size for stable single-domain (SD) behavior. The frequency-dependent measurement on χ shows a moderately high value ranging from about 1.22 % to 14.31 %, with extremely high values captured under section 4.2.1.

These suggest that the contribution of superparamagnetic (SPM) mineral grains to the measurement of χ, is generally high at deeper water depth than at the shallow depth, although some very high frequency-dependent measured values occur at the beach of the lake.

The increasing χ_{arm} values with water depth as well as the stability values plotting in the range close to unity (Fig. 4.3 b) also suggest the abundance of ferrimagnetic mineral with increase in water depth. In addition, the $ARM/SIRM$ plot, also suggests the presence of MD grains fractions at shallow water depth and single-domain to pseudo-single domains at deeper water depth (Fig. 4.3 c). Furthermore, a plot of the ARM and IRM AF demagnetization values of samples on the same axes shows a dominance of multi-domain magnetic mineral grain sizes at shallow water depth to single and pseudo-single domain sizes as water depth

increases (Figs. 4.13 A & B). This is because the mean destructive field (MDF) deduced from the ARM curves MDF_{ARM} are observed to be smaller compared to those deduced from the SIRM curves MDF_{SIRM} on samples at shallow depth. Conversely, the MDF_{ARM} are observed to be larger than MDF_{SIRM} with samples collected from the deeper water depths (Fig. 4.13).

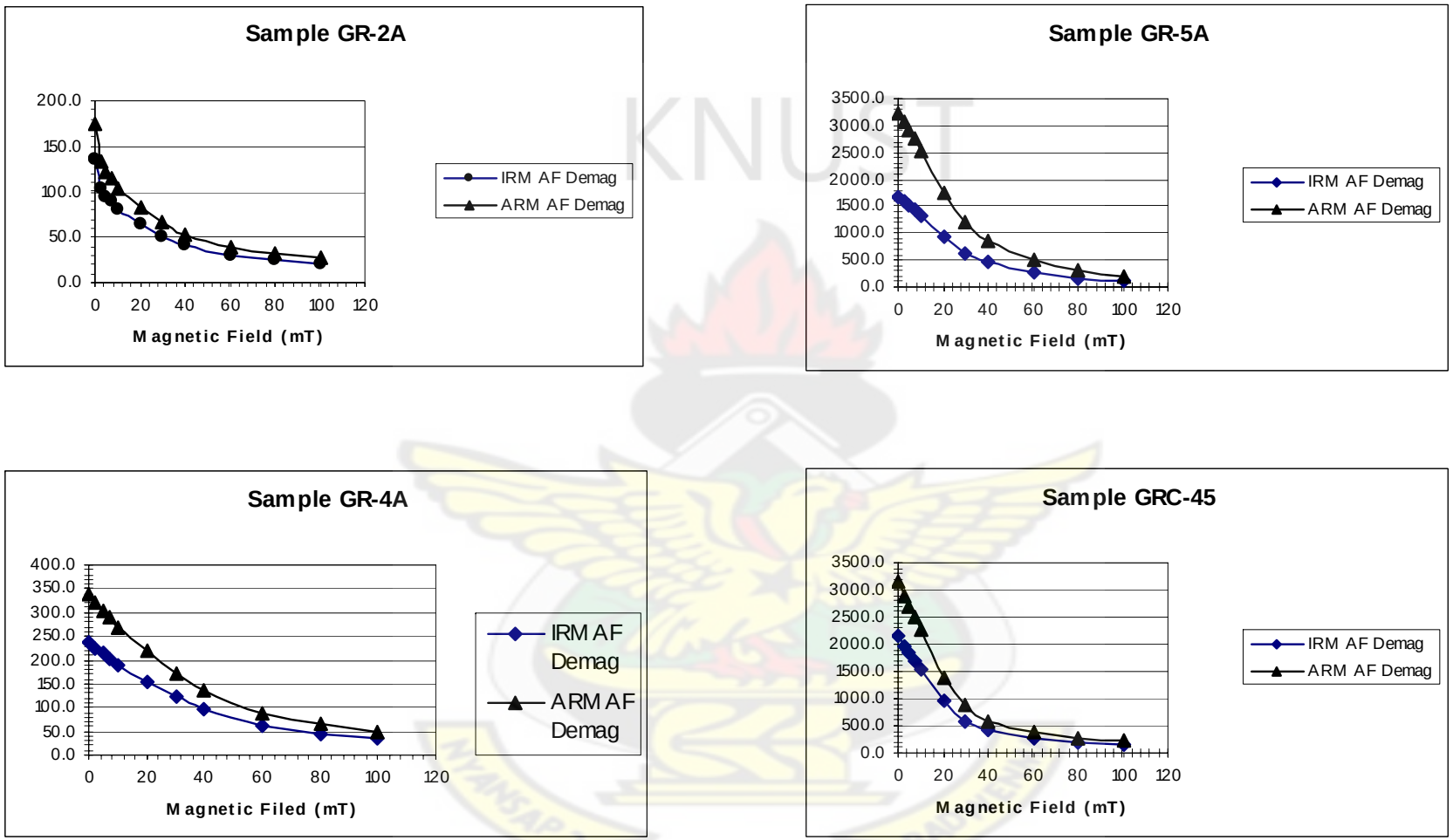

Figure 4.13 A Comparison of ARM and IRM Demagnetization to help determine the magnetic mineral grain size. Samples are from shallow water depth with their $MDF_{ARM} < MDF_{SIRM}$.

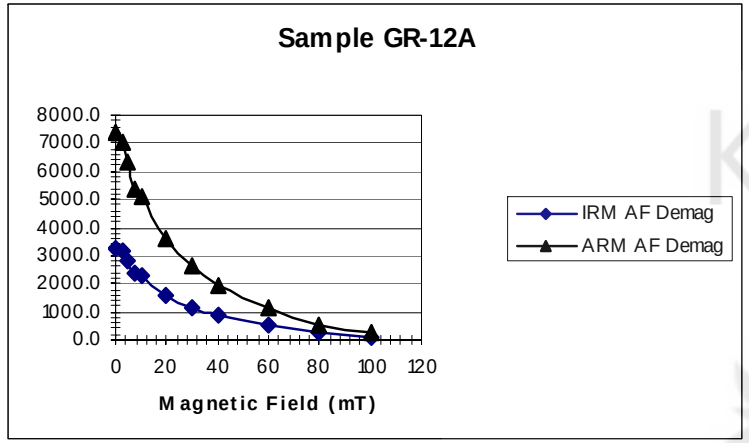

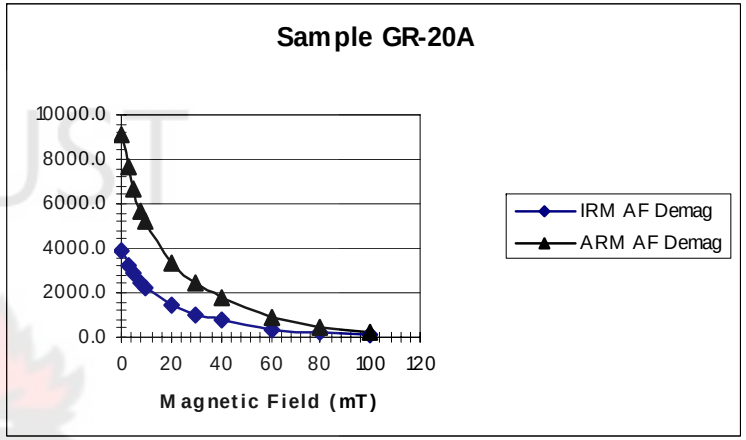

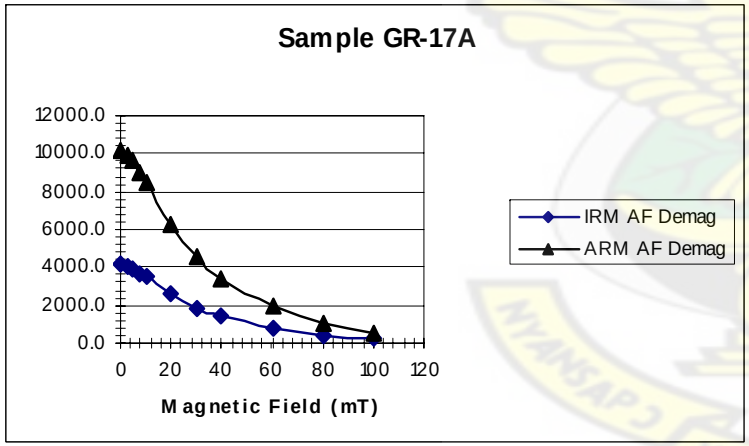

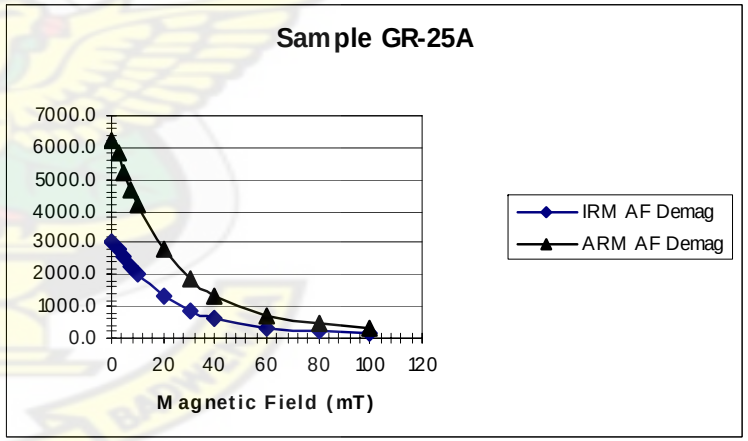

Figure 4.13 B Comparison of ARM and IRM Demagnetization to help determine the magnetic mineral grain size. Samples are from deep-water depth with their $MDF_{ARM} > MDF_{SIRM}$.

The ARM and IRM AF demagnetized curves suggest the presence of low coercivity magnetic mineral such as magnetite and maghaemite at deeper depths since the samples collected from deep waters give off their remanences more easily (Figs 4.4 & 4.5 B). However, the demagnetization graph in Fig. 4.6 shows a general increase in coercivity values with increase in water depth. The higher coercivity value registered by sample GR – 4A at the shallow depth (13.00 m), is rather suggestive of the presence of more stable magnetic mineral grain such as greigite, broken chains or an intact bacterial magnetite chains. This however is certified by the stability plot in Fig. 4.9, giving a value of 0.39 for the sample taken from the 13.00 m water depth (Maher & Thompson, 1999). Furthermore, the coercivity and remanences ratios on the Day plot, clustered samples tightly within the pseudo-single domain region (Fig. 4.8).

The discussion from the grain size analysis (section 4.4), articulates the view that the sediment grain size generally increases with increase in water depth.

CHAPTER FIVE

CONCLUSION AND RECOMMENDATIONS

5.1 CONCLUSION

From the discussions (i.e., sections 4.2.1, 4.2.2, 4.2.3, 4.2.4, 4.3, and 4.4), magnetic mineral grain size is observed to decrease with increase in water depth, while the bulk sediment organic matter content and general bulk sediment grain size also decreases with increase in water depth. It is realized that, at very shallow water depth, the fine grain sand fractions (177 μm) in the bulk sediment are high. The grain size then decreases to very fine sand (88 μm) – coarse silt sizes (44 μm) at water depth 0.17 – 0.81. The grain sizes then maintains its decreasing trend to the higher depths of the lake.

The high values of the measured magnetic parameters (χ, SIRM, ARM etc), together with the ratios computered ($^{\chi}_{ARM}$ and $^{SIRM}/_{ARM}$ etc), show magnetic mineral grain assemblage to be higher in fraction of PSD if not all PSD grains. This is confirmed by the magnetic mineral grains plotting at the PSD zone of the Day plot (Fig. 4.8). This PSD from (Peck et al, 2004), is due to the mixture of SD and SPM grain size fractions. This coupled with the high proportion of low coercivity minerals harness the palaeoclimatic interpretation that, surfacial sediments in the lake to a depth of 8 cm actually accumulated under interglacial conditions of reduced dust flux.

Last and not the least, this research has produced a spatial map of the standings in the dry bulk density, percentage organic matter and percentage water content of the bulk sediment with variations in water depth.

5.2 RECOMMENDATIONS

1. It is recommended that a detailed study into the variation of the organic matter content in the lake: i.e., the cause of the almost stable variation at;
    1. The shallow water depth (up to around 18 m),
    2. The rise between water depths of 20 – 60 m, and
    3. The relative diminutive variation at the center of the lake.

    It is suggested that the variations in the ratios of carbon to nitrogen (C:N) contents of the sediment could be determined. This will give a clue to, and assist in ascertaining the origins of the sediment, because the increase in the C:N ratio within sediment profiles have been interpreted to identify periods in a lake's history when sediments received a high proportion of terrestrial organic matter (Guilizzoni et al., 1996) and conversely, the decrease in the C:N ratio, identifies periods when the lake sediments have received high proportions of algal organic matter (Kanassanen & Jaakkola, 1985). In conclusion, this procedure has been proven to be reliable in determining the historical source of sedimentary organic matter, and can indicate the human disturbance of the watersheds (Kaushal & Binford, 1998).

2 Although the sampling method used in this study is excellent, I suggest that a means to keep the sampling platform stable be devised so that samples can be collected easily in a straight line. This I think will give the opportunity to a more uniform sampling trend and also, a more precise bases for judgment along the samplings made along a transect.

3 Researches of this nature should be encouraged by making funds available. This goes a long way to first and foremost strengthen the researcher as a scientist and also put the country's research status at par with the international standing of countries like the USA, Canada, Germany etc, since this research falls within the current areas of discovery in science.

REFERENCES

Aandahl, A. R. 1948. The Characterization of Slope Positions and their Influence on total Nitrogen Content of few Virgin Soils Of Western Iowa. Soil Sci. Soc. Am Pro. 13: 449 – 454.

As, J. A. and Zidjerveld, J. D. A., 1958. Magnetic cleaning of rocks in palaeomagnetic research. Geophys. J., 1: 308-319.

Banerjee, S. K., 1989, Physics of Rock Magnetism, London Academy, pp. 10, 42 – 43, 52.
Piper, J. D. A, 1987. Palaeomagnetism and the Continental Crust. p.11

Blatt, Harvey, Middleton, Gerald and Murray, Raymond, 1972, Origin of Sedimentary Rocks: Englewood Cliffs, New Jersey, Prentice-Hall, p. 634.

Boggs, S. Jr., 1987. Principle of Sedimentology and Stratigraphy. Merrill Publishing Company, A Bell & Howell Company, Columbus Toronto London Melbourne, pp. 45, 51 and 105, 112 - 118.

Bradshow, R. and Thompson, R., 1985. The use of magnetic measurements to investigate the mineralogy of Icelandic lake sediments and to Study Catchment processes. Boreas, 14, 203 – 215.

Brubaker, S. C., Jones, A. J., Lewis, D. T., and Frank, K., 1993. Soil Properties Associated with Landscape Positions and Management. Soil Sci. Soc. Am. J. 57: 235 – 239.

Butler, R. F., 1982. Magnetic Mineralogy of Continental Deposits, San Juan Basin, New Mexico, and Clark's Fork Basin, Wyoming, J. Geophys. Res., 87B, 7843-7852.

Butler, R. F. 1992. Palaeomagnetism, Magnetic Domains to Geologic Terranes. Blackwell Sc. Publications, p. 106.

Collinson, D. W., 1983. Methods in Rock Magnetism and Palaeomagnetism; Techniques and instrumentation, Chapman and Hall, London. p. 14, 37.

Creer, K. M., 1958. Preliminary palaeomagnetic measurements from S. America. Ann. Geophys., 14: 373-390.

Creer, K. M., 1959. A. C. demagnetization of unstable Triassic Keuper marls from S.W. England. Geophys. J., 2: 261-275.

Danuor, S. K., 2004, Geological Characterization of the Lake Bosumtwi impart crater and comparison with meteorite craters of similar age and size, Phd thesis, KNUST.

Day, R. and Fuller, M., Schmidt, V. A., 1977. Hysteresis properties of titanomagnetite: grain size and compositional dependence, Phys. Earth Planet. Inter. 13, 260 – 267.

Dearing, J. A., Elner, J. K. and Happy – Wood, C. M. 1981: Recent Sediment flux and Erosional processes in a welsh upland lakes catchment based on magnetic susceptibility measurements: Quaternary Research 16, 356-72 or 256-372

Dearing, J., 1999. Environmental Magnetic Susceptibility, Using the Bartington MS2 System, Chi Publishing, England, pp. 8 – 9.

Dunlop, D. J., 1981. The Rock Magnetism of Fine Particles, Phys. Earth Planet. Inter., 26, pp. 1-26.

Dunlop, D. J, and Yu, Y. 2003. The dependence of anhysteretic remanent magnetization on alternating field decay rate: Fundamental origin and palaeomagnetic applications: Eos Trans. AGU, 84 (46), Fall Meet. Suppl., Abstract GP31A-06, 2003.

Folk, R. L., 1974. The Petrology of Sedimentary Rocks: Austin, Tex., Hemphill Publishing Co., p. 182.

Folk, R. L., 1980. Petrology of Sedimentary Rocks. Humphill Publishing Company, Austin, Texas: pp. 15 – 23.

Folk, R. L., and Ward, W. C., 1957, Brazos River bar – a study in the significance of grain size parameters: Journal Sedimentary Petrology, v. 27, pp. 3-26.

Fuller, M., 1987. Experimental methods in rock magnetism and paleomagnetism, in Method of Experimental physics, edited by C. G. Sammis, and T. L. Henyeys, Academic Press, Orlando, p. 314.

Galle, O. K., and Runnels, R. T., 1960, Determination of CO_2 in carbonate rocks by controlled loss on ignition: Jour. Sed. Pretrology, v. 30, pp. 613-618.

Guilizzoni, P., Marchetto, A., Lami, A., Cameron, G., Appleby, P., Schnell, N. L., Schnell, O. A., Belis, C. A., Giorgis, A. & Guzzi, L., 1996. The environmental history of a mountain lake (Lago Paione Superior, Central Alps, Italy) for the last c. 100 years: a multidisciplinary, paleolimnological study. J. Paleolim. 15: 245 – 264.

Hillel, D., 1980. Fundamentals of Soil Physics, Academic Press, Inc. pp. 14 – 16.

Hilton, J. and Lishman, J. P., 1985. The effect of redox changes on the magnetic susceptibility of sediments from a seasonally anoxic lake. Limnol. Oceanogr. 80 (4), 937 – 909.

Inman, D. L., 1952, Measures for describing size of sediments: Journal Sedimentary Petrology, v. 19, pp. 51-70.

Irving, E., Stott, P. M. and Ward, M. A., 1961a. demagnetization of igneous rocks by alternating magnetic fields. Phil. Mag., 6: 225-241.

Jones, A. J., Mielke, L. N., Bartles, C. A., and Miller, C. A., 1989. Relationship of landscape Position and Properties to Crop Production. J. Soil Water Consev. 44: 328 – 332.

Jones W. B., Bacon M., and Hastings D. A. 1981. The Lake Bosumtwi impact crater, Ghana. Geological Society of America Bulletin 92:342–349.

Junner N. R., 1937. The geology of the Bosumtwi caldera and surrounding country. Gold Coast Geological Survey Bulletin 8: 1–38

Kanassanen, P. H. & Jaakkola, T., 1985. Assessment of pollution history from recent sediments in lake Vanajavesi, southern Finland. I. Selection of representative profiles, their dating and chemostratigraphy. Ann. Zool. Fennici 22: 13 – 55.

Kalff, J., 2002. Limnology; Inland Water Ecosystems. Prentice Hall, pp. 294 – 295.

Kane, W. T., and Hubert, J. F., 1962, Fortran program for the calculation of grain-size textural parameters on the IBM 1960 computer: Sedimentology, no. 2, pp. 87-90.

Kaushal, S. and Binford, M. W., 1999. Relationship between C:N ratios of lake sediments, organic matter sources, and historical deforestation in Lake Pleasant, Massachusetts, USA. Kluwer Academic Publishers, Journal of Paleolimno. 22: 439 - 442.

Khan, M. A., 1960. The remanent magnetization of the basic Tertiary igneous rocks of Skye, Inverness-shire. Geophys. J., 3: 45-62.

Koeberl, C., Bottomley, R., Glass, B., Storzer, D, 1997. Geochemistry and age of Ivory Coast tektites and micro-tektites. Geochimica et Cosmochimica Acta, 61: 1745 – 1772.

Kolbe P., Pinson W. H., Saul J. M., and Miller E. W. 1967. Rb-Sr study on country rocks of the Bosumtwi crater, Ghana. Geochimica et Cosmochimica Acta 31:869–875.

Konrad, J. G., Chesters, G., and Keeney, D. R., 1970, Determination of organic- and carbonate-carbon in freshwater lake sediments by a micro-combustion procedure: Jour. Thermal Analysis, v. 2, pp. 199-208.

Leube A., Hirdes W., Mauer R., and Kesse G. O. 1990. The early Proterozoic Birimian Supergroup of Ghana and some aspects of its associated gold mineralization. Precambrian Research 46: 139–165.

Magdoft, F. & Weil, R. R., 2004. Soil Organic Matter In Sustainable Agriculture, CRC Press, p. 67.

Maher, B., Thompson, R., 1999. Quaternary Climates, Environments and Magnetism. Cambridge University Press. pp. 29, 37 & 43.

McCave, I. N., and Syvitski, J. P. M., 1991, Principles and methods of particle size analysis, In J. P. M. Syvitski (ed.), Principles, Methods, and Applications of Particle Size Analysis, New York, Cambridge University Press, p. 3-21.

Michael, E. E., Heller F., 2003. Environmental Magnetism, 'Principles and Applications of Environmagnetics', Academic Press, pp. 7 – 9, 21- 23.

Moon P. A. and Mason D. 1967. The geology of ¼° field sheets 129 and 131, Bompata SW. and NW. Ghana Geological Survey Bulletin 31:1–51

Moskowitz, M. B., 1991. Hitchhiker's Guide to Magnetism, pp. 4 - 5, 9 - 11, 15 – 17, 20 – 23, 25, 31, 35 - 37.

Neel, L., 1955. Advance Phys. 4, 191.

Nicholson, S. E., 1986. The spatial coherence of Africa rainfall anomalies: interhemispheric teleconnections.Journal of Climatology and Applied Meteorology 25, pp. 1365 – 1381.

Oldfield, F., 1977. Lakes and their drainage basins as units of sediment – based ecological study, progress in physical Geophy. 3, 460 – 504.

Opdyke, N. D., 1964. The palaeomagnetism of the Permian red beds of S. W. Tanganyika. J. Geophys. Res., 69: 2477-3487.

Peck, J. A., Green, R. R., Shanahan, T., King, J. W., Overpeck, J. T. and Scholz, C. A., A magnetic mineral record of Late Quaternary tropical climate variability from Lake Bosumtwi, Ghana. Palaeo., 215 (2004) 37 – 57.

Poppe, L. J., Eliason, A. H., Fredericks, J. J., Rendings, R. R., Blackwood, D. and Polloni, C. F., 2000, Grain-size analysis of marine sediments: Methodology and data processing, U. S. Geological Survey East-Coast Sediment Analysis: Procedures, Database, and Georeferenced Displays. Open-File Rep, 00-358.

Prof. T. Nagata, (1961). Rock Magnetism. University of Tokyo, Revised Edition, Maruzen Company, Tokyo. p.144.

Reimold W. U., Brandt D., and Koeberl C. 1998. Detailed structural analysis of the rim of a large, complex impact crater: Bosumtwi crater, Ghana. Geology 26:543–546.

Sawyer, M. B., 1977, Computer program for the calculation of grain-size statistics by the method of moments: U. S. Geological Survey Open-File Report 77-580, p. 15.

Schlee, J., 1966, A modified Woods Hole Rapid Sediment Analyzer: Journal Sedimentary Petrology, v. 30, p. 403-413.

Snowball, I. F., 1993. Geochemical Control of Magnetite dissolution in Subarctic lake sediments and the implications for environmental magnetism. J. Quat. Sci. 8 (4), 339 – 346.

Talbot, M. R. and Delibrias, G., 1977. Holocene variations in the level of Lake Bosumtwi, Ghana. Nature, 268.

Talbot, M. R., Livingstone, D.A., Palmer, P., Maley, J., Melack, J.M., Delibrias, G., Gulliksen, S., 1984. Preliminary results from sediment cores from Lake Bosumtwi, Ghana. Plaeoecology of Africa and the Surrounding Islands 16, pp. 173 – 192.

The IRM Quarterly, Fall 2003. Maintaining Standards III, Pozzolana cement, cross-calibration samples available; Vol. 13, No. 3. pp. 8, 9 – 11.

Thompson, R. and Morton, 1979. Magnetic Susceptibility and Particle – size distribution in recent Sediments of the Loch Lomond drainage basin, Scotland. Journal of Sedimentary Petrology 49, 801 – 812.

Thompson, R., Oldfield, F., 1986. Environmental magnetism, Allen and Unwin, London, 227 pp.

Trask, P. D., 1932, Origin and environment of source sediments of petroleum: Houston, TX, Gulf Publication Company, p. 323.

Turner, B.F., Gardner, L.R., Sharp, W.E., 1995. The hydrology of Lake Bosumtwi, a climatic – sensitive lake in Ghana, West Africa, Journal of Hydrology. p. 245.

Dean W.E. JR, 1974. Determination of Carbonate and Organic Matter in Calcarious Sediments and Sedimentary Rocks by Loss on Ignition: Comparison with other Methods, Journal of Sedimentary Petrology, Vol. 44, No. 1, pp. 242 – 243.

Waugah, W. N., and Hill, W. E., Jr., 1960, Determination of carbon dioxide and other volatiles in pyretic limestones by loss on ignition: Jour. Sed. Petrology, v. 30, p. 144-147.

Wetzel, R. G., 2001. Limnology: Lake and River Ecosystems, Third Edition, Academic Press, pp. 102 – 103.

Woodfield P. D. 1966. The geology of the ¼° field sheet 91, Fumso NW. Ghana Geological Survey Bulletin 30:1–66.

Wright J. B., Hastings D. A., Jones W. B., and Williams H. R. 1985. Geology and mineral resources of West Africa. London: Allen and Unwin. 187 p.

www.ascscientific.com.

www.bartington.com/multisus.htm.

www.rockgateco.com.

Zeigler, J. M., Whitney, G. G., Jr., and Hayes, C. R., 1960, Woods Hole Rapid Sediment Analyzer: Journal of Sedimentary Petrology, v. 30, pp. 490-495.

Appendix A

A: Detail spatial plot of sample sites at Abonu.

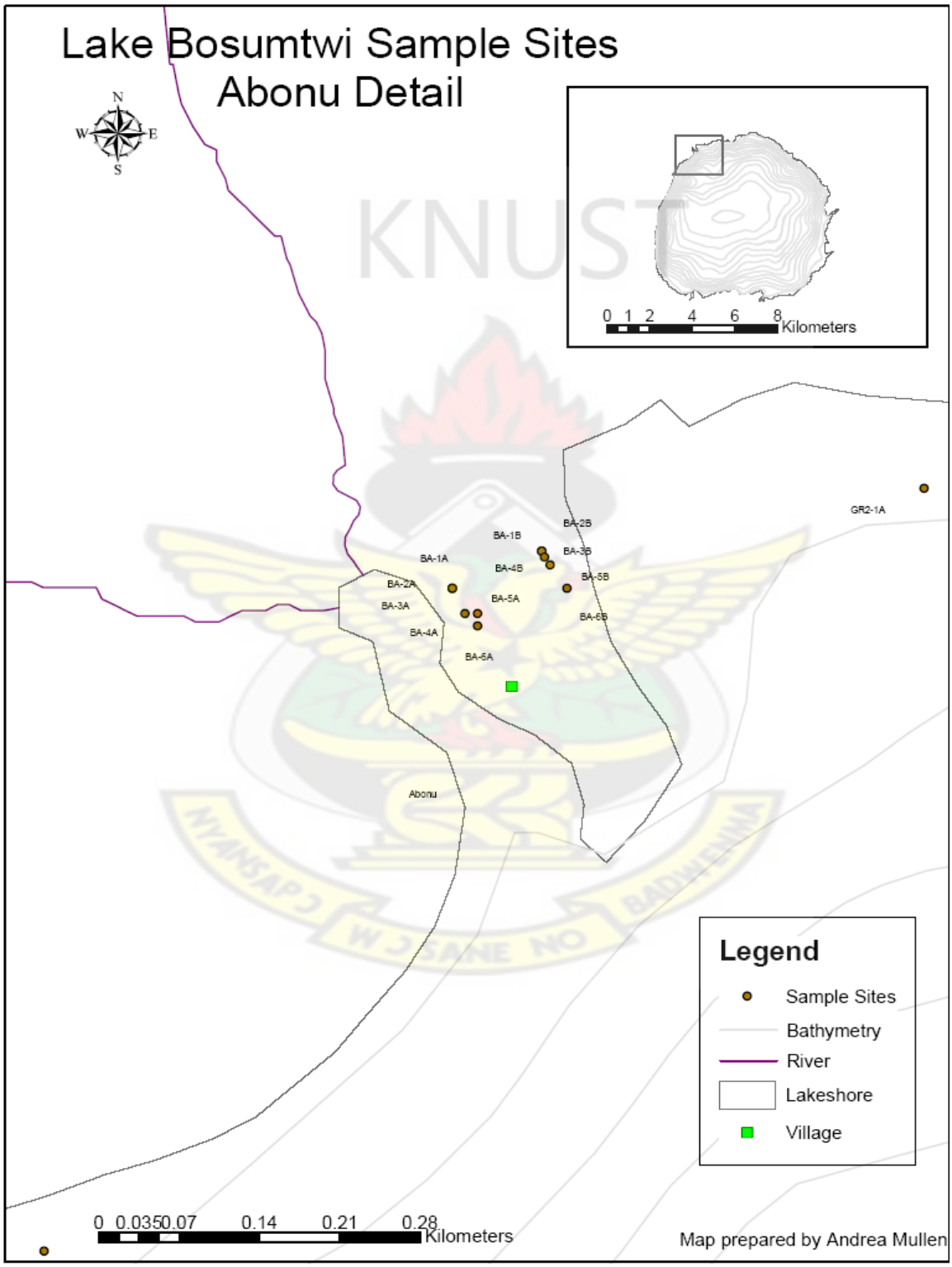

B: Detail spatial plot of sample sites at Anyinatiase.

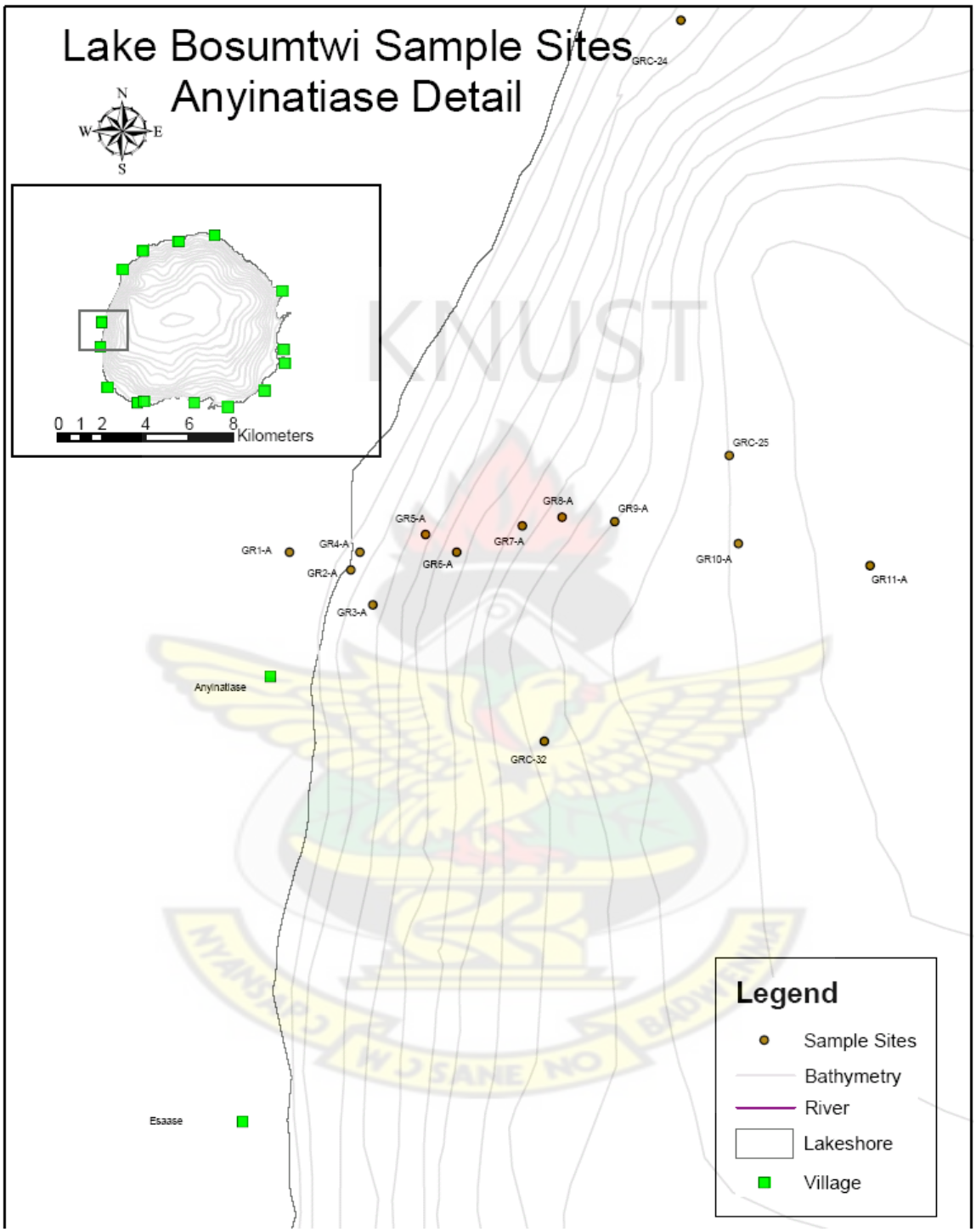

Appendix B

A: Detail plot showing the distribution of percentage organic content of samples collected from Abonu.

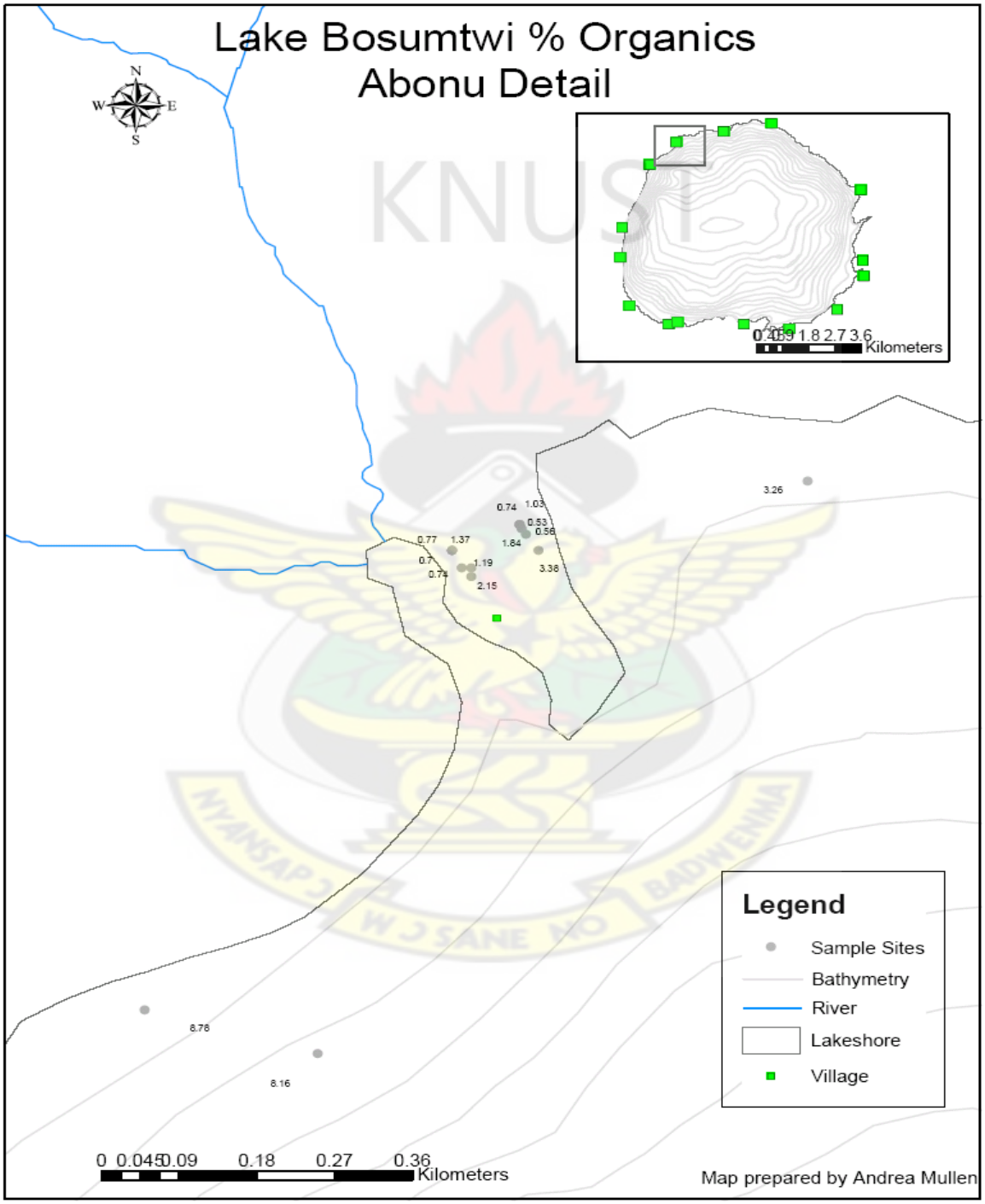

B: Detail plot showing the distribution of the dry bulk density content of samples collected from Abonu.

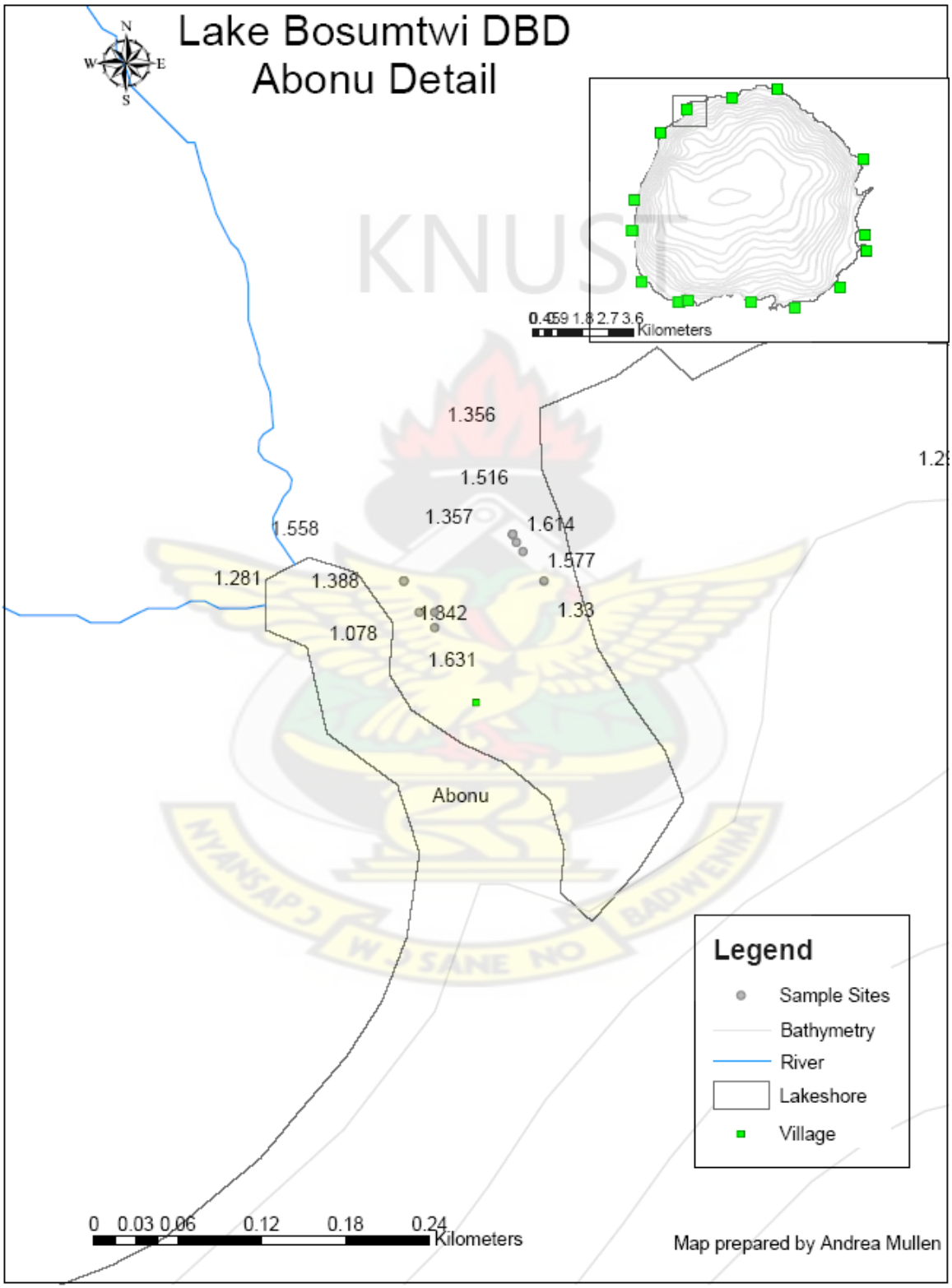

C: Detail plot showing the distribution of the dry bulk density content of samples collected from Anyinatiase.

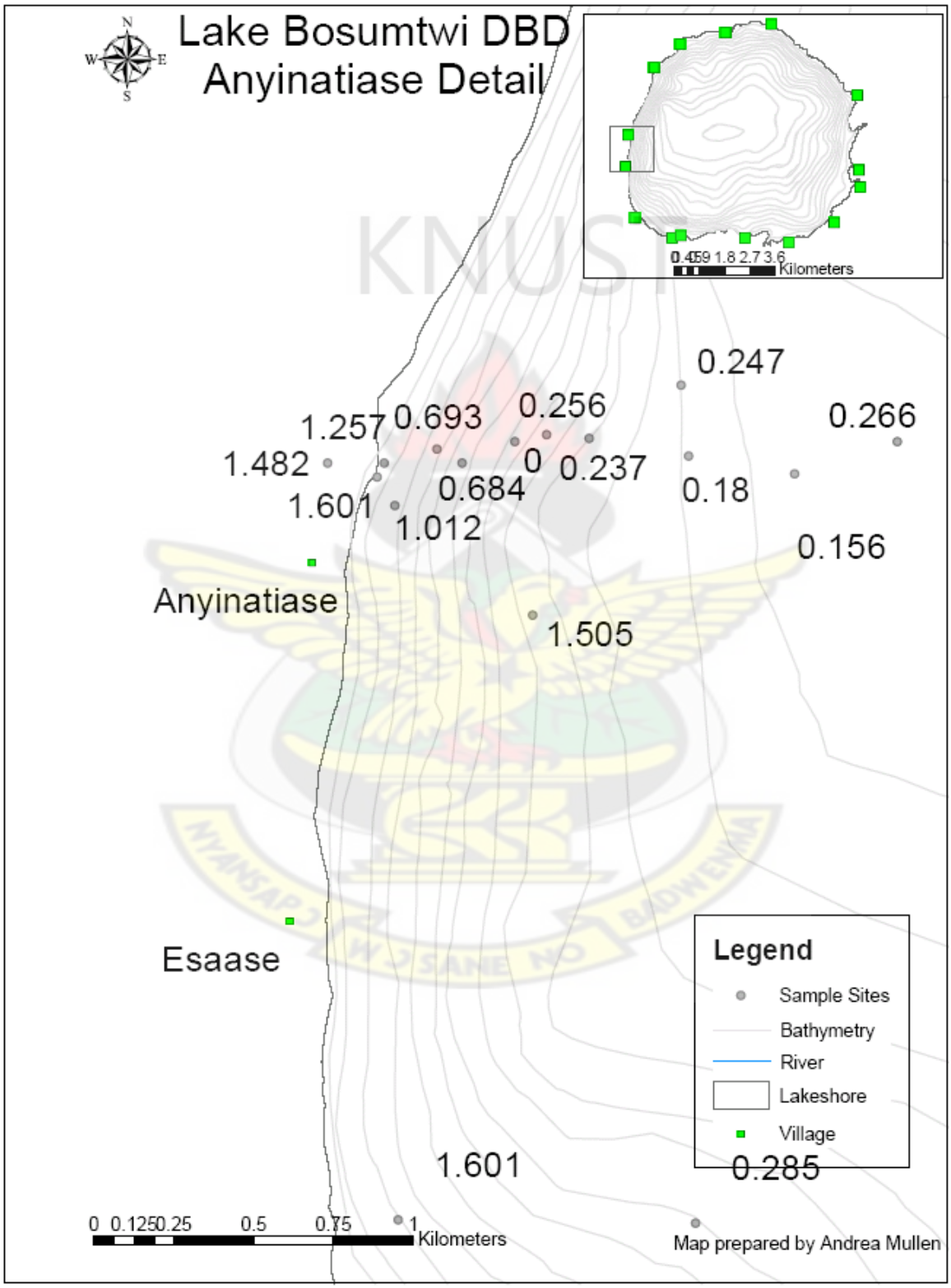

Appendix C

A: Detail plot showing the distribution of percentage water content of samples collected from Abonu.

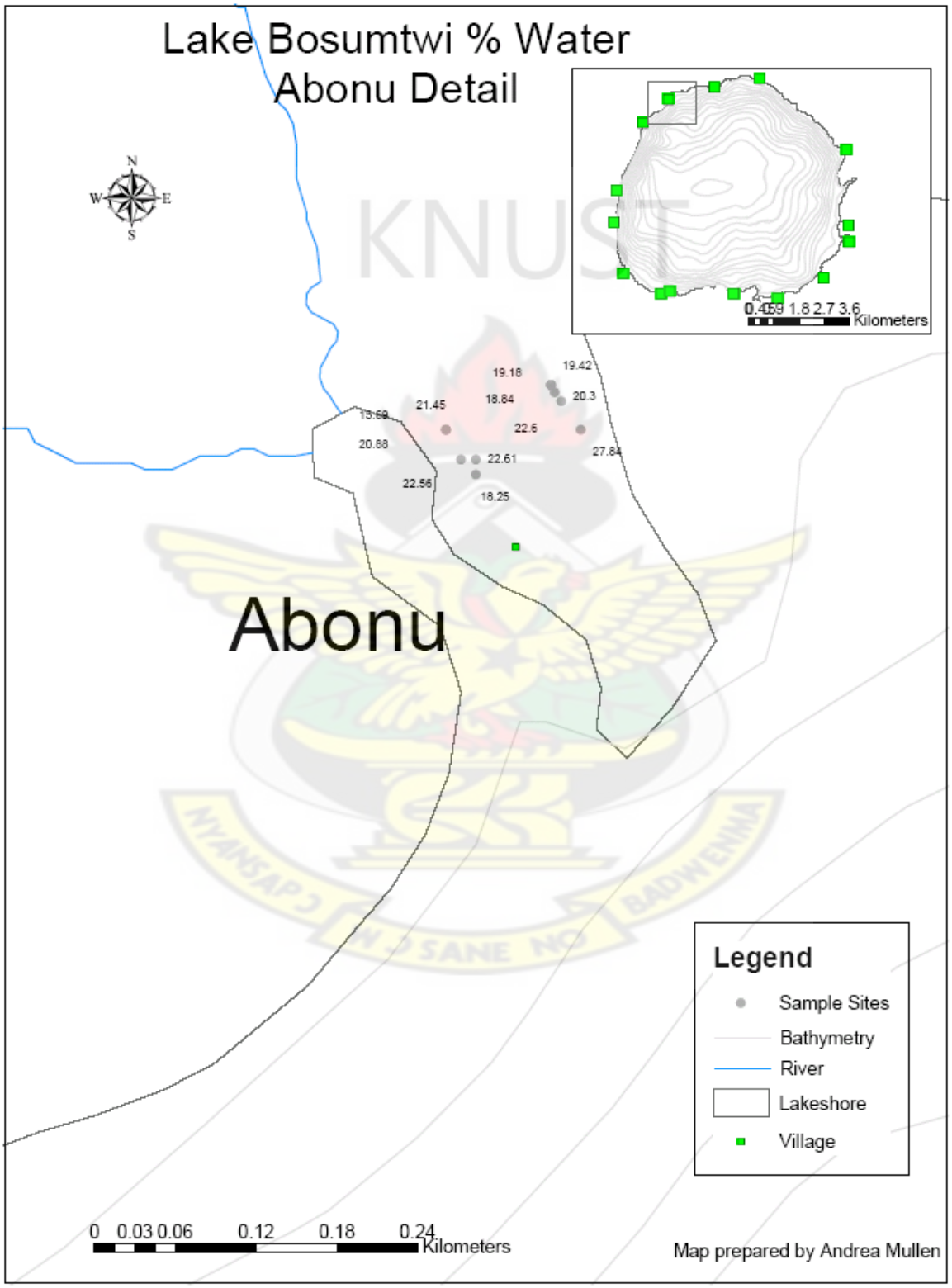

Appendix D

A: Detail plot showing the distribution of low frequency susceptibility content of samples from Abonu.

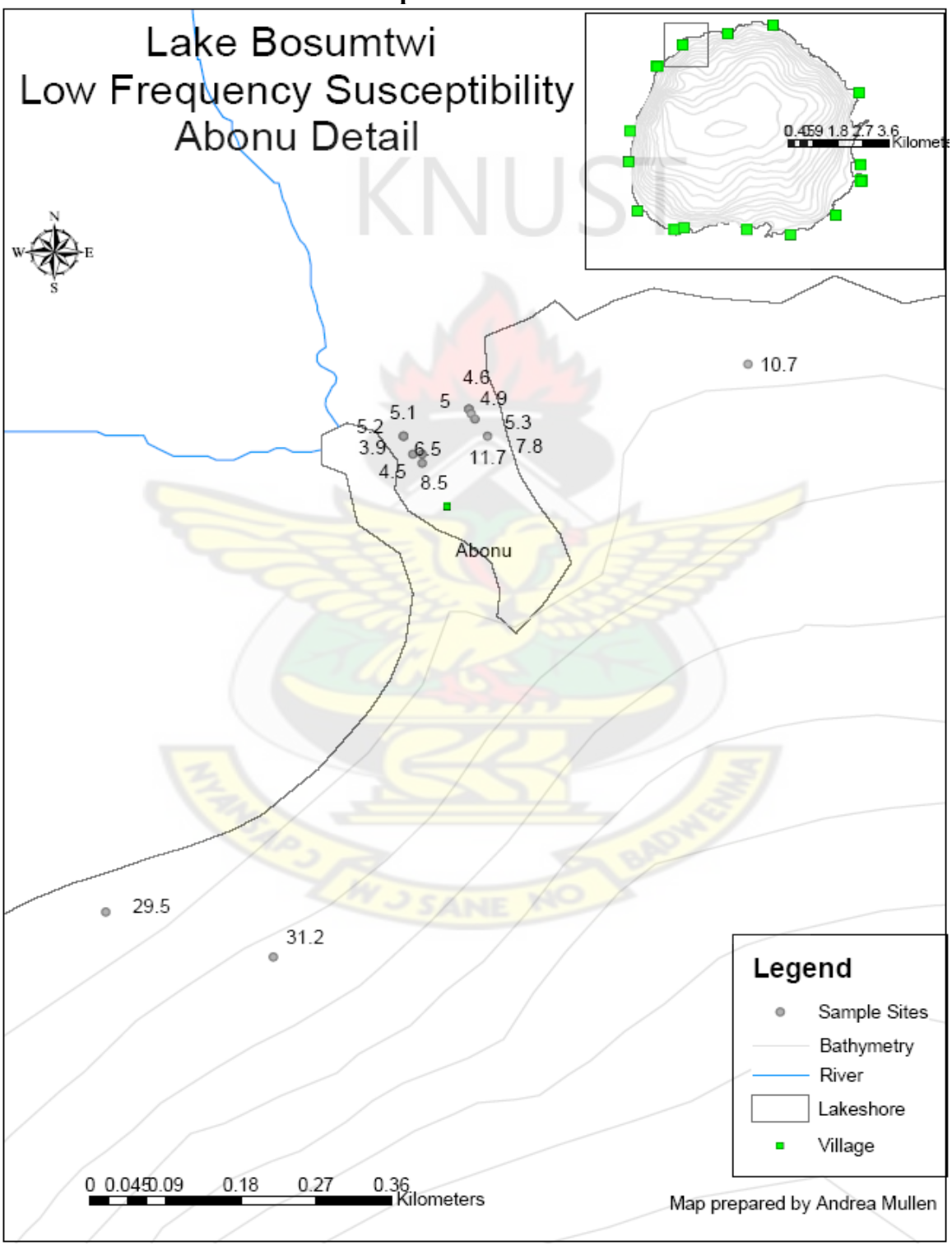

B: Detail plot showing the distribution of low frequency susceptibility content of samples from Anyinatiase.

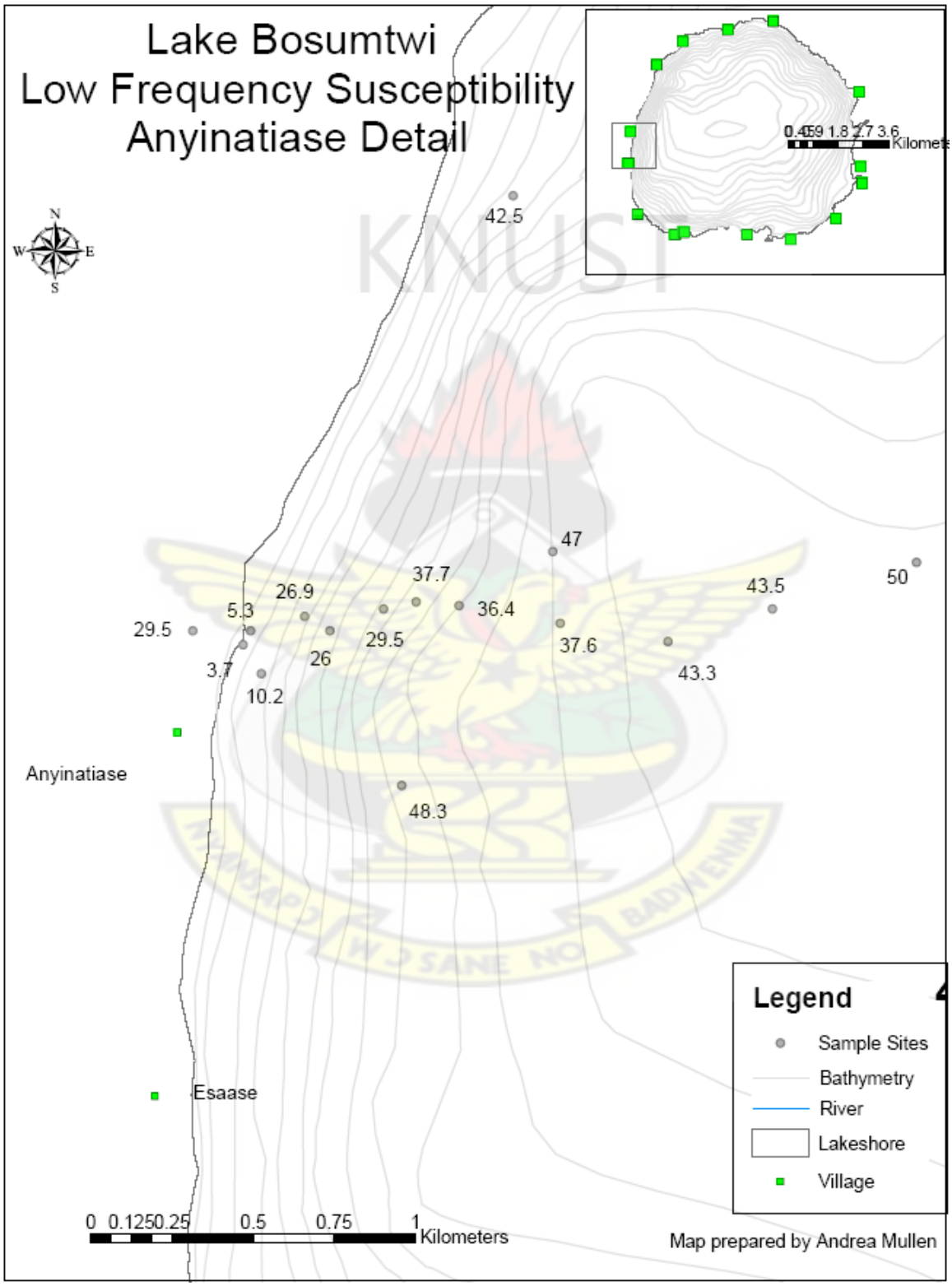

Appendix E

A: Detail plot showing the distribution of frequency dependence content of samples from Anyinatiase.

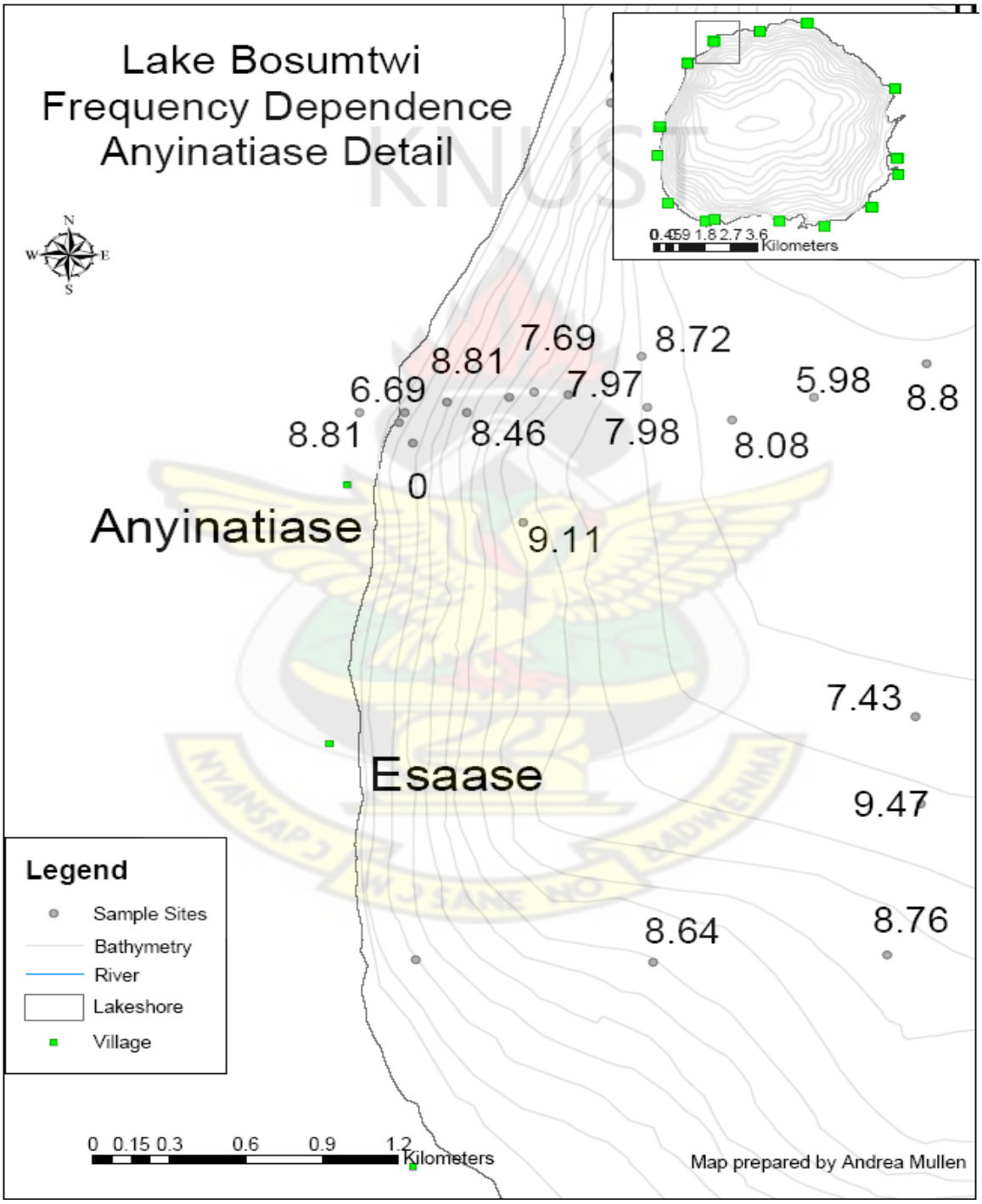

Appendix F

TABLE OF FIELD DATA.

Table 3.1 Table showing name of samples, location coordinates and corresponding water depths.

Lat. DD = Latitude Decimal Degrees and Lon. DD = Longitude Decimal Degrees.

Sample Name	Lat degrees	Lat minutes	Long. Degrees	Long Minutes	Water depth (m)	lat. DD	long DD
BA-1A	6	31.9080	1.0000	25.8230	0.00	6.5318	1.4304
BA-1B	6	31.9260	1.0000	25.7840	0.07	6.5321	1.4297
BA-2A	6	31.9080	1.0000	25.8230	0.00	6.5318	1.4304
BA-3A	6	31.9050	1.0000	25.8230	0.17	6.5318	1.4304
BA-4A	6	31.8970	1.0000	25.8200	0.42	6.5316	1.4303
BA-5A	6	31.8940	1.0000	25.8140	1.06	6.5316	1.4302
BA-6A	6	31.8910	1.0000	25.8110	1.23	6.5315	1.4302
GR1-A	6	30.2800	1.0000	26.7800	0.65	6.5047	1.4463
GR2-A	6	30.2600	1.0000	26.6920	10.60	6.5043	1.4449
GR3-A	6	30.2100	1.0000	26.6630	20.00	6.5035	1.4444
GR4-A	6	30.2820	1.0000	26.6800	13.00	6.5047	1.4447
GR5-A	6	30.3050	1.0000	26.5940	26.60	6.5051	1.4432
GR6-A	6	30.2810	1.0000	26.5480	32.00	6.5047	1.4425
GR7-A	6	30.3170	1.0000	26.4580	38.00	6.5053	1.4410
GR8-A	6	30.3310	1.0000	26.4030	42.80	6.5055	1.4401
GR9-A	6	30.3240	1.0000	26.3360	46.00	6.5054	1.4389
GR10-A	6	30.2920	1.0000	26.1640	56.00	6.5049	1.4361
GR11-A	6	30.2650	1.0000	25.9850	62.00	6.5044	1.4331
GR12-A	6	30.3160	1.0000	25.8090	74.60	6.5053	1.4302
GR15-A	6	30.6140	1.0000	25.1810	84.00	6.5102	1.4197
GR16-A	6	30.6140	1.0000	25.0900	73.00	6.5102	1.4182
GR17-A	6	30.6390	1.0000	24.7640	74.00	6.5107	1.4127
GR18-A	6	30.7080	1.0000	24.3450	71.70	6.5118	1.4058
GR19-A	6	30.6960	1.0000	24.1440	72.00	6.5116	1.4024
GR20-A	6	30.6910	1.0000	23.8900	70.00	6.5115	1.3982
GR21-A	6	30.6970	1.0000	23.7130	67.00	6.5116	1.3952
GR-23A	6	30.6750	1.0000	23.5340	57.00	6.5113	1.3922
GR24-A	6	30.6770	1.0000	23.1360	50.00	6.5113	1.3856
GR25-A	6	30.7060	1.0000	22.9040	39.50	6.5118	1.3817
GR26-A	6	30.7110	1.0000	22.8150	34.50	6.5119	1.3803
GR27-A	6	30.6810	1.0000	22.6800	27.50	6.5114	1.3780
GR2-1A	6	31.9570	1.0000	25.6000	13.00	6.5326	1.4267
GR2-2A	6	31.7790	1.0000	25.4340	24.00	6.5297	1.4239
GR2-3A	6	31.4900	1.0000	25.1550	43.00	6.5248	1.4193
GR2-4A	6	31.3870	1.0000	25.0690	49.00	6.5231	1.4178
GR2-5A	6	31.1640	1.0000	24.9740	59.00	6.5194	1.4162
GR2-6A	6	29.3190	1.0000	24.3270	50.00	6.4887	1.4055
GR2-7A	6	29.1450	1.0000	24.2310	40.00	6.4858	1.4039

GR2-8A	6	29.0170	1.0000	24.1600	33.50	6.4836	1.4027
GR2-9A	6	28.7850	1.0000	24.0170	25.50	6.4798	1.4003
GR2-10A	6	32.0680	1.0000	24.9380	17.50	6.5345	1.4156
GR2-11A	6	31.5320	1.0000	24.8830	49.00	6.5255	1.4147
GR2-12A	6	31.0030	1.0000	24.8590	66.00	6.5167	1.4143
GR2-13A	6	30.4980	1.0000	24.8590	77.00	6.5083	1.4143
GR2-14A	6	29.9940	1.0000	24.8880	78.00	6.4999	1.4148
GR2-15A	6	29.4960	1.0000	24.8800	67.50	6.4916	1.4147
GR2-16A	6	28.9930	1.0000	24.8990	58.00	6.4832	1.4150
GR2-17A	6	28.7330	1.0000	24.8970	42.00	6.4789	1.4150
GR2-18A	6	28.6050	1.0000	24.8980	33.00	6.4768	1.4150
GR2-19A	6	28.5250	1.0000	24.8900	18.00	6.4754	1.4148
GR2-22A	6	28.9070	1.0000	25.3870	45.00	6.4818	1.4231
GR2-23A	6	29.4000	1.0000	25.3760	62.00	6.4900	1.4229
GR2-24A	6	29.9000	1.0000	25.3920	73.50	6.4983	1.4232
GR2-25A	6	30.4010	1.0000	25.3660	76.00	6.5067	1.4228
GR2-26A	6	30.9090	1.0000	25.3950	63.50	6.5152	1.4233
GR2-27A	6	31.4110	1.0000	25.3970	38.75	6.5235	1.4233
GR2-28A	6	31.9760	1.0000	24.3370	36.50	6.5329	1.4056
GR2-29A	6	31.5000	1.0000	24.3360	59.25	6.5250	1.4056
GR2-30A	6	30.9950	1.0000	24.3290	72.75	6.5166	1.4055
GR2-31A	6	30.4880	1.0000	24.3220	78.00	6.5081	1.4054
GR2-32A	6	30.0060	1.0000	24.3370	73.75	6.5001	1.4056
GR2-33A	6	29.4970	1.0000	24.3380	59.75	6.4916	1.4056
GR2-35A	6	30.9170	1.0000	22.9950	40.00	6.5153	1.3833
GR2-36A	6	30.4150	1.0000	23.0060	43.50	6.5069	1.3834
GR2-37A	6	29.9110	1.0000	23.0070	39.50	6.4985	1.3835
GR2-38A	6	29.3980	1.0000	23.0080	31.50	6.4900	1.3835
GR2-39A	6	28.9820	1.0000	23.0080	16.00	6.4830	1.3835
GR2-40A	6	28.8070	1.0000	23.0090	11.00	6.4801	1.3835
GR2-41A	6	28.7010	1.0000	22.9990	6.50	6.4784	1.3833
GR2-42A	6	28.5220	1.0000	23.3410	16.50	6.4754	1.3890
GR2-43A	6	29.0410	1.0000	23.3380	40.00	6.4840	1.3890
GR2-44A	6	29.5150	1.0000	23.3280	46.80	6.4919	1.3888
GR2-45A	6	30.0190	1.0000	23.3330	59.25	6.5003	1.3889
GR2-46A	6	30.5410	1.0000	23.3270	63.50	6.5090	1.3888
GR2-47A	6	31.0450	1.0000	23.3270	51.00	6.5174	1.3888
GR2-48A	6	31.5420	1.0000	23.3340	23.00	6.5257	1.3889
GR2-49A	6	28.9970	1.0000	26.6600	15.00	6.4833	1.4443
GR2-50A	6	28.9940	1.0000	26.1540	34.50	6.4832	1.4359
GR2-51A	6	29.0100	1.0000	25.6530	45.00	6.4835	1.4276
GR2-52A	6	29.0010	1.0000	25.1490	56.00	6.4834	1.4192
GR2-53A	6	28.9830	1.0000	24.6570	47.80	6.4831	1.4110
GR2-54A	6	28.9980	1.0000	24.1670	33.00	6.4833	1.4028
GR2-55A	6	28.9900	1.0000	23.6590	39.00	6.4832	1.3943
GR2-56A	6	28.9910	1.0000	23.1580	25.00	6.4832	1.3860
GR2-57A	6	29.0170	1.0000	22.7980	7.50	6.4836	1.3800
GR2-58A	6	31.6510	1.0000	26.1200	11.00	6.5275	1.4353

GR2-59A	6	31.5890	1.0000	26.0160	17.50	6.5265	1.4336
GR2-60A	6	31.5580	1.0000	25.9060	24.20	6.5260	1.4318
GR2-61A	6	31.5530	1.0000	25.5730	28.50	6.5259	1.4262
GR2-62A	6	31.5460	1.0000	25.0870	42.50	6.5258	1.4181
GR2-63A	6	31.5090	1.0000	24.4890	55.50	6.5252	1.4082
GR2-64A	6	31.4880	1.0000	24.0170	53.70	6.5248	1.4003
GR2-65A	6	31.4750	1.0000	23.5910	34.50	6.5246	1.3932
GR2-66A	6	31.4400	1.0000	23.2730	28.50	6.5240	1.3879
GR2-67A	6	31.3840	1.0000	23.0010	16.00	6.5231	1.3834
GR2-68A	6	31.3790	1.0000	22.8580	8.80	6.5230	1.3810
GRE-1A	6	30.0190	1.0000	22.3530	18.30	6.5003	1.3726
GRC-1	6	28.2490	1.0000	24.3370	3.00	6.4708	1.4056
GRC-2	6	29.3740	1.0000	22.3820	16.40	6.4896	1.3730
GRC-3	6	29.2410	1.0000	22.3820	10.20	6.4874	1.3730
GRC-4	6	29.3640	1.0000	22.5670	31.00	6.4894	1.3761
GRC-5	6	29.4170	1.0000	23.3610	50.00	6.4903	1.3894
GRC-6	6	29.5580	1.0000	23.4050	66.30	6.4926	1.3901
GRC-7	6	30.5650	1.0000	23.4240	51.40	6.5094	1.3904
GRC-8	6	31.1590	1.0000	23.4120	49.80	6.5193	1.3902
GRC-10	6	31.0400	1.0000	23.5820	69.30	6.5173	1.3930
GRC-11	6	31.1740	1.0000	24.1600	51.20	6.5196	1.4027
GRC-12	6	31.3660	1.0000	24.0230	49.20	6.5228	1.4004
GRC-13	6	31.3870	1.0000	23.4430	32.50	6.5231	1.3907
GRC-14	6	31.5570	1.0000	23.5800	28.00	6.5260	1.3930
GRC-22	6	31.0370	1.0000	25.4130	54.50	6.5173	1.4236
GRC-24	6	31.0070	1.0000	26.2450	6.00	6.5168	1.4374
GRC-25	6	30.4140	1.0000	26.1780	44.00	6.5069	1.4363
GRC-26	6	30.3970	1.0000	25.5700	49.00	6.5066	1.4262
GRC-29	6	29.5650	1.0000	25.3970	65.00	6.4928	1.4233
GRC-30	6	29.5670	1.0000	25.5980	63.00	6.4928	1.4266
GRC-32	6	30.0230	1.0000	26.4280	6.50	6.5004	1.4405
GRC-34	6	29.3660	1.0000	25.5810	53.00	6.4894	1.4264
GRC-36	6	29.1770	1.0000	25.4230	51.30	6.4863	1.4237
GRC-39	6	28.4040	1.0000	26.1600	21.00	6.4734	1.4360
GRC-40	6	28.2400	1.0000	26.0180	7.50	6.4707	1.4336
GRC-42	6	28.3980	1.0000	24.1920	25.00	6.4733	1.4032
GRC-45	6	28.2190	1.0000	23.3730	4.90	6.4703	1.3896
GRC-46	6	28.2220	1.0000	23.5950	4.90	6.4704	1.3933
GRC-47	6	28.2830	1.0000	24.5430	3.00	6.4714	1.4091
GRC-48	6	28.3880	1.0000	25.4200	35.90	6.4731	1.4237
station A	6	31.0100	1.0000	23.3300	59.00	6.5168	1.3888
station B	6	30.2300	1.0000	23.3900	66.40	6.5038	1.3898
station C	6	30.2000	1.0000	23.5700	71.00	6.5033	1.3928
station D	6	30.0000	1.0000	24.0200	67.30	6.5000	1.4003
station E	6	29.4100	1.0000	24.0400	59.50	6.4902	1.4007
station F	6	29.2700	1.0000	24.0500	52.30	6.4878	1.4008
station G	6	29.0400	1.0000	23.5800	37.50	6.4840	1.3930
Deep Grab	6	31.3360	1.0000	25.2580	43.60	6.5223	1.4210

Appendix G

TABLE OF MEASURED AND COMPUTERED RESULTS

Table 3.2 Showing measured sample values and calculated results of % water content, Dry bulk density and % organic content of samples.

Sample	Water depth (m)	crucible #	crucible wt (g)	wet sample wt (tared)	sample and crucible 60 C	550 sample and crucible	% water	Dry Bulk density	% organic matter
BA-1A	0.00	34	4.529	1.767	5.917	5.898	21.4488	1.3880	1.3689
BA-1B	0.07	135	5.266	1.679	6.623	6.613	19.1781	1.3570	0.7369
BA-2A	0.00	69	4.763	1.848	6.321	6.309	15.6926	1.5580	0.7702
BA-2B	0.07	95	4.784	1.752	6.140	6.126	22.6027	1.3560	1.0324
BA-3A	0.17	74	5.097	1.619	6.378	6.369	20.8771	1.2810	0.7026
BA-3B	0.00	64	4.732	1.868	6.248	6.240	18.8437	1.5160	0.5277
BA-4A	0.42	96	4.890	1.392	5.968	5.960	22.5575	1.0780	0.7421
BA-4B	0.17	103	5.051	2.025	6.665	6.656	20.2963	1.6140	0.5576
BA-5A	1.06	4	4.430	1.734	5.772	5.756	22.6067	1.3420	1.1923
BA-5B	0.44	12	4.531	1.957	6.108	6.079	19.4175	1.5770	1.8389
BA-6A	1.23	45	4.573	1.995	6.204	6.169	18.2456	1.6310	2.1459
BA-6B	0.81	47	4.586	1.843	5.916	5.871	27.8351	1.3300	3.3835
GR1-A	0.65	59	4.750	1.839	6.232	6.208	19.4127	1.4820	1.6194
GR2-A	10.60	113	5.176	1.983	6.777	6.753	19.2637	1.6010	1.4991
GR-3A	20.00	121	5.230	1.610	6.242	6.205	37.1429	1.0120	3.6561
GR-4A	13.00	114	5.366	1.816	6.623	6.586	30.7819	1.2570	2.9435
GR-5A	26.60	36	4.391	1.468	5.084	5.031	52.7929	0.6930	7.6479
GR6-A	32.00	25	4.050	1.475	4.734	4.684	53.6271	0.6840	7.3099
GR8-A	42.80	120	5.044	1.204	5.300	5.261	78.7375	0.2560	15.2344
GR9-A	46.00	54	4.517	1.178	4.754	4.717	79.8812	0.2370	15.6118

GR10-A	56.00	35	4.665	1.119	4.845	4.811	83.9142	0.1800	18.8889
GR11-A	62.00	56	4.366	1.137	4.522	4.490	86.2797	0.1560	20.5128
GR-12A	74.60	97	5.143	1.202	5.409	5.357	77.8702	0.2660	19.5489
GR-15A	84.00	5	4.394	1.105	4.499	4.474	90.4977	0.1050	23.8095
GR-16A	73.00	11	4.447	1.171	4.674	4.618	80.6149	0.2270	24.6696
GR-17A	74.00	124	5.108	1.124	5.214	5.189	90.5694	0.1060	23.5849
GR-18A	71.70	127	4.905	1.125	5.044	5.012	87.6444	0.1390	23.0216
GR-19A	72.00	62	4.359	1.116	4.499	4.468	87.4552	0.1400	22.1429
GR-20A	70.00	78	5.244	1.118	5.372	5.340	88.5510	0.1280	25.0000
GR-21A	67.00	38	4.679	1.067	4.743	4.724	94.0019	0.0640	29.6875
GR-23A	57.00	89	4.856	1.082	4.933	4.916	92.8835	0.0770	22.0779
GR-24A	50.00	118	5.288	1.040	5.449	5.416	84.5192	0.1610	20.4969
GR-25A	39.50	111	5.362	1.221	5.657	5.600	75.8395	0.2950	19.3220
GR-26A	34.50	18	4.613	1.219	4.913	4.869	75.3897	0.3000	14.6667
GR-27A	27.50	143	5.259	1.182	5.507	5.472	79.0186	0.2480	14.1129
GR2-1A	13.00	6	4.497	1.840	5.787	5.745	29.8913	1.2900	3.2558
GR2-3A	43.00	44	4.720	1.182	4.933	4.901	81.9797	0.2130	15.0235
GR2-4A	49.00	99	5.378	1.144	5.562	5.528	83.9161	0.1840	18.4783
GR2-5A	59.00	77	5.226	1.043	5.355	5.331	87.6318	0.1290	18.6047
GR2-6A	50.00	13	4.381	1.088	4.491	4.463	89.8897	0.1100	25.4545
GR2-7A	40.00	112	5.266	1.150	5.453	5.415	83.7391	0.1870	20.3209
GR2-8A	33.50	29	4.225	1.148	4.410	4.379	83.8850	0.1850	16.7568
GR2-9A	25.50	63	4.496	1.252	4.849	4.814	71.8051	0.3530	9.9150
GR2-10A	17.50	142	4.599	1.634	5.648	5.597	35.8017	1.0490	4.8618
GR2-11A	49.00	126	5.001	1.162	5.235	5.193	79.8623	0.2340	17.9487
GR2-12A	66.00	1	4.409	1.119	4.537	4.510	88.5612	0.1280	21.0938
GR2-13A	77.00	117	5.148	1.104	5.240	5.216	91.6667	0.0920	26.0870
GR2-14A	78.00	76	5.138	1.062	5.204	5.188	93.7853	0.0660	24.2424
GR2-15A	67.50	114	5.366	1.762	5.439	5.422	95.8570	0.0730	23.2877
GR2-16A	58.00	3	4.546	1.111	4.638	4.616	91.7192	0.0920	23.9130
GR2-17A	42.00	40	4.489	1.055	4.603	4.584	89.1943	0.1140	16.6667
GR2-18A	33.00	37	4.600	1.144	4.817	4.789	81.0315	0.2170	12.9032

GR2-19A	18.00	26	4.196	1.247	4.599	4.562	67.6824	0.4030	9.1811
GR2-22A	45.00	84	5.311	1.169	5.511	5.475	82.8914	0.2000	18.0000
GR2-23A	62.00	30	4.396	1.068	4.480	4.462	92.1348	0.0840	21.4286
GR2-24A	73.50	49	4.296	1.146	4.517	4.467	80.7155	0.2210	22.6244
GR2-25A	76.00	42	4.522	1.105	4.610	4.590	92.0362	0.0880	22.7273
GR2-26A	63.50	31	4.132	1.121	4.293	4.264	85.6378	0.1610	18.0124
GR2-27A	38.75	32	4.168	1.198	4.400	4.366	80.6344	0.2320	14.6552
GR2-28A	36.50	24	4.553	1.266	4.921	4.884	70.9321	0.3680	10.0543
GR2-29A	59.25	79	5.176	1.208	5.452	5.399	77.1523	0.2760	19.2029
GR2-30A	72.75	49	4.296	1.144	4.428	4.401	88.4615	0.1320	20.4545
GR2-31A	78.00	63	4.496	1.089	4.605	4.580	89.9908	0.1090	22.9358
GR2-32A	73.75	28	4.249	1.147	4.394	4.359	87.3583	0.1450	24.1379
GR2-33A	59.75	80	4.775	1.139	4.939	4.898	85.6014	0.1640	25.0000
GR2-36A	43.50	51	4.391	1.131	4.551	4.519	85.8532	0.1600	20.0000
GR2-37A	39.50	41	4.343	1.183	4.588	4.537	79.2899	0.2450	20.8163
GR2-38A	31.50	94	5.387	1.217	5.647	5.649	78.6360	0.2600	-0.7692
GR2-39A	16.00	5	4.393	1.583	5.247	5.202	46.0518	0.8540	5.2693
GR2-41A	6.50	65	4.358	1.953	5.805	5.755	25.9089	1.4470	3.4554
GR2-42A	16.50	127	4.906	1.487	5.665	5.621	48.9576	0.7590	5.7971
GR2-43A	40.00	122	5.746	1.213	6.062	6.005	73.9489	0.3160	18.0380
GR2-44A	46.80	139	4.750	1.096	4.863	4.835	89.6898	0.1130	24.7788
GR2-45A	59.25	105	5.206	1.073	5.307	5.282	90.5871	0.1010	24.7525
GR2-46A	63.50	17	4.521	1.142	4.738	4.689	80.9982	0.2170	22.5806
GR2-47A	51.00	14	4.444	1.123	4.561	4.537	89.5815	0.1170	20.5128
GR2-48A	23.00	77	5.226	1.398	5.826	5.777	57.0815	0.6000	8.1667
GR2-49A	15.00	9	4.201	2.008	5.802	5.767	20.2689	1.6010	2.1861
GR2-50A	34.50	58	4.617	1.211	4.902	4.865	76.4657	0.2850	12.9825
GR2-51A	45.00	75	5.166	1.144	5.340	5.310	84.7902	0.1740	17.2414
GR2-52A	56.00	28	4.925	1.117	5.049	5.025	88.8988	0.1240	19.3548
GR2-53A	47.80	115	5.112	0.983	5.245	5.218	86.4700	0.1330	20.3008
GR2-54A	33.00	125	4.687	1.105	4.856	4.828	84.7059	0.1690	16.5680
GR2-55A	39.00	88	5.111	1.092	5.204	5.186	91.4835	0.0930	19.3548

GR2-56A	25.00	27	4.655	1.118	4.790	4.771	87.9249	0.1350	14.0741
GR2-57A	7.50	132	5.048	2.046	6.663	6.611	21.0655	1.6150	3.2198
GR2-58A	11.00	43	4.623	2.044	6.235	6.201	21.1350	1.6120	2.1092
GR2-59A	17.50	67	4.466	1.356	4.967	4.923	63.0531	0.5010	8.7824
GR2-60A	24.20	94	5.385	1.434	5.998	5.948	57.2524	0.6130	8.1566
GR2-61A	28.50	53	4.252	1.206	4.559	4.526	74.5439	0.3070	10.7492
GR2-62A	42.50	20	4.420	1.132	4.572	4.545	86.5724	0.1520	17.7632
GR2-63A	55.50	88	5.110	1.317	5.569	5.532	65.1481	0.4590	8.0610
GR2-64A	53.70	64	4.733	1.127	4.870	4.849	87.8438	0.1370	15.3285
GR2-65A	34.50	76	5.138	1.500	5.870	5.813	51.2000	0.7320	7.7869
GR2-66A	28.50	134	5.080	1.306	5.529	5.480	65.6202	0.4490	10.9131
GR2-67A	16.00	73	5.006	1.894	6.517	6.446	20.2218	1.5110	4.6989
GR2-68A	8.80	53	4.252	2.031	5.832	5.809	22.2058	1.5800	1.4557
GRE-1A	18.30	85	5.069	1.645	6.328	6.302	23.4650	1.2590	2.0651
GRC-1A	3.00	100	4.874	1.817	6.134	6.089	30.6549	1.2600	3.5714
GRC-2A	16.40	2	4.580	1.603	5.488	5.437	43.3562	0.9080	5.6167
GRC-3A	10.20	91	4.710	2.111	6.462	6.426	17.0062	1.7520	2.0548
GRC-4A	31.00	66	4.473	1.219	4.776	4.730	75.1436	0.3030	15.1815
GRC-5A	50.00	23	4.506	1.123	4.630	4.601	88.9581	0.1240	23.3871
GRC-6A	66.30	119	5.307	1.114	5.462	5.420	86.0862	0.1550	27.0968
GRC-7A	51.40	116	4.753	1.165	4.902	4.868	87.2103	0.1490	22.8188
GRC-8A	49.80	21	4.446	1.069	4.684	4.648	77.7362	0.2380	15.1261
GRC-10A	69.30	68	4.303	1.255	4.666	4.615	71.0757	0.3630	14.0496
GRC-11A	51.20	73	5.007	1.219	5.294	5.260	76.4561	0.2870	11.8467
GRC-12A	49.20	140	5.272	1.268	5.678	5.638	67.9811	0.4060	9.8522
GRC-13A	32.50	98	4.840	1.518	5.589	5.524	50.6588	0.7490	8.6782
GRC-14A	28.00	104	4.528	1.125	4.757	4.726	79.6444	0.2290	13.5371
GRC-22A	54.50	109	5.574	1.285	5.973	5.931	68.9494	0.3990	10.5263
GRC-24A	6.00	15	4.447	2.052	6.122	6.099	18.3723	1.6750	1.3731
GRC-25A	44.00	56	4.367	1.181	4.614	4.581	79.0855	0.2470	13.3603
GRC-29A	65.00	93	4.321	1.167	4.508	4.469	83.9760	0.1870	20.8556
GRC-32A	6.50	90	4.829	1.889	6.334	6.306	20.3282	1.5050	1.8605

GRC-34A	53.00	72	4.424	1.062	4.514	4.495	91.5254	0.0900	21.1111
GRC-36A	51.30	131	5.017	1.132	5.172	5.142	86.3074	0.1550	19.3548
GRC-39A	21.00	55	4.486	1.310	4.959	4.921	63.8931	0.4730	8.0338
GRC-40A	7.50	132	5.049	1.809	6.321	6.272	29.6849	1.2720	3.8522
GRC-42A	25.00	7	4.230	1.374	4.769	4.719	60.7715	0.5390	9.2764
GRC-45	4.90	101	4.962	1.921	6.454	6.417	22.3321	1.4920	2.4799
GRC-46A	4.90	51	4.392	1.553	5.216	5.179	46.9414	0.8240	4.4903
GRC-47A	3.00	9	4.200	1.812	5.455	5.415	30.7395	1.2550	3.1873
GRC-48A	35.90	144	5.605	1.281	6.011	5.969	68.3060	0.4060	10.3448
GRC-50A	63.00	102	4.470	1.884	6.020	5.990	17.7282	1.5500	1.9355
station-A	59.00	87	5.204	1.142	5.337	5.305	88.3538	0.1330	24.0602
station B	66.40	86	4.778	1.087	4.888	4.859	89.8804	0.1100	26.3636
station C	71.00	19	4.417	1.098	4.516	4.490	90.9836	0.0990	26.2626
station D	67.30	138	5.162	1.064	5.245	5.225	92.1992	0.0830	24.0964
station E	59.50	33	4.230	1.085	4.331	4.308	90.6912	0.1010	22.7723
station F	52.30	35	4.665	0.951	4.763	4.740	89.6951	0.0980	23.4694
station G	37.50	136	4.779	1.098	4.900	4.876	88.9800	0.1210	19.8347
deep-grab	43.60	32	4.169	1.040	4.266	4.241	90.6731	0.0970	25.7732

Appendix H

TABLE OF MEASURED AND COMPUTERED RESULTS.

Table 3.3 Table showing sample locations and their magnetic measured parameters

Sample	lat. DD	long DD	Water depth (m)	LF Sus.	% Freq. Dep.	ARM 10^{-8} Am^2	ARM 10^{-6} (Am2/kg)	X_{arm} 10^{-6} m3/kg	X_{arm}/X
BA-1A	6.5318	1.4304	0.00	3.9	-2.56	7.92	9.67	0.12	0.03
BA-1B	6.5321	1.4297	0.07	5	12.00	9.24	11.35	0.14	0.03
BA-2A	6.5318	1.4304	0.00	5.1	-1.96	10.51	12.97	0.16	0.03
BA-2B	0.0000	0.0000	0.07	4.6	6.52	6.31	8.03	0.10	0.02
BA-3A	6.5318	1.4304	0.17	5.2	9.62	10.41	13.50	0.17	0.03
BA-3B	0.0000	0.0000	0.00	4.9	8.16	12.54	16.90	0.21	0.04
BA-4A	6.5316	1.4303	0.42	4.5	6.67	10.64	14.69	0.18	0.04
BA-4B	0.0000	0.0000	0.17	5.3	28.30	6.35	8.03	0.10	0.02
BA-5A	6.5316	1.4302	1.06	6.5	3.08	14.47	20.61	0.26	0.04
BA-5B	0.0000	0.0000	0.44	7.8	7.69	13.29	20.35	0.26	0.03
BA-6A	6.5315	1.4302	1.23	8.5	8.24	17.8	25.87	0.32	0.04
BA-6B	0.0000	0.0000	0.81	11.7	7.69	23.31	37.47	0.47	0.04
GR1-A	6.5047	1.4463	0.65	29.5	8.81	11.14	24.64	0.31	0.01
GR2-A	6.5043	1.4449	10.60	3.7	8.11	8.54	11.05	0.14	0.04
GR3-A	6.5035	1.4444	20.00	10.2	0	33.98	57.98	0.73	0.07
GR4-A	6.5047	1.4447	13.00	5.3	1.89	20.06	28.57	0.36	0.07
GR5-A	6.5051	1.4432	26.60	26.9	6.69	110.65	211.93	2.66	0.10
GR6-A	6.5047	1.4425	32.00	26	8.46	84.98	168.91	2.12	0.08
GR7-A	6.5053	1.4410	38.00	29.5	8.81	115.13	254.66	3.20	0.11
GR8-A	6.5055	1.4401	42.80	37.7	7.69	174.53	374.45	4.70	0.12
GR9-A	6.5054	1.4389	46.00	36.4	7.97	166.03	373.02	4.69	0.13
GR10-A	6.5049	1.4361	56.00	37.6	7.98	228.47	493.35	6.20	0.16
GR11-A	6.5044	1.4331	62.00	43.3	8.08	284.1	558.04	7.01	0.16

GR12-A	6.5053	1.4302	74.60	43.5	5.98	229.11	515.90	6.48	0.15
GR15-A	6.5102	1.4197	84.00	45.8	9.17	265.38	562.13	7.06	0.15
GR16-A	6.5102	1.4182	73.00	44	8.41	281.14	574.81	7.22	0.16
GR17-A	6.5107	1.4127	74.00	40.1	7.48	254.76	621.21	7.80	0.19
GR18-A	6.5118	1.4058	71.70	40.1	7.98	283.49	566.87	7.12	0.18
GR19-A	6.5116	1.4024	72.00	45.3	7.28	319.5	622.69	7.82	0.17
GR20-A	6.5115	1.3982	70.00	43.4	8.29	258.95	602.07	7.56	0.17
GR21-A	6.5116	1.3952	67.00	43.7	9.15	245.84	606.86	7.62	0.17
GR-23A	6.5113	1.3922	57.00	48.9	7.98	263.9	566.92	7.12	0.15
GR24-A	6.5113	1.3856	50.00	51.7	9.09	231.92	483.07	6.07	0.12
GR25-A	6.5118	1.3817	39.50	52.7	10.06	211.81	437.53	5.50	0.10
GR26-A	6.5119	1.3803	34.50	45.4	8.15	115.09	353.58	4.44	0.10
GR27-A	6.5114	1.3780	27.50	44.1	8.16	169.95	336.47	4.23	0.10
GR2-1A	6.5326	1.4267	13.00	10.7	7.48	43.88	82.16	1.03	0.10
GR2-3A	6.5248	1.4193	43.00	43.7	8.39	175.71	365.23	4.59	0.10
GR2-4A	6.5231	1.4178	49.00	45.3	8.39	234.64	464.54	5.84	0.13
GR2-5A	6.5194	1.4162	59.00	46.3	7.99	210.65	487.50	6.12	0.13
GR2-6A	6.4887	1.4055	50.00	92.5	9.3	210.17	871.71	10.95	0.12
GR2-7A	6.4858	1.4039	40.00	55.5	9.01	225.12	449.25	5.64	0.10
GR2-8A	6.4836	1.4027	33.50	48.7	8.42	189.09	415.49	5.22	0.11
GR2-9A	6.4798	1.4003	25.50	35.9	8.08	133.45	284.48	3.57	0.10
GR2-10A	6.5345	1.4156	17.50	18	7.78	77.06	156.59	1.97	0.11
GR2-11A	6.5255	1.4147	49.00	47.3	9.51	247.14	482.60	6.06	0.13
GR2-12A	6.5167	1.4143	66.00	52.8	8.33	220.91	538.67	6.77	0.13
GR2-13A	6.5083	1.4143	77.00	45.1	8.87	295.81	652.86	8.20	0.18
GR2-14A	6.4999	1.4148	78.00	46.6	10.09	208.09	551.82	6.93	0.15
GR2-15A	6.4916	1.4147	67.50	49.5	9.9	290.39	610.58	7.67	0.15
GR2-16A	6.4832	1.4150	58.00	50.5	9.9	251.03	515.36	6.47	0.13
GR2-17A	6.4789	1.4150	42.00	48.9	10.22	227.69	420.79	5.29	0.11
GR2-18A	6.4768	1.4150	33.00	43.2	8.33	188.84	361.00	4.54	0.10
GR2-19A	6.4754	1.4148	18.00	25.6	7.81	93.37	182.33	2.29	0.09
GR2-22A	6.4818	1.4231	45.00	46.3	9.72	212.91	448.14	5.63	0.12

GR2-23A	6.4900	1.4229	62.00	50.5	11.09	288.72	581.98	7.31	0.14
GR2-24A	6.4983	1.4232	73.50	50.4	9.52	222.25	479.92	6.03	0.12
GR2-25A	6.5067	1.4228	76.00	45.9	9.8	246.32	537.70	6.76	0.15
GR2-26A	6.5152	1.4233	63.50	44.9	8.02	188.94	468.72	5.89	0.13
GR2-27A	6.5235	1.4233	38.75	42.1	9.26	167.91	364.15	4.57	0.11
GR2-28A	6.5329	1.4056	36.50	48.1	10.6	155.59	322.07	4.05	0.08
GR2-29A	6.5250	1.4056	59.25	40.7	7.37	220.24	416.25	5.23	0.13
GR2-30A	6.5166	1.4055	72.75	43.2	7.64	313.09	618.63	7.77	0.18
GR2-31A	6.5081	1.4054	78.00	44.1	7.48	245.21	553.40	6.95	0.16
GR2-32A	6.5001	1.4056	73.75	45.7	7.88	241.96	578.71	7.27	0.16
GR2-33A	6.4916	1.4056	59.75	50.7	8.68	275.92	608.96	7.65	0.15
GR2-36A	6.5069	1.3834	43.50	54.3	9.02	222.05	437.88	5.50	0.10
GR2-37A	6.4985	1.3835	39.50	54.4	9.38	227.16	492.65	6.19	0.11
GR2-38A	6.4900	1.3835	31.50	52.9	8.51	222.33	419.41	5.27	0.10
GR2-39A	6.4830	1.3835	16.00	20.7	5.31	112.92	186.61	2.34	0.11
GR2-41A	6.4784	1.3833	6.50	40.3	7.44	126.33	196.44	2.47	0.06
GR2-42A	6.4754	1.3890	16.50	24.1	7.88	101.85	200.06	2.51	0.10
GR2-43A	6.4840	1.3890	40.00	56.8	9.33	233.01	437.08	5.49	0.10
GR2-44A	6.4919	1.3888	46.80	54.5	9.17	211.1	516.01	6.48	0.12
GR2-45A	6.5003	1.3889	59.25	49.6	9.48	261.6	612.50	7.69	0.16
GR2-46A	6.5090	1.3888	63.50	49.9	9.22	286.2	572.29	7.19	0.14
GR2-47A	6.5174	1.3888	51.00	47.4	7.17	219.17	480.53	6.04	0.13
GR2-48A	6.5257	1.3889	23.00	24.4	4.92	64.87	130.23	1.64	0.07
GR2-49A	6.4833	1.4443	15.00	9.6	8.33	30.73	39.65	0.50	0.05
GR2-50A	6.4832	1.4359	34.50	42.8	8.64	177.11	334.11	4.20	0.10
GR2-51A	6.4835	1.4276	45.00	46.8	8.76	173.11	398.78	5.01	0.11
GR2-52A	6.4834	1.4192	56.00	48.9	10.22	291.68	565.16	7.10	0.15
GR2-53A	6.4831	1.4110	47.80	50.6	8.3	248.87	521.63	6.55	0.13
GR2-54A	6.4833	1.4028	33.00	51	14.31	222.43	427.67	5.37	0.11
GR2-55A	6.4832	1.3943	39.00	54.7	9.32	181.25	401.80	5.05	0.09
GR2-56A	6.4832	1.3860	25.00	51.7	8.9	209.46	385.67	4.85	0.09
GR2-57A	6.4836	1.3800	7.50	26.6	5.64	78.47	103.37	1.30	0.05

GR2-58A	6.5275	1.4353	11.00	7.1	5.63	21.8	28.57	0.36	0.05
GR2-59A	6.5265	1.4336	17.50	29.5	9.83	120.41	239.81	3.01	0.10
GR2-60A	6.5260	1.4318	24.20	31.2	7.69	91.19	173.33	2.18	0.07
GR2-61A	6.5259	1.4262	28.50	37.4	8.56	93.25	219.36	2.76	0.07
GR2-62A	6.5258	1.4181	42.50	42.8	8.18	248	471.39	5.92	0.14
GR2-63A	6.5252	1.4082	55.50	40.1	8.98	149.58	311.56	3.91	0.10
GR2-64A	6.5248	1.4003	53.70	47.6	11.76	198.33	388.81	4.88	0.10
GR2-65A	6.5246	1.3932	34.50	33.3	7.51	69.2	155.47	1.95	0.06
GR2-66A	6.5240	1.3879	28.50	35.8	6.98	102.29	236.73	2.97	0.08
GR2-67A	6.5231	1.3834	16.00	8.2	1.22	30.61	36.88	0.46	0.06
GR2-68A	6.5230	1.3810	8.80	7.6	2.63	14.31	20.38	0.26	0.03
GRE-1A	6.5003	1.3726	18.30	11.3	3.54	25.86	31.23	0.39	0.03
GRC-1	6.4708	1.4056	3.00	9.4	6.38	58.55	75.15	0.94	0.10
GRC-2	6.4896	1.3730	16.40	14.1	6.38	68.25	112.98	1.42	0.10
GRC-3	6.4874	1.3730	10.20	21.2	4.72	80.38	99.10	1.24	0.06
GRC-4	6.4894	1.3761	31.00	54.1	8.87	202.97	410.79	5.16	0.10
GRC-5	6.4903	1.3894	50.00	47.1	7.43	192.8	584.07	7.34	0.16
GRC-6	6.4926	1.3901	66.30	50.7	8.88	275.75	639.64	8.04	0.16
GRC-7	6.5094	1.3904	51.40	47.9	8.98	268.08	617.55	7.76	0.16
GRC-8	6.5193	1.3902	49.80	43.3	8.08	135.5	306.49	3.85	0.09
GRC-10	6.5173	1.3930	69.30	47.9	9.19	175.53	340.11	4.27	0.09
GRC-11	6.5196	1.4027	51.20	45.7	9.19	174.19	351.83	4.42	0.10
GRC-12	6.5228	1.4004	49.20	39.1	8.95	98.03	223.76	2.81	0.07
GRC-13	6.5231	1.3907	32.50	39.1	9.46	91.19	193.57	2.43	0.06
GRC-14	6.5260	1.3930	28.00	45.7	9.41	162.06	314.01	3.94	0.09
GRC-22	6.5173	1.4236	54.50	34.2	8.77	104.63	224.96	2.83	0.08
GRC-24	6.5168	1.4374	6.00	5.3	-3.77	7.61	9.69	0.12	0.02
GRC-25	6.5069	1.4363	44.00	42.5	8	156.59	330.99	4.16	0.10
GRC-26	6.5066	1.4262	49.00	47	8.72	209.32	459.94	5.78	0.12
GRC-29	6.4928	1.4233	65.00	50	8.8	252.98	552.24	6.94	0.14
GRC-32	6.5004	1.4405	6.50	14.4	6.94	27.8	37.82	0.48	0.03
GRC-34	6.4894	1.4264	53.00	48.3	9.11	228.13	510.24	6.41	0.13

GRC-36	6.4863	1.4237	51.30	50.7	9.47	240.1	511.83	6.43	0.13
GRC-39	6.4734	1.4360	21.00	26.6	7.14	106	199.96	2.51	0.09
GRC-40	6.4707	1.4336	7.50	15.2	4.61	38.54	65.98	0.83	0.05
GRC-42	6.4733	1.4032	25.00	37.5	9.87	150.85	282.44	3.55	0.09
GRC-45	6.4703	1.3896	4.90	21.3	5.63	74.1	108.79	1.37	0.06
GRC-46	6.4704	1.3933	4.90	20.4	6.37	65.95	113.49	1.43	0.07
GRC-47	6.4714	1.4091	3.00	13	4.62	36.43	53.49	0.67	0.05
GRC-48	6.4731	1.4237	35.90	36.7	7.36	130.08	274.95	3.45	0.09
GRC-30	6.4928	1.4266	63.00	8.4	5.95	23.24	29.34	0.37	0.04
station A	6.5168	1.3888	59.00	48.9	9.2	331.12	663.43	8.33	0.17
station B	6.5038	1.3898	66.40	47.5	8.42	316.58	673.43	8.46	0.18
station C	6.5033	1.3928	71.00	46.4	8.84	336.99	691.83	8.69	0.19
station D	6.5000	1.4003	67.30	48.8	8.61	335.9	698.19	8.77	0.18
station E	6.4902	1.4007	59.50	49	9.8	277.99	582.67	7.32	0.15
station F	6.4878	1.4008	52.30	51.2	8.79	239.08	535.93	6.73	0.13
station G	6.4840	1.3930	37.50	52.4	8.97	250.01	501.93	6.31	0.12
deep drab	6.5223	1.4210	43.60	43.7	10.07	276.69	565.71	7.11	0.16

Table 3.4 Table showing calculated magnetic ratios from measured experimental values.

Sample	X_{arm}/SIRM	ARM/SIRM	SIRM/X	bIRM/SIRM	HIRM
GR1-A	0.0006	0.022	17.1525	0.9492	12.8650
GR2-A	0.0013	0.082	28.2351	0.9289	3.7150
GR3-A	0.0023	0.107	31.0333	0.9272	11.5250
GR4-A	0.0022	0.121	31.3321	0.9192	6.7050
GR5-A	0.0030	0.126	32.7353	0.9605	17.3900
GR6-A	0.0032	0.128	25.5900	0.9207	26.3650
GR7-A	0.0042	0.152	25.7285	0.9688	11.8300
GR8-A	0.0038	0.141	32.7594	0.9443	34.4050
GR9-A	0.0040	0.141	32.3019	0.9444	32.7150
GR10-A	0.0043	0.160	38.0104	0.9382	44.1850
GR11-A	0.0037	0.149	43.9048	0.9609	37.1500
GR12-A	0.0044	0.157	33.5786	0.9666	24.3800
GR15-A	0.0040	0.151	38.4537	0.9663	29.7000
GR16-A	0.0042	0.163	39.2241	0.9855	12.5300
GR17-A	0.0045	0.148	42.8132	0.9836	14.1200
GR18-A	0.0040	0.158	44.8357	0.9382	55.5150
GR19-A	0.0037	0.149	47.3024	0.9651	37.4350
GR20A	0.0045	0.153	39.0041	0.9970	2.5300
GR21-A	0.0050	0.160	35.2080	0.9571	32.9850
GR23-A	0.0040	0.147	36.6115	0.9421	51.7950
GR24-A	0.0036	0.138	32.5236	0.9538	38.8500
GR25-A	0.0038	0.145	27.7085	0.9590	29.9300
GR26-A	0.0053	0.137	18.5711	0.9068	39.3100
GR27-A	0.0032	0.127	30.4175	0.9519	32.2650
GRE-1A	0.0011	0.075	30.4584	0.9377	10.7150
GRC-1A	0.0014	0.090	69.5596	0.9407	19.4000
GRC-2A	0.0023	0.112	43.0397	0.9347	19.8100
GRC-3A	0.0008	0.053	71.1627	0.9328	50.6750
GRC-4A	0.0032	0.126	29.7736	0.9286	57.5050
GRC-5A	0.0056	0.147	27.8743	0.9292	46.4700
GRC-6A	0.0044	0.151	36.1160	0.9531	42.9350
GRC-7A	0.0045	0.154	36.3564	0.9508	42.8200
GRC-8A	0.0038	0.133	23.5799	0.9495	25.7750
GRC-10A	0.0032	0.130	28.0965	0.9442	37.5300
GRC-11A	0.0035	0.138	27.6621	0.9365	40.1550
GRC-12A	0.0033	0.117	21.4798	0.9313	28.8700
GRC-13A	0.0029	0.110	21.2079	0.9388	25.3850
GRC-14A	0.0031	0.129	27.5173	0.9165	52.4750
GRC-22A	0.0037	0.138	22.1336	0.9372	23.7850
GRC-24A	0.0010	0.065	22.0642	0.9022	5.7200
GRC-25A	0.0037	0.141	26.1224	0.9300	38.8600
GRC-26A	0.0040	0.144	30.9747	0.9576	30.8700

GRC-29A	0.0041	0.150	33.6886	0.9330	56.3900
GRC-32A	0.0007	0.040	48.8340	0.9754	8.6600
GRC-34A	0.0039	0.140	33.6569	0.9441	45.4100
GRC-36A	0.0038	0.142	33.3765	0.9246	63.7950
GRC-39A	0.0029	0.124	32.2090	0.9264	31.5250
GRC-40A	0.0013	0.059	42.6776	0.9640	11.6700
GRC-42A	0.0027	0.114	35.2923	0.9307	45.8550
GRC-45	0.0009	0.051	68.7563	0.9291	51.9050
GRC-46A	0.0019	0.086	37.6221	0.8986	38.9000
GRC47A	0.0016	0.085	33.1569	0.9463	11.5800
GRC-48A	0.0032	0.120	29.6466	0.9385	33.4600
GRC-50A	0.0008	0.048	58.2262	0.8961	25.4000
station-a	0.0035	0.138	48.9072	0.9543	54.6850
station-b	0.0040	0.148	45.0425	0.9429	61.1100
station-c	0.0038	0.148	48.9427	0.9447	62.7950
station-d	0.0038	0.147	46.9455	0.9667	38.0900
station-e	0.0038	0.144	39.4235	0.8981	98.3950
station-f	0.0037	0.131	35.5180	0.9404	54.1550
station-g	0.0034	0.133	35.8118	0.9257	69.7250
deep-grab	0.0048	0.187	33.7998	0.8814	87.5900

Appendix I TABLE OF MEASURED AND COMPUTERED RESULTS.

Table 3.6 Showing measured and calculated Anhysteretic Remanent Magnetization AF Demagnetization as well as calculated ARM susceptibility values.

	Meter N moment 10^{-8} A/m											
AF Demag Steps (mT)	**GR-2A**	**10^{-6} Am^2kg^{-1}**	**X_{ARM} 10^{-6} m^3kg^{-1}**	**GR-4A**	**10^{-6} Am^2kg^{-1}**	**X_{ARM} 10^{-6} m^3kg^{-1}**	**GR-5A**	**10^{-6} Am^2kg^{-1}**	**X_{ARM} 10^{-6} m^3kg^{-1}**	**GRC-45**	**10^{-6} Am^2kg^{-1}**	**X_{ARM} 10^{-6} m^3kg^{-1}**
0	7.94	10.2703	0.1290	20.66	29.4260	0.3697	113.84	218.0425	2.7392	73.06	107.2677	1.3476
2.5	7.46	9.6495	0.1212	20.35	28.9845	0.3641	113.28	216.9699	2.7258	70.31	103.2301	1.2969
5	7.24	9.3649	0.1176	19.8	28.2011	0.3543	111.13	212.8519	2.6740	67.9	99.6917	1.2524
7.5	7.06	9.1321	0.1147	19.82	28.2296	0.3546	105.25	201.5897	2.5325	64.65	94.9200	1.1925
10	6.75	8.7311	0.1097	18.94	26.9762	0.3389	101.88	195.1350	2.4514	60.37	88.6360	1.1135
20	5.91	7.6445	0.0960	16.65	23.7146	0.2979	81.34	155.7939	1.9572	43.93	64.4986	0.8103
30	4.3	5.5620	0.0699	11.42	16.2655	0.2043	59.95	114.8247	1.4425	25.62	37.6156	0.4726
40	3.15	4.0745	0.0512	8.62	12.2775	0.1542	44.03	84.3325	1.0595	13	19.0868	0.2398
60	0.92	1.1900	0.0149	4.37	6.2242	0.0782	22.71	43.4974	0.5464	4.28	6.2840	0.0789
80	0.38	0.4915	0.0062	1.38	1.9655	0.0247	8.41	16.1080	0.2024	1.35	1.9821	0.0249
100	0.37	0.4786	0.0060	0.4	0.5697	0.0072	0.24	0.4597	0.0058	0.77	1.1305	0.0142
AF Demag Steps (mT)	**GR-12A**	**10^{-6} Am^2kg^{-1}**	**X_{ARM} 10^{-6} m^3kg^{-1}**	**GR-17A**	**10^{-6} Am^2kg^{-1}**	**X_{ARM} 10^{-6} m^3kg^{-1}**	**GR-20A**	**10^{-6} Am^2kg^{-1}**	**X_{ARM} 10^{-6} m^3kg^{-1}**	**GR-25A**	**10^{-6} Am^2kg^{-1}**	**X_{ARM} 10^{-6} m^3kg^{-1}**
0	234.47	527.9667	6.6327	257.37	627.5786	7.8842	269.81	627.3192	7.8809	206.95	427.4943	5.3705
2.5	211.22	475.6136	5.9750	252.31	615.2402	7.7291	237.87	553.0574	6.9480	193.22	399.1324	5.0142
5	199.73	449.7410	5.6500	247.16	602.6823	7.5714	225.12	523.4132	6.5755	185.54	383.2679	4.8149
7.5	185.77	418.3067	5.2551	241.98	590.0512	7.4127	203.92	474.1223	5.9563	173.07	357.5088	4.4913
10	169.52	381.7158	4.7954	232.75	567.5445	7.1300	183.35	426.2962	5.3555	159.88	330.2623	4.1490
20	151.36	340.8241	4.2817	203.58	496.4155	6.2364	154.99	360.3581	4.5271	125.7	259.6571	3.2620
30	122.93	276.8070	3.4775	165.82	404.3404	5.0797	119.85	278.6561	3.5007	92	190.0434	2.3875
40	88.6	199.5046	2.5063	137.44	335.1378	4.2103	100.67	234.0618	2.9405	67.94	140.3429	1.7631
60	54.59	122.9228	1.5443	82.13	200.2682	2.5159	57.45	133.5736	1.6781	36.92	76.2652	0.9581
80	21.22	47.7820	0.6003	30.83	75.1768	0.9444	20.92	48.6399	0.6111	13.63	28.1553	0.3537
100	2.05	4.6161	0.0580	0.7	1.7069	0.0214	3.7	8.6027	0.1081	1.46	3.0159	0.0379

Appendix J TABLE OF MEASURED AND COMPUTERED RESULTS.

Table 3.7 (A) Showing measured and calculated acquired Isothermal Remanent Magnetization values.

	Meter N moment 10^{-8} A/m							
IRM Acq. Steps mT	**GR-2A**	**10^{-6} Am^2kg^{-1}**	**GR-4A**	**10^{-6} Am^2kg^{-1}**	**GR-5A**	**10^{-6} Am^2kg^{-1}**	**GRC-45**	**10^{-6} Am^2kg^{-1}**
0	0.37	0.4786	0.4	0.5697	0.24	0.4597	0.77	1.1305
5	0.36	0.4657	0.55	0.7834	2.26	4.3287	1.64	2.4079
10	1.68	2.1731	2.56	3.6462	19.43	37.2151	15.08	22.1407
20	14.25	18.4323	17.55	24.9964	145.92	279.4867	179.46	263.4855
30	32.33	41.8187	43.87	62.4840	337.42	646.2747	539.81	792.5562
40	45.57	58.9445	64.22	91.4685	463.94	888.6037	790.83	1161.1070
50	50.26	65.0110	82.61	117.6613	551.42	1056.1578	960.26	1409.8664
100	76.45	98.8876	133.32	189.8875	779.78	1493.5453	1272.61	1868.4628
300	94.16	121.7954	158.31	225.4807	850.43	1628.8642	1392.12	2043.9289
400	98.66	127.6161	159.42	227.0617	845.59	1619.5939	1401.51	2057.7155
1100	104.47	135.1313	166.06	236.5190	880.58	1686.6118	1464.51	2150.2129
IRM Acq. Steps mT	**GR-12A**	**10^{-6} Am^2kg^{-1}**	**GR-17A**	**10^{-6} Am^2kg^{-1}**	**GR-20A**	**10^{-6} Am^2kg^{-1}**	**GR-25A**	**10^{-6} Am^2kg^{-1}**
0	2.05	4.6161	0.7	1.7069	3.7	8.6027	1.46	3.0159
5	4.63	10.4256	3.29	8.0224	5.13	11.9275	3.92	8.0975
10	30.4	68.4531	29.62	72.2263	28.8	66.9612	36.85	76.1206
20	211.78	476.8746	218.86	533.6747	200.25	465.5894	278.11	574.4887
30	516.23	1162.4184	510.76	1245.4523	525.02	1220.6929	623.8	1288.5767
40	703.32	1583.6974	751.56	1832.6262	738.2	1716.3450	834.25	1723.3010
50	906.75	2041.7699	968.33	2361.2046	916.98	2132.0158	996.5	2058.4590
100	1360.67	3063.8820	1459.86	3559.7659	1578.78	3670.7277	1383.31	2857.4881
300	1407.36	3169.0160	1685.24	4109.3392	1626.94	3782.7017	1429.52	2952.9436
400	1407.07	3168.3630	1686.36	4112.0702	1606.15	3734.3641	1430.28	2954.5135
1100	1460.67	3289.0565	1716.81	4186.3204	1692.78	3935.7824	1460.24	3016.4016

Table 3.7 (B) Showing measured and calculated Isothermal Remanent Magnetization AF Demagnetization values.

	Meter N moment 10^{-8} A/m							
IRM AF Demag Steps (mT)	**GR-2A**	**10^{-6} Am^2kg^{-1}**	**GR-4A**	**10^{-6} Am^2kg^{-1}**	**GR-5A**	**10^{-6} Am^2kg^{-1}**	**GRC-45**	**10^{-6} Am^2kg^{-1}**
0	104.77	135.52	166.06	236.52	880.58	1686.61	1464.51	2150.21
2.5	79.19	102.43	158.57	225.85	841.91	1612.55	1341.59	1969.74
5	73.23	94.72	150.52	214.39	799.7	1531.70	1245.54	1828.72
7.5	68.55	88.67	142.55	203.03	753.16	1442.56	1159.73	1702.73
10	62.43	80.75	132.96	189.37	684.2	1310.48	1043.9	1532.67
20	50.02	64.70	107.82	153.57	480.3	919.94	645.69	948.01
30	39.68	51.33	85.07	121.17	327.09	626.49	403.85	592.94
40	31.97	41.35	67.35	95.93	235.43	450.93	275.53	404.54
60	23.55	30.46	44.26	63.04	140.92	269.91	179.08	262.93
80	19.4	25.09	31.71	45.16	84.19	161.25	129.59	190.27
100	16.24	21.01	24.38	34.72	54.24	103.89	105.49	154.88
IRM AF Demag Steps (mT)	**GR-12A**	**10^{-6} Am^2kg^{-1}**	**GR-17A**	**10^{-6} Am^2kg^{-1}**	**GR-20A**	**10^{-6} Am^2kg^{-1}**	**GR-25A**	**10^{-6} Am^2kg^{-1}**
0	1460.67	3289.06	1716.81	4186.32	1692.78	3935.78	1460.24	3016.40
2.5	1390.96	3132.09	1666.47	4063.57	1409.34	3276.77	1359.32	2807.93
5	1249.12	2812.70	1613.68	3934.85	1232.99	2866.75	1226.59	2533.75
7.5	1060.94	2388.97	1504.74	3669.20	1050.56	2442.59	1087.84	2247.14
10	1009.71	2273.61	1421.47	3466.15	959.36	2230.55	990	2045.03
20	714.97	1609.93	1055.47	2573.69	613.83	1427.18	649.12	1340.88
30	519.77	1170.39	773.06	1885.05	446.53	1038.20	430.75	889.80
40	373.02	839.95	574.53	1400.95	329.16	765.31	302.77	625.43
60	220.8	497.19	324.94	792.34	160.82	373.91	168.17	347.39
80	108.18	243.59	171.47	418.12	86.28	200.60	100.62	207.85
100	58.55	131.84	90.05	219.58	47.45	110.32	64.1	132.41

Appendix K

Table 3.9 Shows measured SIRM DC Demagnetization values for twenty samples.

IRM Demag Steps	GR-2A	X 10^{-6} Am^2kg^{-1}	GR-4A	X 10^{-6} Am^2kg^{-1}	GR-5A	X 10^{-6} Am^2kg^{-1}	GR-10A	X 10^{-6} Am^2kg^{-1}	GR-12A	X 10^{-6} Am^2kg^{-1}
0	102.02	131.96	164.63	234.48	861.71	1650.47	1425.6	3078.38	1431.07	3222.40
5	89.15	115.31	157.28	224.01	850.97	1629.90	1319.81	2849.95	1260.8	2839.00
10	77.63	100.41	145.39	207.08	759.61	1454.91	1184.43	2557.61	1022.42	2302.23
15	57.56	74.45	122.88	175.02	567.93	1087.78	908.86	1962.56	747.28	1682.68
20	42.16	54.53	99.2	141.29	401.4	768.82	680.35	1469.12	489.17	1101.49
30	5.68	7.35	42.67	60.77	10.54	20.19	111.04	239.78	-43.45	-97.84
40	-15.37	-19.88	3.39	4.83	-227.13	-435.03	-259.7	-560.79		
50			-33.45	-47.64						

IRM Demag Steps	GR-15A	X 10^{-6} Am^2kg^{-1}	GR-17A	X 10^{-6} Am^2kg^{-1}	GR-18A	X 10^{-6} Am^2kg^{-1}	GR-20A	X 10^{-6} Am^2kg^{-1}	GR-25A	X 10^{-6} Am^2kg^{-1}
0	1822.68	3860.79	1693.33	4129.07	1829.86	3658.99	1733.57	4030.62	1508.55	3116.20
5	1723.81	3651.37	1651.94	4028.14	1708.22	3415.76	1438.76	3345.18	1325.86	2738.81
10	1498.65	3174.43	1432.76	3493.68	1532.69	3064.77	1206.8	2805.86	1154.33	2384.49
15	1130.33	2394.26	1189.21	2899.80	1160.8	2321.14	899.5	2091.37	758.2	1566.21
20	843.08	1785.81	932.5	2273.84	893.14	1785.92	638.22	1483.89	488.38	1008.84
30	130.94	277.36	275.2	671.06	198.95	397.82	12.98	30.18	-150.75	-311.40
40	-351.23	-743.97	-178.35	-434.89	-278.55	-556.99	-377.56	-877.84		
50										

Continuation of Table 3.9

IRM Demag Steps	GRC-3A	X 10^{-6} Am^2kg^{-1}	GRC-12A	X 10^{-6} Am^2kg^{-1}	GRC-25A	X 10^{-6} Am^2kg^{-1}	GRC-32A	X 10^{-6} Am^2kg^{-1}	GRC-40A	X 10^{-6} Am^2kg^{-1}
0	1518.23	1871.82	848.29	1936.29	1120.75	2368.95	740.29	1007.06	718.58	1230.23
5	1380.94	1702.55	802.22	1831.13	1053	2225.75	658.5	895.80	581.43	995.43
10	1157.48	1427.05	698.33	1594.00	999.28	2112.20	485.31	660.20	323.04	553.06
15	730.45	900.57	451.18	1029.86	643.71	1360.62	165.67	225.37	198.59	339.99
20	334.52	412.43	248.81	567.93	409.16	864.85	-51.2	-69.65	67.09	114.86
30	-496.37	-611.97	-163.83	-373.96	-99.23	-209.74			-157.66	-269.92
40										
50										

IRM Demag Steps	GRC-45	X 10^{-6} Am^2kg^{-1}	GRC-48A	X 10^{-6} Am^2kg^{-1}	Station A-dk1	X 10^{-6} Am^2kg^{-1}	Station-D-a	X 10^{-6} Am^2kg^{-1}	Station-F-a	X 10^{-6} Am^2kg^{-1}
0	1469.18	2157.07	1103.81	1620.63	2418.76	4846.24	2265.75	4709.52	1770.96	3969.87
5	1360.83	1997.99	1061.81	1558.96	2318	4644.36	2137.99	4443.96	1581.64	3545.48
10	1203.37	1766.80	946.52	1389.69	2084.24	4176.00	1855.9	3857.62	1248.12	2797.85
15	885.97	1300.79	681.47	1000.54	1671.95	3349.93	1451.8	3017.67	984.04	2205.87
20	599.69	880.47	463.89	681.09	1300.8	2606.29	1099.45	2285.28	668.07	1497.58
30	-98.87	-145.16	-48.44	-71.12	366.38	734.08	237.04	492.70	-42.41	-95.07
40					-276.92	-554.84	-346.81	-720.87		
50										

Appendix L **TABLE OF RESULTS**

Table 3.14 Shows the measured and calculated results for the grain size analysis of sample BA – 2B out of the twenty-five samples selected.

sample name		BA-2B								
total weight start (g)		65.589								
percent error		0.3644								
Phi	mm	Sample Wt	Individual % Wt	Cumulative Wt (g)	Cumulative Wt %	Remarks (Composition, Roundness)				
-2.00		0.00	0.00	0.00	0.00					
-1.25		0.00	0.00	0.00	0.00					
-1.00		0.00	0.00	0.00	0.00					
-0.50		0.02	0.03	0.02	0.03					
0.00		0.08	0.11	0.10	0.15					
0.50		0.10	0.15	0.19	0.30					
1.00		1.39	2.12	1.58	2.42					
1.50		11.42	17.48	13.00	19.89					
2.00		34.55	52.87	47.55	72.77					
2.50		12.49	19.11	60.04	91.88					
3.00		1.82	2.79	61.86	94.66					
3.50		0.54	0.82	62.40	95.48					
4.00		0.34	0.52	62.74	96.00					
pan		2.61	4.00	65.35	100.00					
total		65.35								

Table built for Computing moment statistics using $^1/_2\,\Phi$										
class interval (~~θ~~)	m Midpoint (~~θ~~)	f Weight %	fm Product	(m - x) Deviation	$(m - x)^2$ Deviation squared	$f(m - x)^2$ Product	$(m - x)^3$ Deviation cubed	$f(m - x)^3$ Product	$(m - x)^4$ Deviation quadrupled	$f(m - x)^4$ Product
2.0 - 1.6	1.8	0.00	0.00	-0.53	0.28	0.00	-0.15	0.00	0.08	0.00
1.5 - 1.1	1.3	0.00	0.00	-1.03	1.06	0.00	-1.09	0.00	1.13	0.00
1.0 - 0.6	0.8	0.00	0.00	-1.53	2.34	0.00	-3.58	0.00	5.48	0.00
0.5 - 0.1	0.3	0.03	0.01	-2.03	4.12	0.14	-8.37	-0.28	16.98	0.57
0.0 - 0.4	0.2	0.11	0.02	-2.13	4.54	0.52	-9.66	-1.11	20.58	2.36
0.5 - 0.9	0.7	0.15	0.10	-1.63	2.66	0.39	-4.33	-0.64	7.06	1.05
1.0 - 1.4	1.2	2.12	2.55	-1.13	1.28	2.71	-1.44	-3.06	1.63	3.46
1.5 - 1.9	1.7	17.48	29.71	-0.63	0.40	6.94	-0.25	-4.37	0.16	2.75
2.0 - 2.4	2.2	52.87	116.32	-0.13	0.02	0.89	0.00	-0.12	0.00	0.02
2.5 - 2.9	2.7	19.11	51.60	0.37	0.14	2.62	0.05	0.97	0.02	0.36
3.0 - 3.4	3.2	2.79	8.91	0.87	0.76	2.11	0.66	1.83	0.57	1.60
3.5 - 3.9	3.7	0.82	3.03	1.37	1.88	1.54	2.57	2.11	3.52	2.89
4.0 - 4.4	4.2	0.52	2.19	1.87	3.50	1.82	6.54	3.40	12.23	6.36
≥ 4.5	4.7	4.00	18.79	2.37	5.62	22.45	13.31	53.21	31.55	126.10
		100.00	233.23			42.13		51.94		147.52

Table 1 of 25.

Calculation:

From equation (2.3), $Mean = {}^{233.33}\!/_{100} = 2.3333$

From equation (2.4), $S\tan dard\ Deviation = \sqrt{\frac{42.13}{100}} = 0.6491$

From equation (2.5), $Skewness = \frac{51.94}{100 \times 0.6491^3} = 1.8992$

From equation (2.6), $Kurtosis = \frac{147.52}{100 \times 0.6491^4} = 8.3101$

Table 3.15 Table showing samples, water depth and their measured statistical parameters

Sample Name	Water Depth	Mean Grain Size (N)	Mean grain size (:m)	Standard Deviation	Skewness
BA – 1A	0.00	2.6328	177	0.5120	1.0885
BA – 2A	0.00	1.4605	350	1.1989	1.2526
BA – 2B	0.00	2.3333	210	0.6491	1.8992
BA – 1B	0.07	2.3344	210	0.9837	0.7858
BA – 3A	0.17	3.5414	88	0.8187	0.0567
BA - 3B	0.17	1.8993	250	0.8803	1.5402
BA – 4B	0.17	2.6889	149	0.9166	0.4301
BA – 4A	0.42	3.6948	74	0.7382	-0.0554
BA – 5B	0.44	4.0145	62.5	0.8606	-1.1131
BA – 6B	0.81	4.5064	44	0.4213	-2.8538
BA – 6A	1.23	4.0494	62.5	0.8329	-1.2589
GRE – 1A	18.30	3.356	105	1.4588	-0.6206
GR – 1A	0.65	2.0712	250	0.9941	0.5308
GR – 2A	10.60	3.2249	105	1.3390	-0.0441
GR – 4A	13.00	3.9966	62.5	1.2137	-1.6770
GR – 20A	70.00	1.7684	300	1.0518	1.4460
GR2 – 57A	7.50	2.2343	210	1.1419	0.0939
GR2 – 68A	8.80	3.3279	105	1.1785	-0.7184
GR2 -58A	11.00	3.4373	88	1.3268	-0.5812
GR2 – 49A	15.00	2.8295	149	1.4573	-0.1418
GR2 - 67A	16.00	2.1929	250	1.2658	0.3118
GRC – 45	4.90	3.3633	88	1.2137	-0.7141
GRC – 32A	6.50	2.8745	125	1.1819	-0.4404
GRC – 3A	10.20	3.1889	105	1.3371	-0.5453
GRC – 50A	63.00	1.3896	350	0.7558	0.4009

Appendix M

Plots from the hysteresis measurements